# DESIGN AND SIMULATION OF SINGLE-CRYSTAL DIAMOND DIODES FOR HIGH VOLTAGE, HIGH POWER AND HIGH TEMPERATURE APPLICATIONS

Ву

Nutthamon Suwanmonkha

## A DISSERTATION

Submitted to
Michigan State University
in partial fulfillment of the requirements
for the degree of

Electrical Engineering - Doctor of Philosophy

2016

#### ABSTRACT

# DESIGN AND SIMULATION OF SINGLE-CRYSTAL DIAMOND DIODES FOR HIGH VOLTAGE, HIGH POWER AND HIGH TEMPERATURE APPLICATIONS

By

#### Nutthamon Suwanmonkha

Diamond has exceptional properties and great potentials for making high-power semiconducting electronic devices that surpass the capabilities of other common semiconductors including silicon. The superior properties of diamond include wide bandgap, high thermal conductivity, large electric breakdown field and fast carrier mobilities. All of these properties are crucial for a semiconductor that is used to make electronic devices that can operate at high power levels, high voltage and high temperature.

Two-dimensional semiconductor device simulation software such as Medici assists engineers to design device structures that allow the performance requirements of device applications to be met. Most physical material parameters of the well-known semiconductors are already compiled and embedded in Medici. However, diamond is not one of them. Material parameters of diamond, which include the models for incomplete ionization, temperature-and-impurity-dependent mobility, and impact ionization, are not readily available in software such as Medici. Models and data for diamond semiconductor material have been developed for Medici in the work based on results measured in the research literature and in the experimental work at Michigan State University.

After equipping Medici with diamond material parameters, simulations of various diamond diodes including Schottky, PN-junction and merged Schottky/PN-junction diode structures are reported. Diodes are simulated versus changes in doping concentration, drift layer thickness and operating temperature. In particular, the diode performance metrics

studied include the breakdown voltage, turn-on voltage, and specific on-resistance. The goal is to find the designs which yield low power loss and provide high voltage blocking capability. Simulation results are presented that provide insight for the design of diamond diodes using the various diode structures. Results are also reported on the use of field plate structures in the simulations to control the electric field and increase the breakdown voltage.

#### **ACKNOWLEDGEMENTS**

First and foremost, I would like to express my sincere appreciation to my advisor, Professor Dr. Timothy Grotjohn for his guidance, encouragement and support throughout the development of this research and the writing of this dissertation. His attention to details and patience allowed me learn the way to apply theoretical knowledge to the actual practice of semiconductor device designing.

I would also like to thank the other members of my dissertation committee: Professor Dr. Donnie Reinhard, Professor Dr. Tim Hogan and Professor Dr. Greg Swain for their knowledgeable insights and constructive comments during my study. I have gained good understandings in physical electronics from the course ECE-874 taught by Dr. Reinhard. He also spent some time going through my experimental data at the beginning of my research study and helped me make sense of it from which my knowledge expands. I received several helps from Dr. Hogan when I was working in the cleanroom and on the cryogenic probing station. Through observations, I learned from Dr. Swain the techniques to give effective and comprehensible academic presentations. All of this support has been much appreciated.

I would also like to mention the following members of the research group, MSU staff members and colleagues, including Professor Dr. Jes Asmussen, Michael Becker, Karl Dersch, Brian Wright, Dzung Tri Tran, Robert Rechenberg, Jing Lu, Yajun Gu, Ayan Bhattacharya and Shreya Nad who have contributed their knowledge and expertise to my research study and personal growth as an engineer.

Importantly, I would like to thank my family members, relatives and good friends whose support has been my cornerstone. My grandparents, aunts, uncles, cousins and Rob, my brother have been very supportive. Grandma Sukanya, the pillar of our family, has always given me wise words and sent good wishes. Likewise, I would like to give special thanks to my Spartan parents, Professor Dr. Christopher Wheeler and his wife, Penny Wheeler for their advice, encouragement and many wonderful home-cooked meals. Their kind actions have touched my family and I since before I came to MSU to my commencement day and beyond. Furthermore, I am thankful for and very much appreciate the longtime friendship with a few of my elementary school classmates especially Da and Dr. Ling. Also, I am sincerely grateful to have Ton, Dr. Natee Limsuwan, in my life. Thank you for keeping me smiling.

Finally, I would like to express my deepest gratitude to my dearest parents, Dr. Rungsit and Dr. Siripaarn Suwanmonkha who have been everything to me, and everything that I am. Thank you for being my super backbone, always sending me love and cheering me on from the other side of the Pacific Ocean for the past 18 years. Your tremendous support, encouragement and understanding have enabled me to overcome many obstacles in my academic and life journey. This PhD thesis is dedicated to you, Mom and Dad.

# TABLE OF CONTENTS

| LIST OF TABLES  | viii |
|---|------|
| LIST OF FIGURES   | ix   |
| KEY TO SYMBOLS  | xii  |
| CHAPTER1  |      |
| INTRODUCTION  | 1    |
| 1.1 Motivation  | 1    |
| 1.2 Research Objectives   | 3    |
| 1.3 Outline of Dissertation   |      |
| CHAPTER 2   |      |
| CURRENT STATE OF THE ART OF HIGH POWER DIAMOND DEVICES              | 5    |
| 2.1 Theory of Diodes  |      |
| 2.2 Challenges of Diamond Diodes                                    |      |
| 2.3 Literature Review   |      |
| CHAPTER 3   |      |
| SINGLE-CRYSTAL DIAMOND MATERIAL MODELS AND PARAMETERS FOR           |      |
| SEMICONDUCTOR DEVICE SIMULATION                                     | 23   |
| 3.1 Medici Device Simulator   |      |
| 3.2 Diamond Parameters  | 26   |
| 3.2.1 Bulk Properties   | 26   |
| 3.2.2 Incomplete Ionization Model                                   |      |
| 3.2.3 Temperature-and-impurity-dependent Mobility Model             | 29   |
| 3.2.4 Impact Ionization Model                                       | 31   |
| 3.2.5 Metal Contacts to Diamond                                     |      |
| 3.3 Summary of Diamond Parameters for the Simulations in this Study | 32   |
| CHAPTER 4   |      |
| SCHOTTKY DIAMOND DIODE DESIGN AND SIMULATION                        | 34   |
| 4.1 Schottky Diode Fundamentals                                     |      |
| 4.1.1 Design Parameters in Power Devices                            | 37   |
| 4.1.2 Space Charge Limited Conduction (SCLC)                        |      |
| 4.2 Simulation Setup for Schottky Diamond Diodes                    |      |
| 4.2.1 Schottky Diamond Diode Simulations in Forward Bias            |      |
| 4.2.2 Schottky Diamond Diode Simulations in Reverse Bias            |      |
| 4.3 Schottky Diamond Diode with Field Plate Structures              |      |
| 4.4 Summary of Chapter  |      |

| CHAPTER 5  |     |
|--|-----|
| COMPARISON OF DIAMOND DIODE DESIGNS  | 64  |
| 5.1 PN-junction Diamond Diode  | 64  |
| 5.1.1 Basic Operation of PN-junction Diode   | 65  |
| 5.1.2. Structure Setup and Simulation of PN-junction Diamond Diode                           | 67  |
| 5.1.3 Performance Comparison of Schottky and PN-junction                                     |     |
| Diamond Diode  | 72  |
| 5.2 Merged Diamond Diode   | 77  |
| 5.2.1 Basic Operation of Merged Diode Structures   | 77  |
| 5.2.2 Structure Setup and Simulation of Merged Diamond Diode                                 | 78  |
| 5.2.3 Comparison of Schottky, PN-junction and  |     |
| Merged Diamond Diodes  | 80  |
| 5.3 Summary of Chapter   | 83  |
| CHAPTER 6 CONCLUSION AND FUTURE RESEARCH6.1 Conclusion of Findings6.2 Future Research        | 84  |
| APPENDICES   | 89  |
| APPENDIX A: Input File of Schottky Diamond Diode   |     |
| $(p^{-} = 1x10^{17} \text{ cm}^{-3}; 450 \text{ K})$   | 90  |
| APPENDIX B: Input File of Schottky Diamond Diode with Field Plate                            |     |
| $(p^{-} = 1x10^{17} \text{ cm}^{-3}; 450 \text{ K})$   | 92  |
| APPENDIX C: Input File of PN-junction Diamond Diode  |     |
| $(p^{-} = 1x10^{17} \text{ cm}^{-3}; 450 \text{ K})$   | 95  |
| APPENDIX D: Input File of Merged Diamond Diode   |     |
| $(p^{-} = 1 \times 10^{17} \text{ cm}^{-3}; 450 \text{ K}; \text{ spacing} = 1 \mu\text{m})$ | 97  |
| DVDV 10 CD A DVVV  | 0.0 |
| BIBLIOGRAPHY   | 99  |

# LIST OF TABLES

| Table 1.1: | Basic Bulk Properties of Diamond Compared to Si, GaAs, 4H-SiC and GaN at 300K  |
|------------|--|
| Table 3.1: | Bulk Properties of Diamond Compared to Si, GaAs, 4H-SiC and GaN at 300K  |
|            | Hall Mobility Data Obtained from Hall Measurement of the Actual Diamond Samples Grown in MSU Lab   |
| Table 3.3: | Diamond Material Parameters Used in All the Simulations of this Work 33  |
|            | Breakdown Voltages, Specific On-resistance and Maximum Electric Field of Schottky Diamond Diode Simulations at 300 K when Drift Layer was 5 μm 54  |
| Table 4.2: | Electric Field at the Edge of Schottky Contact and Breakdown Voltage at 700 V Reverse Bias when Varying Thickness of Field Plate was Used  |
| Table 5.1: | Results of PN-junction Diamond Diode Simulations (structure displayed in figure 5.1) with Varying Temperature and Doping Concentration   |
|            | Peak Electric Field at Breakdown of PN-junction and Schottky Diode at 450 K76  |
| 1          | Breakdown Voltage, Turn-on Voltage and Specific On-resistance for PN-junction, Schottky and Merged Diamond Diodes Simulated at 450 K and Drift Layer Doping of 1x10 <sup>17</sup> cm <sup>-3</sup> |

# LIST OF FIGURES

| Figure 2.1 | (a) Sign convention of a diode; (b) Ideal diode I-V characteristic; (c) Non-ideal diode I-V characteristic; | 6          |
|------------|---|------------|
|            | (d) Forward current and ideality factor, η  | 0          |
| Figure 2.2 | : Schematics of (a) a Schottky diode and (b) a PN-junction diode  | 7          |
| Figure 2.3 | : Comparison of I-V characteristic of Schottky and PN-junction diodes                                       | 8          |
| Figure 2.4 | : Unipolar vertical Schottky diode structure  | 11         |
| Figure 2.5 | : Structure of the merged diode   | 12         |
| Figure 2.6 | : IV Characteristic of PN-junction diode and merged diode<br>(from 100-µm diameter diode)                   | 13         |
| Figure 2.7 | : Structure of the SPND diamond diode   | 15         |
| Figure 2.8 | : Structure of Schottky diode with field plates   | 16         |
| Figure 2.9 | : Measurement of boron concentration versus device distance<br>from delta doping technique                  | 17         |
| Figure 2.1 | 0: Diamond MESFET structure   | 18         |
| Figure 2.1 | 1: Mobility measurement of delta doping diamond MESFET  | 19         |
| Figure 2.2 | 2: Structure of H-terminated diamond MISFET   | 20         |
| Figure 2.2 | 3: Proposed MISFET structure  | <b>2</b> 1 |
| Figure 2.2 | 3: MISFET I <sub>D</sub> -V <sub>DS</sub> performance   | <b>2</b> 1 |
| Figure 3.1 | : Summary of Medici solution process  | <b>2</b> 3 |
| Figure 3.2 | : N-type and P-type dopant levels in single-crystal diamond   | 28         |
| Figure 3.3 | : Ionized impurity carriers versus temperature in single-crystal diamond                                    | 28         |
| Figure 3.5 | : Hall measurements of boron doped diamond samples  | 30         |
| Figure 4.1 | Structure of Schottky diamond diode   | 31         |

| Figure 4.2: | Band diagram of Schottky diode   | 36 |
|-------------|--|----|
| Figure 4.3: | Block of semiconductor (left); Electric field distribution in the drift region in reverse bias (right)   | 37 |
| Figure 4.4: | Four basic transport processes in forward bias: (1) thermionic emission (2) tunneling (3) recombination and (4) diffusion  | 40 |
| Figure 4.5: | Band diagram of Schottky diamond diode in SCLC regime  | 42 |
| Figure 4.6: | I-V Characteristic of Schottky diamond diode at 300K and p $^{\text{-}}$ was $1 \times 10^{16}$ cm $^{\text{-}3}$ for different thicknesses of the p $^{\text{-}}$ layer   | 46 |
| Figure 4.7: | Semi-log plot of current density versus forward bias voltage of Schottky diamond diode simulations at 300K and p $^{\text{-}}$ was $1 \times 10^{16}$ cm $^{\text{-}3}$ for different thicknesses of p $^{\text{-}}$ layer | 47 |
| Figure 4.8: | Log plot of current densities versus voltage of Schottky diamond diode simulations at 300K and p $^{\text{-}}$ was $1x10^{16}\ \text{cm}^{\text{-}3}$  | 48 |
| Figure 4.9: | Log plot of current densities versus voltage of Schottky diamond diode simulations for varying thickness and temperature based on $p^- = 1 \times 10^{16} \text{ cm}^{-3}$   | 49 |
| Figure 4.10 | ): Slope 'm' vs. draft layer thickness W   | 50 |
| Figure 4.11 | 1: Log plot of current density versus voltage at 300K and $p^- = 2 \mu m$ thick  | 51 |
| Figure 4.12 | 2: Schottky diode structure and dimension for easy electric field comparison   | 52 |
| Figure 4.13 | 3: Electric field versus drift layer when biased at V <sub>BR</sub>  | 53 |
| Figure 4.14 | 4: Semi-log plot of current versus voltage in the reverse bias at 300 K  | 54 |
| Figure 4.15 | 5: Electric field versus drift layer dimension at 300 K at 1000 V reverse bias   | 55 |
| Figure 4.16 | 6: Breakdown voltage versus doping concentration of Schottky diamond diode with drift layer (p-) of 5 μm thick   | 57 |
| Figure 4.17 | 7: Breakdown voltage versus p- layer thickness when p- doping was fixed at $1 \mathrm{x} 10^{16}  \mathrm{cm}^{-3}$  | 58 |
| Figure 4.18 | 3: Breakdown voltage versus temperature for varying p- layer thickness when p- doping was fixed at $1 \times 10^{16}$ cm <sup>-3</sup>   | 59 |

| Figure 4.19 | : Specific on-resistance versus breakdown voltage when $p^-$ layer thickness was fixed at 5 $\mu$ m and $p^-$ doping was fixed at $1x10^{16}$ cm <sup>-3</sup>                               | 60 |
|-------------|--|----|
| Figure 4.20 | : Simulation setup and results of electric field vectors in the device at 400 V reverse bias, 300 K  | 61 |
| Figure 4.21 | : Electric field at the edge and middle of Schottky contact without field plate (left); with 1.0 μm thick field plate (middle); with 0.5 μm thick field plate (right)                        | 62 |
| Figure 5.1: | Basic operations of a PN-junction diode  | 66 |
| Figure 5.2: | Setup structure of PN-junction diode   | 68 |
|             | J-V plot of a PN-junction diamond diode when $N_{\rm A}$ in p- layer was $1x10^{17}$ cm $^{-3}$ and 5 $\mu m$ thick  | 69 |
|             | J-V plot of a PN-junction diamond diode when p- layer was μm thick and operating temperature was 450K  | 70 |
|             | Specific on-resistance versus doping concentration in the drift layer of PN-junction diode   | 70 |
| _           | Breakdown voltage versus drift layer doping concentration of a PN-junction diamond diode based on 5-µm thick drift layer   | 71 |
|             | Specific on-resistance versus breakdown voltage of PN-junction diamond diode at 300 K  | 72 |
|             | Comparison of the turn-on voltages ( $V_{on}$ ) of Schottky and PN-junction diodes at 450 K based on N <sub>A</sub> of 1 x $10^{17}$ cm <sup>-3</sup> and p <sup>-</sup> was 5 $\mu$ m thick | 73 |
| Figure 5.9: | Comparison of R <sub>on,sp</sub> of PN junction and Schottky diamond diodes  | 74 |
| Figure 5:10 | Semi-log plot of current versus voltage in reverse bias of Schottky and PN-junction diamond diodes at 450 K and drift layer doping of $4 \times 10^{17}$ cm <sup>-3</sup>                    | 75 |
| Figure 5.11 | : Breakdown voltage versus p- layer doping concentration of Schottky and PN-junction diamond diodes based on p- layer of 5 $\mu m$ thick and operating temperatures at 300 K and 450 K       | 76 |
| Figure 5.12 | : Structure of merged diode design   | 77 |
| Figure 5.13 | : The intersection of depletion regions in merged diamond diode under reverse bias   | 78 |

| Figure 5.14: | Merged diode setup for simulations   | 78 |
|--------------|--|----|
| Figure 5.15: | Dimension configurations of merged diode dimensions  | 79 |
| •            | Electric field vector of the merged diode with 2- $\mu$ m spacing, drift layer doping of $1x10^{17}$ cm <sup>-3</sup> and simulated at 450 K   | 31 |
|              | Forward conduction of Schottky, PN junction and merged diamond diode simulated at 450 K and drift layer doping of $1 \times 10^{17}$ cm <sup>-3</sup> (the inset is zoomed in on the x and y axes) | 32 |

# **KEY TO SYMBOLS**

| Ron                    | On-state resistance              |
|------------------------|----------------------------------|
| $V_{\text{BR}}$        | Breakdown voltage                |
| $E_{max} \\$           | Peak electric field at breakdown |
| n                      | Electron concentration           |
| p                      | Hole concentration               |
| $N_D^+$                | Ionized donor concentration      |
| $N_A^-$                | Ionized acceptor concentration   |
| $\epsilon$             | Dielectric permittivity          |
| $\psi$                 | Intrinsic Fermi potential        |
| $ ho_s$                | Surface charge density           |
| $E_A$                  | Activation energy                |
| $F_n$                  | Electron quasi-Fermi energy      |
| $F_p$                  | Hole quasi-Fermi energy          |
| $\overrightarrow{J_n}$ | Electron current density vector  |
| $\overrightarrow{J_p}$ | Hole current density vector      |
| $U_n$                  | Electron recombination rate      |
| $U_p$                  | Hole recombination rate          |
| $\mu_n$                | Electron mobility                |
| $\mu_p$                | Hole mobility                    |
| $D_n$                  | Electron diffusivity             |
| $D_p$                  | Hole diffusivity                 |

- $\xi$  Measured electric field
- $\alpha_p$  Hole impact ionization rates
- $\alpha_n$  Electron impact ionization rates
- $\psi_s$  Surface potential
- $\psi_{bi}$  Built-in potential
- E<sub>g</sub> Bandgap energy
- $\chi_{semi}$  Electron affinity of the semiconductor
- N<sub>c</sub> Electron density of state
- N<sub>v</sub> Hole density of state
- q Electric charge which equals to  $1.6 \times 10^{-19}$  C
- k Boltzmann constant, equals to 8.62 x 10<sup>-5</sup> eV/K
- N<sub>A</sub> Doping concentration of boron in the lowly doped (p<sup>-</sup>) layer
- N<sub>D</sub> Doping concentration of phosphorus
- T Operating temperature
- $\Phi_m$  Metal work function
- $\Phi_p$  Barrier potential
- Ec Conduction band energy
- Ev Valence band energy
- $E_{F,m} \hspace{0.5cm} \text{Femi energy level of metal} \\$
- E<sub>vac</sub> Vacuum energy level
- $E_{F,p}$  Femi energy level of p-type semiconductor
- J Current density
- A\* Richardson's constant

- m\* Effective mass of carrier
- h Planck's constant which is  $6.626 \times 10^{-34} \text{ Js}$

#### **CHAPTER 1**

#### INTRODUCTION

#### 1.1 Motivation

Energy consumption has become the essential part of human everyday life. Our modern societies are driven by telecommunication systems, transportation systems and electrical systems, all of which require some forms of energy to run. In fact electricity is a kind of energy that is very versatile. Several natural resources such as oil, natural gas and nuclear reactions are used to create electrical energy. But these resources are limited and the production of electricity yields CO<sub>2</sub> emission, which contributes to global warming and climate change. The International Energy Agency (IEA) estimates the global electricity demand to rise over 70% from 16,400 terawatt-hours per year (TWh/year) in 2007 to 29,000 TWh/year in 2030. [1,2] Moreover, IEA estimates CO<sub>2</sub> emission due to electricity production to increase by 40% from 28 gigatonnes per year (Gt/year) in 2007 to 40 Gt/year in 2030. [1,2] As a result, efficient energy management and reduction of environmental impact are major concerns for the sustainable development of all countries across the globe.

To handle the issues of rising demands of energy while keeping the environmental impact minimal, engineers and scientists have begun to find ways to improve the efficiency of electronic devices. Silicon has been the well-known material and it is the material used in most appliances for control of electrical systems. However, it dissipates energy, so it does not handle high power levels efficiently. Plus, its physical properties have limits beyond which it cannot operate at high temperature and high power due to the material's

breakdown. Therefore, the field of power electronics for many applications is now shifting to wide bandgap semiconductors such as gallium nitride (GaN), silicon carbide (SiC) and diamond, which possess better electrical properties than silicon. The comparison of material properties between diamond and other semiconductors are shown in table 1.1. Among several wide bandgap materials, diamond has the most exceptional properties. This is due to its superior physical and electrical properties such as wide bandgap (5.5 eV) and high thermal conductivity (20W/cm K), which is useful for electronic devices operating at high power levels [3]. Moreover, diamond possesses a high electric breakdown field of up to 10 MV/cm and high carrier mobilities (4500 cm²/V·s for electrons and 3800 cm²/V·s for holes at room temperature) allowing diamond to be a potential choice for high frequency and high voltage electronic devices.

| Property  | Si   | GaAs | 4H-SiC | GaN  | Diamond |
|---|------|------|--------|------|---------|
| Bandgap Energy, Eg (eV)                           | 1.1  | 1.4  | 3.2    | 3.4  | 5.45    |
| Electric Breakdown Field, E <sub>c</sub> (MV/cm)  | 0.3  | 0.4  | 3      | 5    | 20      |
| Electron Mobility, $\mu_n$ (cm <sup>2</sup> /V·s) | 1450 | 8500 | 900    | 2000 | 4500    |
| Hole Mobility, $\mu_p$ (cm <sup>2</sup> /V·s)     | 480  | 400  | 120    | 200  | 3800    |
| Thermal Conductivity, κ (W/cm·K)                  | 1.5  | 0.55 | 3.7    | 1.3  | 24      |

Table 1.1: Basic Bulk Properties of Diamond Compared to Si, GaAs, 4H-SiC and GaN at 300K [4, 5, 6]

Being a new material, unlike silicon, diamond-based devices are mostly still at the research and development stage in Japan, Europe and the US. The recent progresses in diamond growth, doping, surface treatment, and etching has allowed scientists and engineers to fabricate diamond electronic devices. [7,8] Both fabrication processes and device designs are the keys for achieving efficient high-power diamond electronics. A computer-based semiconductor device simulator is an efficient tool for exploring the

possible and best designs of single-crystal diamond devices that are suitable for high power and high temperature applications. The design process can be less expensive and more efficient by using the simulator to come up with the best design that meets the requirements. Then the structure of the device can be fabricated according to the design the simulator yields. Medici is the commercialized semiconductor device simulation software that is available at Michigan State University and is the simulator used throughout this study [9].

## 1.2 Research Objectives

Since single-crystal diamond is not a traditional semiconductor, many of its physical material parameters are not readily available in Medici as is the case for other well-known semiconductors such as silicon. So the objective of this study is to gather diamond parameters and use them to simulate various diode structures. They are listed as follows:

- 1. To develop a complete set of material parameters for single-crystal diamond, which include the effects of incomplete ionization, carrier mobility temperature and impurity scattering dependence, and impact ionization, for the simulator.
- 2. To simulate various structures of diamond diodes including Schottky diodes, PN-junction diodes and merged diodes.
- 3. To investigate the simulation results in details for both the forward-bias and reversebias mechanisms through the analysis of the IV characteristic, on-resistance and breakdown field versus device dimension and temperature.
- 4. To compare simulation results with existing experimental data that has been obtained in our research group.

## 1.3 Outline of Dissertation

The layout of this research is described as follows. Following the brief introduction of the need for diamond-based electronic devices, the theory of diodes and the state of the art of diamond diodes as found in the literature are discussed in chapter 2. In chapter 3, physical parameters of diamond for Medici simulations have been compiled. These include the bulk properties, incomplete ionization, impact ionization, mobility models and values from Hall measurements. The design and simulation of Schottky diamond diodes are presented in chapter 4. The effect of ohmic current and space-charge-limited current is studied in the forward bias. Avalanche breakdown is studied in the reverse bias. Chapter 5 presents the simulations of three different diode structures, which are Schottky, PN-junction and merged. Performance is compared between different diode structures and with existing experimental data. The summary of the work done in this research is presented in chapter 6.

#### CHAPTER 2

## CURRENT STATE OF THE ART OF HIGH POWER DIAMOND DEVICES

A brief overview of diodes in general is presented below followed by the challenges in making diamond diodes and a literature review of diamond-based power electronic devices.

## 2.1 Theory of Diodes

A diode is a two-terminal electronic device, which allows current to pass through one direction while blocking current from flowing in the opposite direction. The sign convention and symbol of a diode is shown in figure 2.1a. The I-V characteristic of an ideal diode is displayed in figure 2.1b, while figure 2.1c exemplifies the non-ideal case.

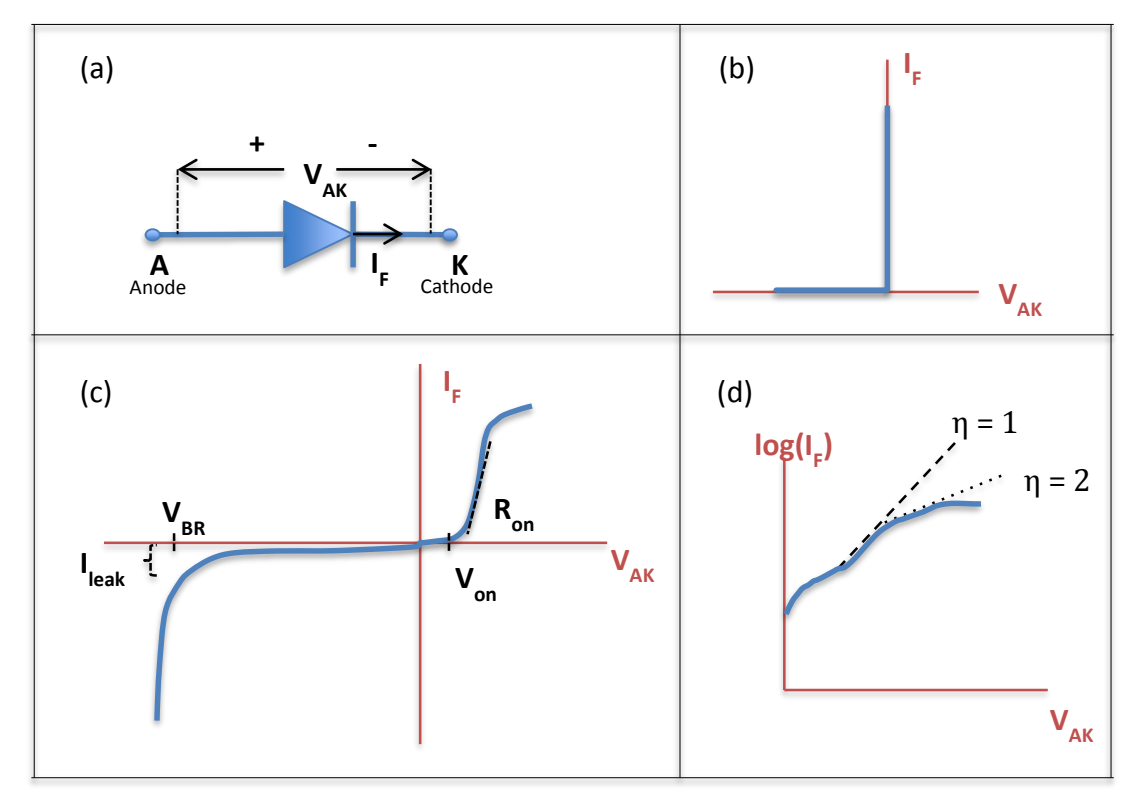


Figure 2.1: (a) Sign convention of a diode; (b) Ideal diode I-V characteristic; (c) Non-ideal diode I-V characteristic; (d) Forward current and ideality factor, η

The specific on-state resistance ( $R_{on,sp}$ ) is the combination of the resistance along the current flow path including all the interfaces when the diode is conducting current in the forward bias multiplied by the surface area of the current flow. So the unit is  $\Omega$ -cm<sup>2</sup>. As shown in the *figure 1a*,  $V_{AK}$  is the voltage drop across a diode and  $I_F$  is the current through a diode in forward bias. Hence,

$$R_{on,sp} = \frac{\Delta V_{AK}}{\Delta I_F} \times surface \ area \ of \ current \ flow \tag{2.1}$$

 $V_{on}$  is  $V_{AK}$  when the diode is on. The breakdown voltage or  $V_{BR}$  is where the magnitude of the current starts to increase indefinitely in the reverse bias. The leakage current,  $I_{leak}$ , is the current in the reverse bias direction before breakdown occurs and typically very small ( $\sim nA$  range). It is the result of an increase in generation current as the

reverse bias is increased. Figure 2.1d depicts the ideality factor,  $\eta$ , which entails the process that the current is being injected at a certain  $V_{AK}$  in the forward direction. Usually  $\eta$  is between 1 and 2. It tends towards 1 when diffusion current dominates. When recombination current dominates,  $\eta$  tends towards 2.

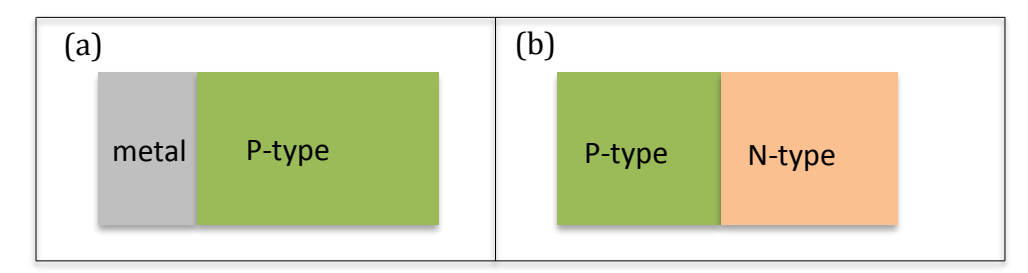


Figure 2.2: Schematics of (a) a Schottky diode and (b) a PN-junction diode

Two common types of semiconductor diodes are the Schottky diodes and PN-junction diodes. The Schottky diode, shown in figure 2.2(a), is formed when a metal-to-semiconductor interface is created. It is considered a majority carrier device where the depletion region is only formed on the semiconductor side. This results in smaller turn-on voltage  $(V_{on})$  and hence performs generally well in the forward-bias direction. The PN-junction diode, shown in figure 2.2(b), has a semiconductor-to-semiconductor interface. It is when two types (n and p) of semiconductors are brought together. It is a minority carrier device and the depletion width extends on both sides of semiconductor junction. It has higher  $V_{on}$  and also larger  $V_{BR}$ . Therefore, the PN-junction diode generally performs better in the reverse bias. These comparisons are exemplified in the I-V plot in figure 2.3.

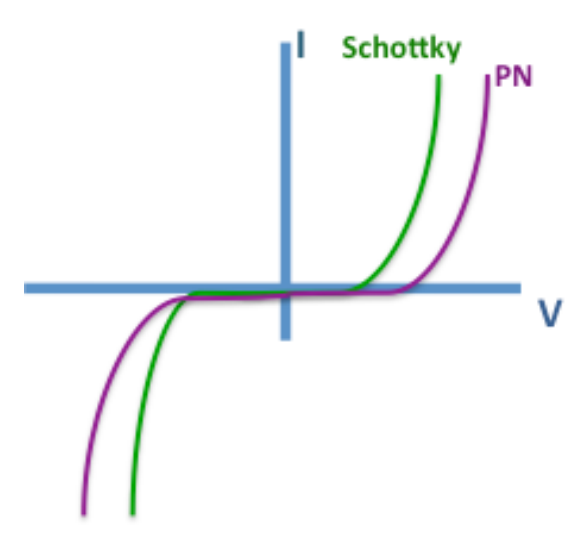


Figure 2.3: Comparison of I-V characteristic of Schottky and PN-junction diodes

## 2.2 Challenges of Diamond Diodes

Diamond is an allotropic form of carbon. Strong covalent  $sp^3$  bonds hold the tetrahedral arrangement of carbon atoms that crystallizes into the diamond lattice, which is a variation of the face centered cubic structure. Diamond diodes are expected to out perform diodes fabricated from Si, SiC or GaN because of the more superior bulk properties of diamond. Among all the other existing semiconductors, diamond has the widest bandgap, which affords diamond devices to have greater  $V_{BR}$  allowing for greater blocking voltage capability and subsequently the ability to function in high power circuits. It also has better thermal conductivity, which provides diamond devices with greater heat sink capability. Thus, it will be able to operate at very high temperatures.

Previously reported challenges in fabricating diamond diodes involve the difficulty to synthesize large, high-quality, single-crystal diamond, as well as, to make the n-type and p-type doping layers that are good quality with low resistance. Nowadays, two types of diamond substrates are available in the market. The first is created from graphite phase by the high pressure and high temperature process (HPHT). The second is created from the

gaseous phase under low pressure in a chemical vapor deposition process (CVD). A substrate size of  $3x3 \text{ mm}^2$  with (100) top surface orientation is commonly available in the market.

The most important donors (phosphorus) and acceptors (boron) in diamond have large activation energies. Nevertheless, p-type doping by boron as an acceptor with activation energy of 0.37 eV has been quite well controlled. [10] N-type doping still needs more research to make it efficient. Thus this has restrained the design fabrication of the diamond-based devices to be mostly unipolar p-type devices. The deep donors and acceptors of diamond along with the wide bandgap lead to incomplete ionization of the donors and acceptors at room temperature. At very high temperature, ionization of carriers becomes more complete. Higher impurity concentration, which will improve conductivity, may be necessary for diamond devices that operate at room temperature. At high doping levels, the carriers flow by a hopping conduction between dopant sites as the current flow mechanism.

In terms of device design, some physical parameters of diamond are not well known. Updated values of diamond parameters are also not readily embedded in Medici, the device simulator. Although most of the bulk properties of diamond have been well studied, some parameters for charged carrier mobility and impact ionization rate model have been interpolated from the values of other semiconductors including silicon and silicon carbide. [11] This causes the simulation to yield inaccurate results. Thus, the design in question will not represent the expected performance of the fabricated device precisely.

#### 2.3 Literature Review

Several types of diamond devices such as Schottky diodes and field effect transistors (FETs) have been fabricated in the past decades. This section highlights some technological breakthroughs that several research groups have made on the fabrication of diamond-based power devices and their performances.

In 2001, diamond PN junctions were successfully fabricated for the first time. [12] This achievement is a result of successfully creating n-type diamond by phosphorus doping. Nevertheless, the n-type diamond presented quite high resistivity of about  $10^5$  -  $10^6 \Omega$ -cm at phosphorous concentrations of 10<sup>18</sup> cm<sup>-3</sup>. This causes the R<sub>on</sub> for PN-junction diode to be too high, which is not good for fast switching and high power diodes. In the literature, the state-of-the-art of p-type diamond is more advanced than the n-type. [3] Specific contact resistance,  $\rho_c$ , is an area-independent parameter and includes a part of metal immediately above the contact and semiconductor below it. Experimentally, it can be defined from an I-V measurement by taking the reciprocal of the slope when the voltage tends to zero (since the voltage required to drive current through a good ohmic contact is small) and the unit is  $\Omega$ -cm<sup>2</sup>. The specific contact resistance is as low as  $10^{-5}$   $\Omega$ -cm<sup>2</sup> for p-type diamond with boron concentration of 10<sup>20</sup> cm<sup>-3</sup>. For n-type diamond with phosphorus concentration of  $10^{20}$  cm<sup>-3</sup>, the specific contact resistance is reported to be around 14  $\Omega$ -cm<sup>2</sup>. [13] Therefore, using just p-type diamond to create Schottky diodes have advantages such as lower built-in voltage and faster turn-on/turn-off properties than those of PN diodes.

In 2004, a group of researchers led by D. J. Twitchen and A. J. Whitehead reported successful results of their high-voltage single-crystal Schottky diamond diode. [14] This diode was implemented with a vertical structure and designed to be a unipolar device and

is favorable to achieve large operating input currents. The intrinsic layer serves as the drift region in the forward conduction and depletion region in the reverse bias. Due to its thin thickness, space charge limited current was observed. The result shows that  $V_{BR}$  was - 2.5kV. The electric field was 4 MV/cm. The hole mobility was measured to be 4100  $\pm$ 400 cm<sup>2</sup>/Vs.

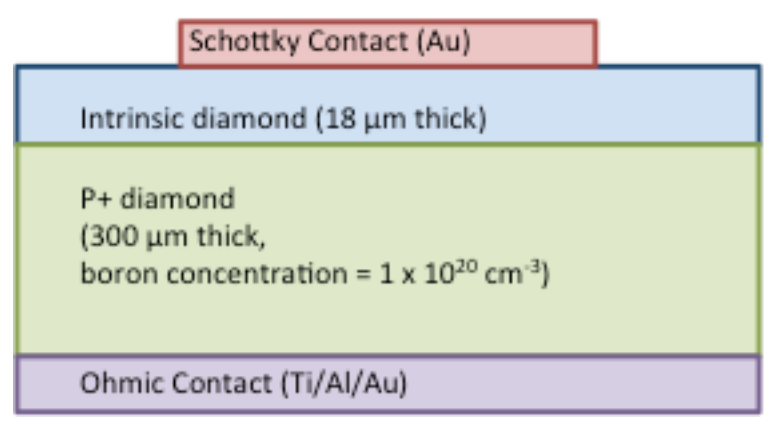


Figure 2.4: Unipolar vertical Schottky diode structure

Next, in 2007 M.Kubovic, H. El-Hajj, J.E. Butler and E. Kohn reported a merged Schottky junction and PN junction diode structure. [15] Merged diodes between PN junction and Schottky junction are composed of small size Schottky contacts embedded into the PN junction. Schottky contact contributes to a low forward threshold voltage since the metal-semiconductor junction results in a lower barrier in the forward bias. However, the Schottky barrier on the reverse bias gives high current leakage and low breakdown voltage. Therefore, a PN junction, which has a low reverse leakage current and a high breakdown voltage on reverse bias was implemented. The merging the two kinds of junctions together yielded a better performance in both forward and reverse biases. Thus, a PN junction is placed next to a Schottky barrier on that same contact in order to create a merged structure as shown in figure 2.5.

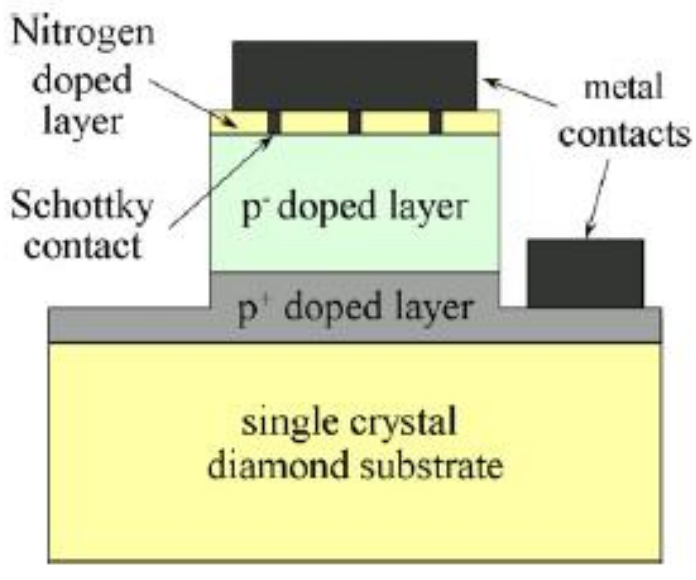


Figure 2.5: Structure of the merged diode [15]

The IV characteristics of the PN junction diode (taken before the Schottky contacts were patterned) and the merged diode (taken after the Schottky contact areas were patterned) are shown in figure 2.6. This was measured from a diode with a diameter of 100  $\mu$ m (diameter of the p<sup>-</sup> layer). The results show improvements of the merged diodes over those with just PN junction diodes.

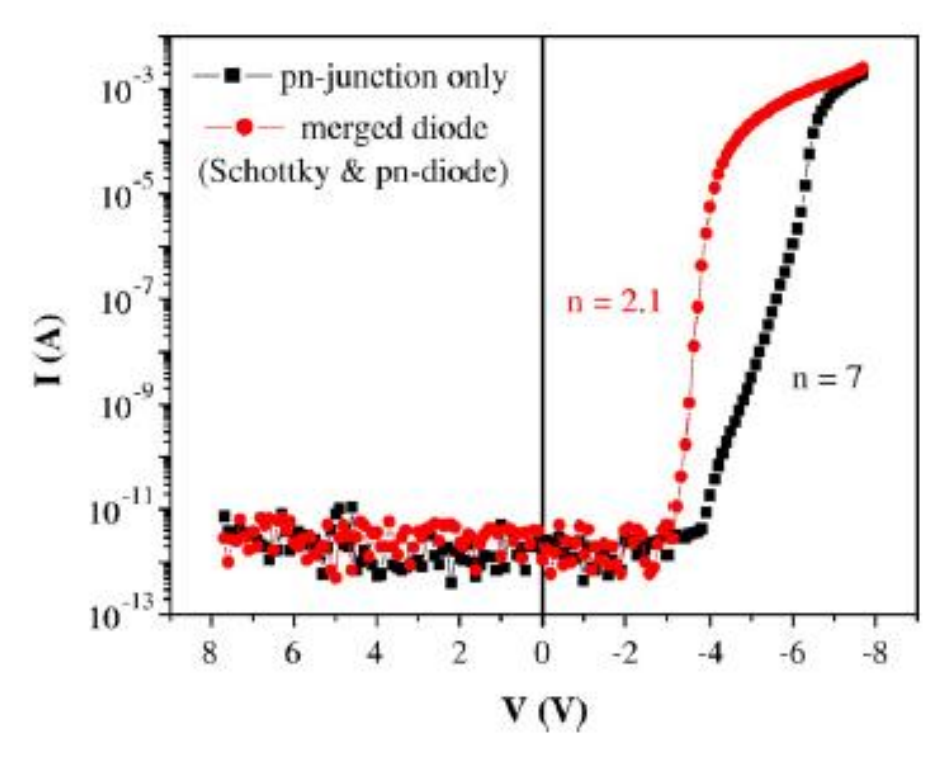


Figure 2.6: IV Characteristic of PN-junction diode and merged diode (from 100-µm diameter diode) [15]

In the range of ±8V, both diodes exemplified a high current rectification ratio of about 10°. The ideality factor in the forward for the merged diode is 2.1 and for the PN junction is 7. In the ideal case, the ideality factory is 1 resulting from zero defects and that the total diode current is diffusion current. More defects give more space-charge recombination, which increases the ideality factor. The ideality factor of 7 for the PN junction diodes indicated that there was current injection in the forward direction by defect states at the interface. The merged diode yielded an improved ideality factor of 2, indicating fewer defects at the interface. Additionally, figure 7 also confirms that the forward turn-on voltage for the PN junction diode is higher than that of the merged. Thus the merged diode outperformed the PN junction diode in both ideality factory as well as turn-on voltage. Additionally, the breakdown voltage is reported to be approximately -25 V,

which corresponds to a breakdown field of 2.5 MV/cm. This measured value of breakdown voltage is lower because of the thinner drift layer (p<sup>-</sup> doped region) than the design by another research group that achieve the blocking voltages in the kV range. [15]

Thus far, the fabricated merged diode utilizes the better characteristics of a Schottky diode in forward bias, and the PN junction behavior in reverse bias. However, this diode still has a trade-off relationship between  $R_{on}$  and  $V_{BR}$  shown in equation 2.2. In order to decrease the  $R_{on}$ , it is needed to decrease the resistance of the p-type layer. This can be done by increasing the acceptor concentration or decreasing the p-type layer thickness. [7,8] However, this induces narrowing of the space-charge layer width of the p-type layer causing  $V_{BR}$  to decrease [12]

$$\frac{V_{BR}}{R_{on.sp}} = \frac{1}{2} q E_{max} \mu_p p \tag{2.2}$$

where  $E_{max}$  = peak electric field at breakdown,  $\mu_p$  = hole mobility, p = hole concentration in the drift layer.

In order to overcome the trade-off relationship between R<sub>on</sub> and V<sub>BR</sub> of the merged diode, Makino and his team of scientists in Tsukuba and Kanazawa Japan have published a paper on a merged diode without any trade-off relationship between R<sub>on</sub> and V<sub>BR</sub>. [12] They referred to their new design as the Schottky-PN diode (SPND), which is composed of a lightly phosphorus-doped n-type layer placed in between highly boron-doped p-type layer and Schottky metal layer. [12] This structure is similar to the merged diode in [15], but the difference is the PN junctions were formed tandem to the Schottky junctions instead of the PN junctions being embedded in the Schottky. The n-type layer, which is the key structure of the SPND, was designed to be fully depleted in both forward and reverse operations.

Thus, only the width of the n-type layer determines  $V_{BR}$  of the diode. In addition, the forward current and  $R_{on}$  are controlled only by the resistivity in the p-type layer. Essentially, this means having a highly boron-doped p-layer, which will give low resistivity or low  $R_{on}$  and thus high forward current. It also means having a wide n-type layer to have high  $V_{BR}$  as long as the layer is fully depleted. Therefore  $R_{on}$  and  $V_{BR}$  can be designed independently as they are determined by different device parameters. [12]

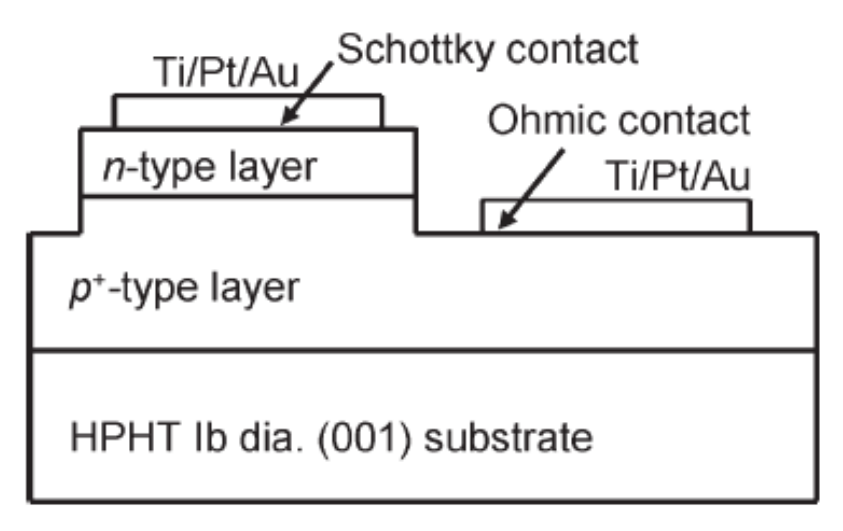


Figure 2.7: Structure of the SPND diamond diode [12]

The thickness and doping concentration of each layer are as follows:  $N_A = 4x10^{20}$  cm<sup>-3</sup> and 1.3 microns for p<sup>+</sup> layer;  $N_A = 6x10^{18}$  cm<sup>-3</sup> and 700nm for p layer; and  $N_D = 7x10^{16}$  cm<sup>-3</sup> and 70nm for n-layer. SPND showed an improved result and reached over 60,000 A/cm<sup>2</sup> with specific on resistance of 0.03 m $\Omega$ cm<sup>2</sup> at the forward bias of 6V. This is comparable to the estimation from the bulk resistivity of the p+ layer (about 5 m $\Omega$ cm<sup>2</sup>). The author noted the important part that the high resistance of the n-type layer (in the order of  $10^2 \Omega$ cm<sup>2</sup>) does not affect the total value of the series resistance of the SPND, which is consistent to the analysis of the operation mechanisms. [12] V<sub>BR</sub> was measured to be 55 V at which the

electric field reached 3.4 MV/cm. The authors elucidated that the higher  $V_{BR}$  was a result of the larger width in the n layer as described by the operational mechanism. Although, it is worth mentioning that n-type doping is still a great challenge nowadays. Thus creating thicker layer of n-type doping puts the limit on the value of  $V_{BR}$  this design tries to achieve.

In 2014, Umezawa and his coworkers at National Institute of Advanced Industrial Science and Technology and Osaka University, demonstrated a vertical-structured high current diamond Schottky diode using a thick Al<sub>2</sub>O<sub>3</sub> field plate as the edge termination technique to reduce large field crowding at Schottky contacts. [16] The structure is shown in figure 2.8.

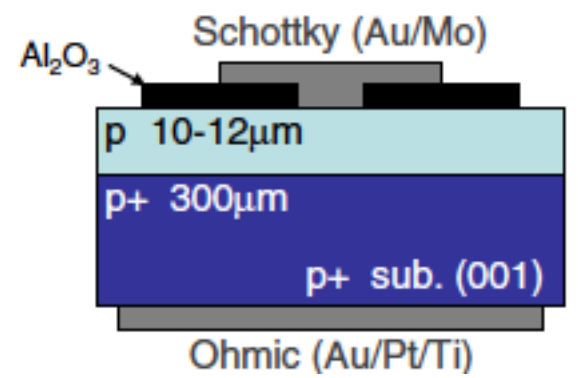


Figure 2.8: Structure of Schottky diode with field plates [16]

The thickness of the  $Al_2O_3$  field plate is 1.8 um. The estimated effective Schottky barrier height was 1.85 eV. The maximum forward currents reached 1 A at 2.4 V and 5 A at 7.3 V. The specific on-resistance was 29.2 m $\Omega$ -cm $^2$  at RT. The maximal blocking voltage of 300 V with the breakdown field of 0.3 MV/cm reported.

Apart from many diamond diode structures previously discussed, many designs and fabrication schemes for diamond FET's have been presented in the literature. The performance of diamond FET's is aimed at high frequency to utilize the higher carrier

mobilities of the bulk material. A few groups have studied the delta doping technique for the p-type layer. This is when boron concentration is heavily doped near the surface to allow for a full activation at room temperature. [17,18]

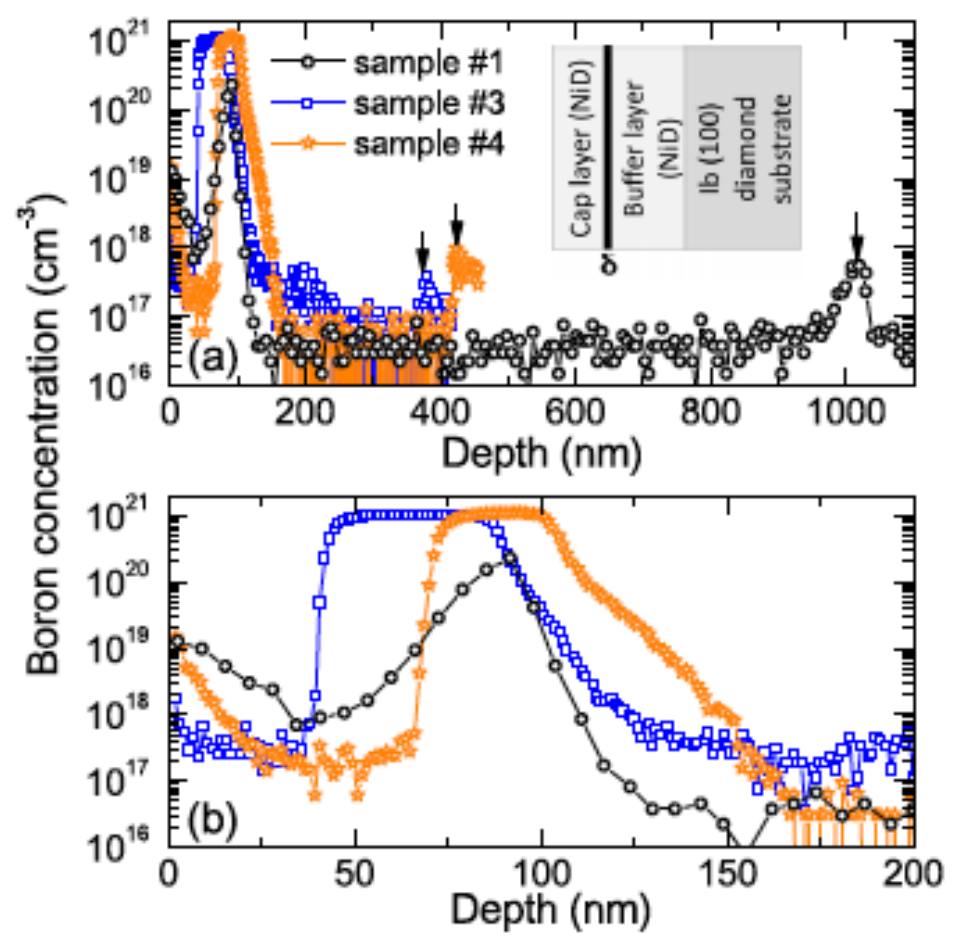


Figure 2.9: Measurement of boron concentration versus device distance from delta doping technique [17, 18]

Kuech et al presented a metal-semiconductor FET (MESFET) structure which incorporated delta doping technique for the p-layer is shown in figure 2.10. [19]

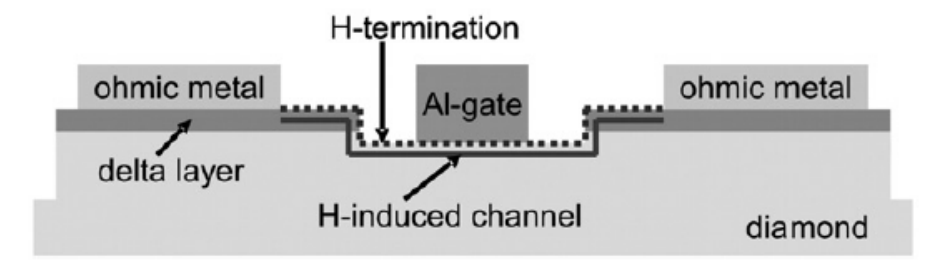


Figure 2.10: Diamond MESFET structure [19]

The point worth mentioning is that the ohmic contacts for this MESFET by treating the surface with oxygen (O-termination) followed by the deposition of Au. In most practice, Ohmic contacts on diamond are formed by Ti/Au. Ohmic contacts are done by treating the surface with hydrogen (H-termination) immediately followed by Au sputtering or evaporation are the less popular method. The H-termination induces a hole conductive channel near the surface and in cooperation with Au, the work function difference is low at the interface resulting a tunneling path. However, the adhesion of Au to the H-terminated diamond surface relies on the van der Waals bonding and is considered weak. The covalent bonding yields stronger adhesion. Nevertheless, this delta-doping technique of boron yielded low hole mobility at room temperature. The hole mobility less than 100 cm²/V-s was measured, so it was not a good device for high frequency operation. [18]

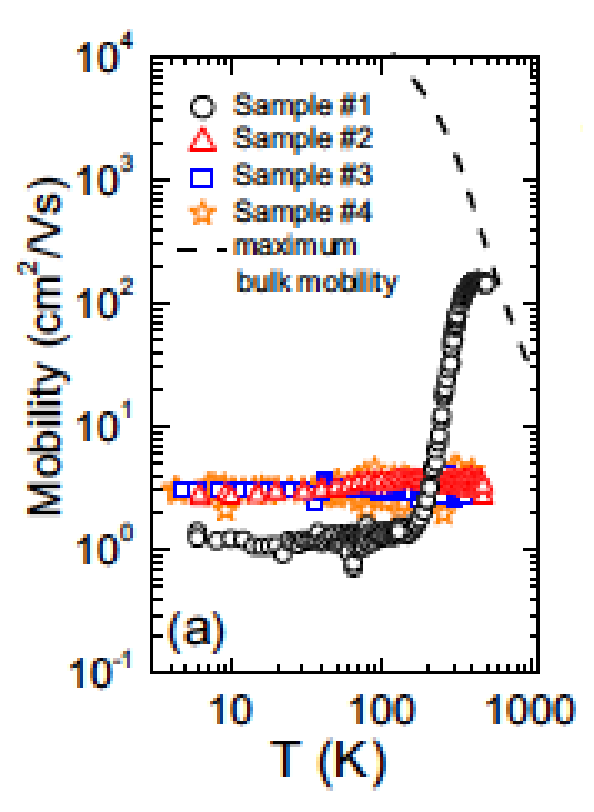


Figure 2.11: Mobility measurement of delta doping diamond MESFET [19]

With the goal of improving hole mobility, H-termination was used instead of delta doping technique. In 2014, Kawarada et al demonstrated H-terminated diamond FET with an oxide layer of Al<sub>2</sub>O<sub>3</sub> that was capable to operate at 500 V, 400 C and 40 GHz. [20] Normally, the C-H bonds created by H-termination are lost when the temperature goes beyond 200 C, but the technique to use atomic layer deposition (ALD) of Al<sub>2</sub>O<sub>3</sub> in this case prevents the bonds from being destroyed at very high temperature.

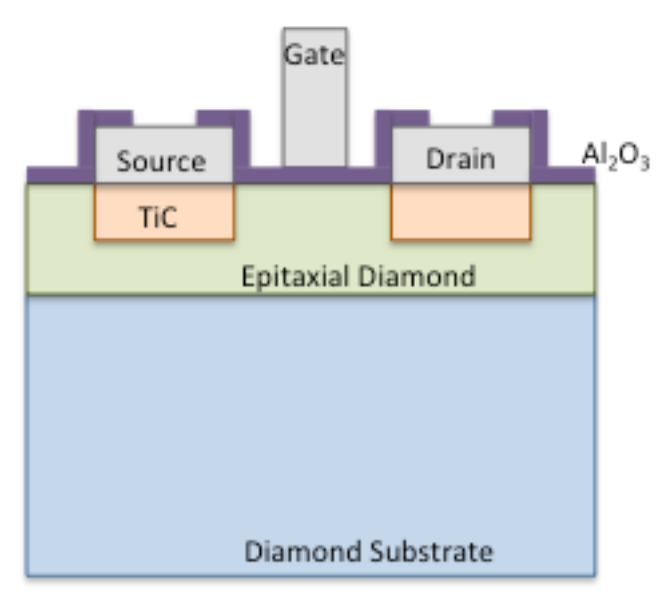


Figure 2.22: Structure of H-terminated diamond MISFET

Also in 2014, a researcher group from collaboration across Japan has fabricated a diamond MISFET. [21] The group intended to utilize the gate insulator to suppress the leakage current and increase the breakdown voltage. H-terminated diamond surface was the chosen technique over delta doping in this study due to the difficulty to control the abruptness of the doping profile [22]. Ta<sub>2</sub>O<sub>5</sub> was the insulator chosen because it has high k value, larger than 20, on diamond. An insulator with high k value can provide the same charge response at a smaller electric field [23]. A thin layer of Al<sub>2</sub>O<sub>3</sub> is used to prevent damage to the diamond surface when Ta<sub>2</sub>O<sub>5</sub> is sputtered onto hydrogenated diamond surface. The electrode contacts for gate, drain and source are identical and are composed of 200 nm Au, 20 nm Ti and 10 nm Pd. The structure is shown in figure 2.23.

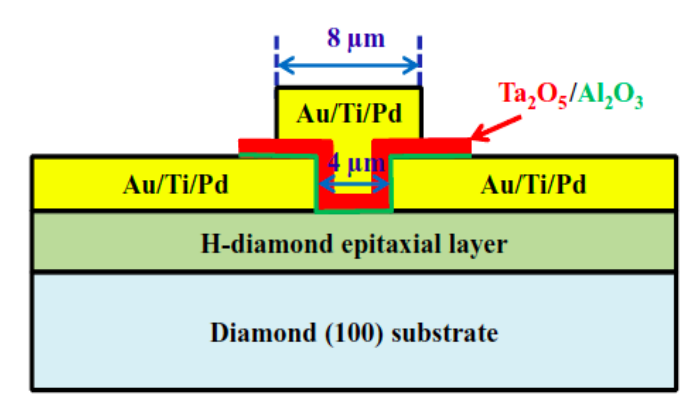


Figure 2.23: Proposed MISFET structure [21]

For the channel length ( $L_G$ ) of 4 um, the maximal  $I_{DS}$  is 97.7 mA/mm shown in figure 2.23. This research group is satisfied with  $Ta_2O_5$  as the choice of insulator since they acquired the largest  $I_{DS}$  value for diamond MISFET to date.

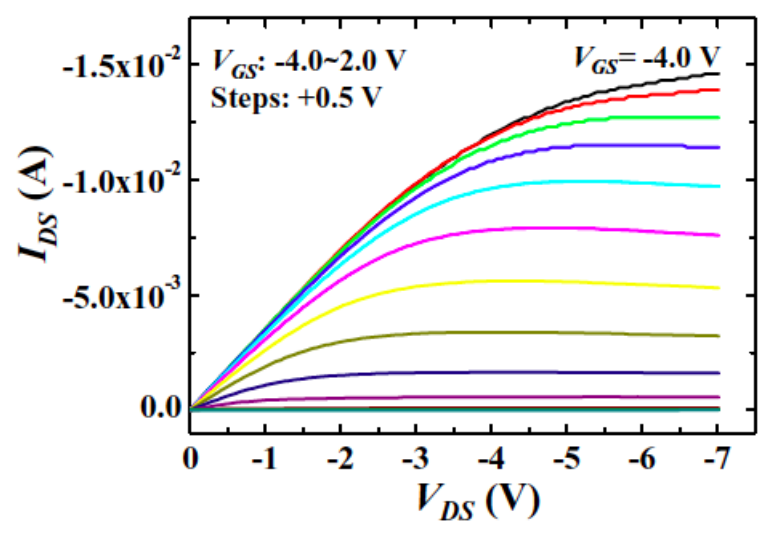


Figure 2.23: MISFET I<sub>D</sub>-V<sub>DS</sub> performance [25]

Through the discussion of several diamond-based devices in this section, the keys to achieve successful performance include advancement in diamond synthesis and doping, having good fabrication schemes and techniques, and having the right structural design.

The focus of this research is in the design. The next chapter will present the tool, which will allow device structures to be simulated and designed.

#### CHAPTER 3

# SINGLE-CRYSTAL DIAMOND MATERIAL MODELS AND PARAMETERS FOR SEMICONDUCTOR DEVICE SIMULATION

This chapter introduces the semiconductor simulator software that was used in this study. Then it presents physical models for material parameters of single-crystal diamond.

#### 3.1 Medici Device Simulator

Medici<sup>TM</sup> is an industry-standard semiconductor device simulation tool that predicts electrical, thermal and optical characteristics of arbitrary 2-D structures under user-specified operating conditions. A wide variety of devices can be modeled in 1-D and 2-D such as pn-diodes, BJTs and MOSFETs. Medici allows device designs to be optimized for best performance without having to go through the entire process of fabrication, which eliminates the need for costly experiments. Furthermore, it assists the fabrication methods in helping to verify experimental results.

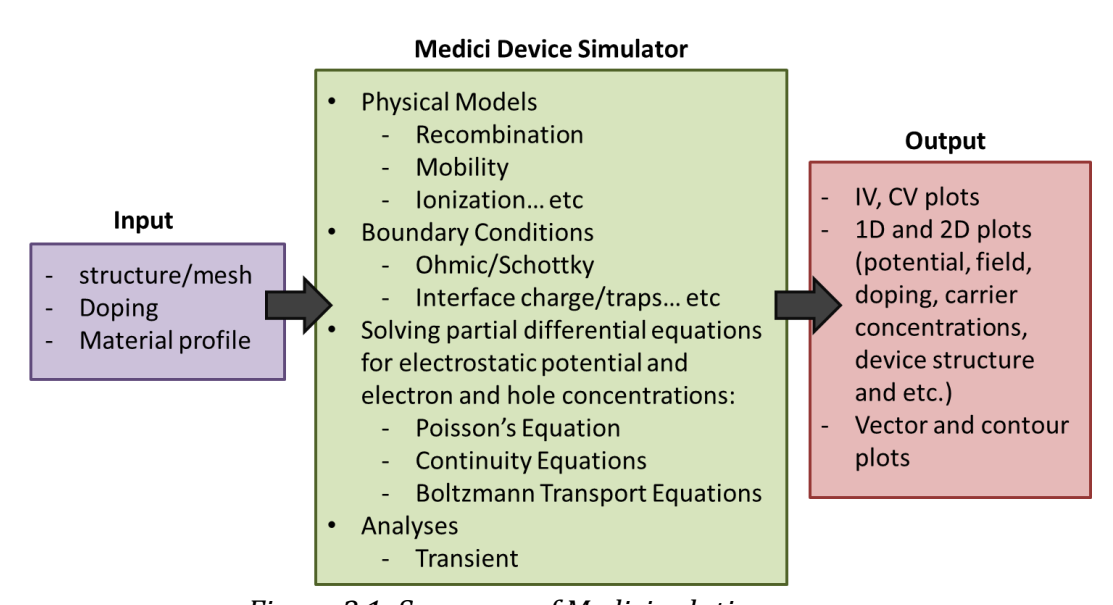


Figure 3.1: Summary of Medici solution process

To analyze a device, five basic equations are solved numerically in Medici. These equations are as follows:

Poisson's equation:

$$\varepsilon \nabla^2 \psi = -q(p - n + N_D^+ - N_A^-) - \rho_s \tag{3.1}$$

This governs the electrical behavior of semiconductor devices.

Continuity equations for electrons and holes:

$$\frac{\partial n}{\partial t} = \frac{1}{q} \overrightarrow{\nabla} \cdot \overrightarrow{J_n} - (U_n - G_n) = F_n(\psi, n, p)$$
(3.2)

$$\frac{\partial p}{\partial t} = \frac{1}{q} \vec{\nabla} \cdot \vec{J_p} - (U_p - G_p) = F_p(\psi, n, p)$$
(3.3)

These also govern the electrical behavior of semiconductor devices.

• Electron and hole transport equations:

$$\overrightarrow{J_n} = -q\mu_n n \overrightarrow{E_a} + q D_n \overrightarrow{\nabla} n \tag{3.4}$$

$$\overrightarrow{J_p} = -q\mu_p p \overrightarrow{E_a} + q D_p \overrightarrow{\nabla} p \tag{3.5}$$

This governs the drift and diffusion aspect of the carriers.

The definitions of the parameters in the above five equations are:

*n* is the electron concentration

p is the hole concentration

 $N_D^+$  is the ionized donor concentration

 $N_A^-$  is the ionized acceptor concentration

 $\varepsilon$  is the dielectric permittivity

 $\psi$  is the intrinsic Fermi potential

 $ho_s$  is the surface charge density

 $E_a$  is the applied field

 $F_n$  is the electron quasi-Fermi energy

 $F_p$  is the hole quasi-Fermi energy

 $\overrightarrow{J_n}$  is the electron current density vector

 $\overrightarrow{J_p}$  is the hole current density vector

 $U_n$  is the electron recombination rate

 $U_p$  is the hole recombination rate

 $\mu_n$  is the electron mobility

 $\mu_p$  is the hole mobility

 $D_n$  is the electron diffusivity

 $D_p$  is the hole diffusivity

Medici employs the finite element method to solve the 5 basic equations above such that the area of the simulated device is discretized into a simulation grid. This discretization process yields a set of coupled nonlinear algebraic equations, which are then calculated for a number of grid points with the different potentials and carrier concentrations. This set of coupled nonlinear algebraic equations must be solved by a nonlinear iteration method. There are two iteration methods available in Medici namely, the Gummel's method and the Newton's method. Regardless of which method is used, the solutions will be carried out over the entire grid until a self-consistent potential  $(\psi)$  and carrier concentrations (n, p) are achieved. Once the potential and carrier concentrations have been calculated at a given bias, it is possible to obtain the quasi-Fermi levels  $(F_n$  and  $F_p)$  and the hole and electron currents  $(\overline{J_p})$  and  $\overline{J_n}$ .

For accurate results, Medici incorporates a number of physical models such as recombination, impact ionization, bandgap narrowing, band-to-band tunneling, mobility,

Fermi-Dirac and Boltzmann statistics. [9] Arbitrary device geometries can be simulated. The user can define types of material, regions, impurity concentrations and electrodes for a specific device structure and simulation process. A summary of processes in Medici to yield a solution is shown in figure 3.1.

## 3.2 Diamond Parameters

Diamond is still new compared to other traditional semiconductors such as silicon (Si) and gallium arsenide (GaAs). Hence, its material parameters are not readily available in Medici like the others. In order to perform simulations of diamond devices, it is required that proper values of diamond parameters have been input into Medici for the accuracy of the results. Fortunately, Medici allows users to define new materials arbitrarily. The rest of this chapter discusses the models and parameters that are used for diamond throughout the Medici simulations in this project.

## 3.2.1 Bulk Properties

Since 1797 when diamond was discovered as pure carbon, many of its bulk properties were investigated and the values published. [4, 5, 6] From table 3.1, silicon carbide (SiC), gallium nitride (GaN) and diamond are considered wide bandgap semiconductors with diamond being the widest. Wide bandgap semiconductors have higher thermal stability and breakdown field compared to silicon, the most popular semiconductor. This means wide bandgap semiconductors can withstand higher field strength intrinsically without the breakdown of the material.

| Property   | Si   | GaAs | 4H-SiC | GaN  | Diamond |
|--|------|------|--------|------|---------|
| Bandgap Energy, Eg (eV)                                    | 1.1  | 1.4  | 3.2    | 3.4  | 5.47    |
| Electric Breakdown Field, Ec (MV/cm)                       | 0.3  | 0.4  | 3      | 5    | 20      |
| Electron Mobility, $\mu_n$ (cm <sup>2</sup> /V·s)          | 1450 | 8500 | 900    | 2000 | 4500    |
| Hole Mobility, $\mu_p$ (cm <sup>2</sup> /V·s)              | 480  | 400  | 120    | 200  | 3800    |
| Thermal Conductivity, к (W/cm·K)                           | 1.5  | 0.55 | 3.7    | 1.3  | 24      |
| Dielectric constant, $\epsilon_r$                          | 11.9 | 13.1 | 10.1   | 9    | 5.5     |
| Saturated Electron Drift Velocity, (x10 <sup>7</sup> cm/s) | 1    | 1    | 2      | 2.2  | 2.7     |

Table 3.1: Bulk Properties of Diamond Compared to Si, GaAs, 4H-SiC and GaN at 300K [4, 5, 6]

In terms of carrier mobilities, diamond also possesses very high values for both electrons and hole. This is beneficial for electronic devices that require fast response and operate at high frequency. Even though the electron mobility of GaAs surpasses that of diamond, the hole mobility is significantly less. So while GaAs is suitable for some high-speed electronics such as mobile phones and satellite communication, there are many other high-energy and high-temperature applications which diamond is more promising. Moreover, this is especially true for high power electronic devices that suffer from high generation of heat. Since the thermal conductivity of diamond is high, it can better conduct the heat away from the active device region of heat generation.

## 3.2.2 Incomplete Ionization Model

To make electronic devices out of diamond; it is doped so that the material is more conductive. The problem of dopant activation originates from the wide 5.45 eV bandgap of diamond and the large ionization energies of dopants in the material. Phosphorus and boron are known donor and acceptor species in diamond and exhibit activation energies of 590 and 360 meV respectively. As shown in figure 3.2, the dopant levels for n-type and p-

type diamond are rather deep which effect the thermal excitation of the carriers at room temperature. From the Pearson and Bardeen approximation, the activation energy in the freeze-out region is a function of temperature and impurity concentration. [11] The parameters and equations in [11] have been verified and plotted as shown in figure 3.3, the number of ionized impurity carriers increases with the increasing temperature. This model has been input in the subsequent Medici simulations.

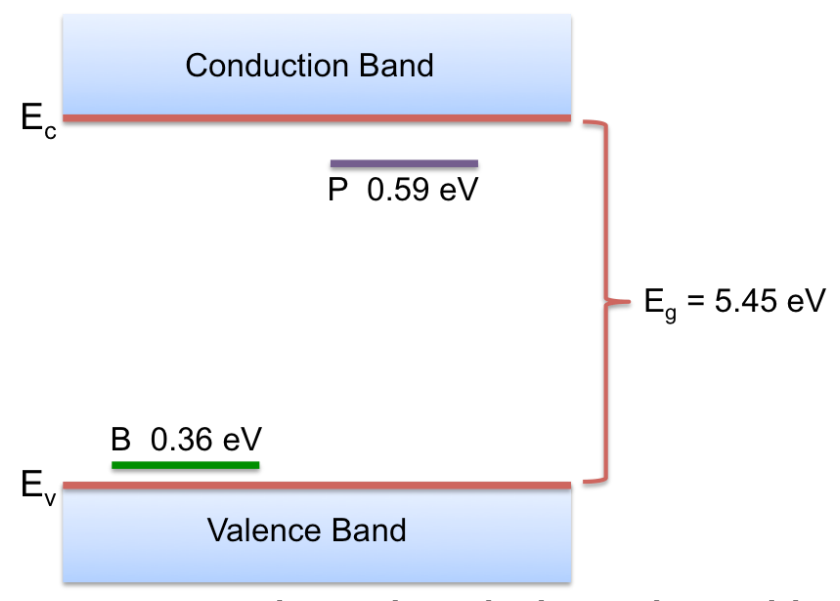


Figure 3.2: N-type and P-type dopant levels in single-crystal diamond

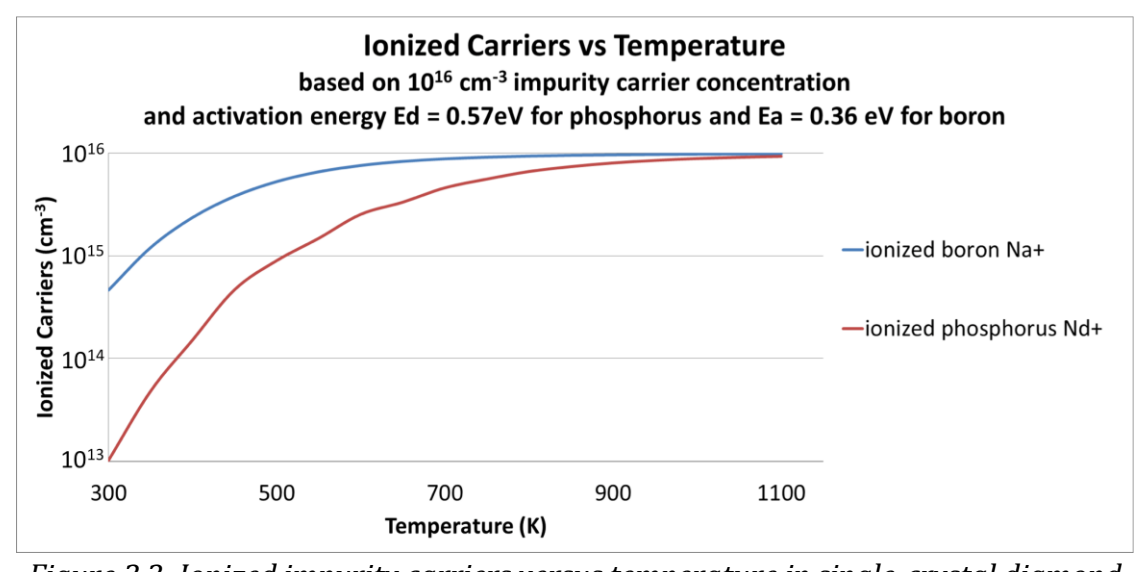


Figure 3.3: Ionized impurity carriers versus temperature in single-crystal diamond

# 3.2.3 Temperature-and-impurity-dependent Mobility Model

At the beginning of the study, the concentration dependent mobility model from [11] was implemented in Medici for the simulations (equation 3.6). However, as experimental data from the Hall measurement became available. The first model in equation 3.6 was no longer used. All of the results presented in this dissertation are based on the Hall measurement values, which were manually entered into Medici files. For completion, a brief description on the first model from [11] is given below. This model was developed from concentration-dependent Hall and time-of-flight (TOF) hole mobility values reported in [24, 25] for heavily boron-doped diamond, which yielded the following empirical expression:

$$\mu_p(N_A) = \mu_0 \exp\left(-\frac{p_c}{N_A}\right) + \frac{\mu_{max} - \mu_0}{1 + \left(\frac{N_A}{C_r}\right)^{\alpha_2}} - \frac{\mu_1}{1 + \left(\frac{C_s}{N_A}\right)^{\beta_2}}$$
(3.6)

where  $\mu_p(N_A)$  is the doping dependence mobility. The terms  $\mu_0$ ,  $\mu_1$ ,  $\mu_{max}$ ,  $p_c$ ,  $C_r$ ,  $C_s$ ,  $\alpha_2$ ,  $\beta_2$  are fitting factors obtained from the data in [26].

More recently, researchers in our group have conducted Hall measurements on several of our boron doped diamond samples grown in our lab and the results are shown in figure 3.5. [27] A tabulated data set of doping concentration and the associated hole and electron mobilities was created based on the findings in [27]. This set of data replaced the first model. The simulation results presented in the next chapters are based on this data set whose values are shown in table 3.2 below.

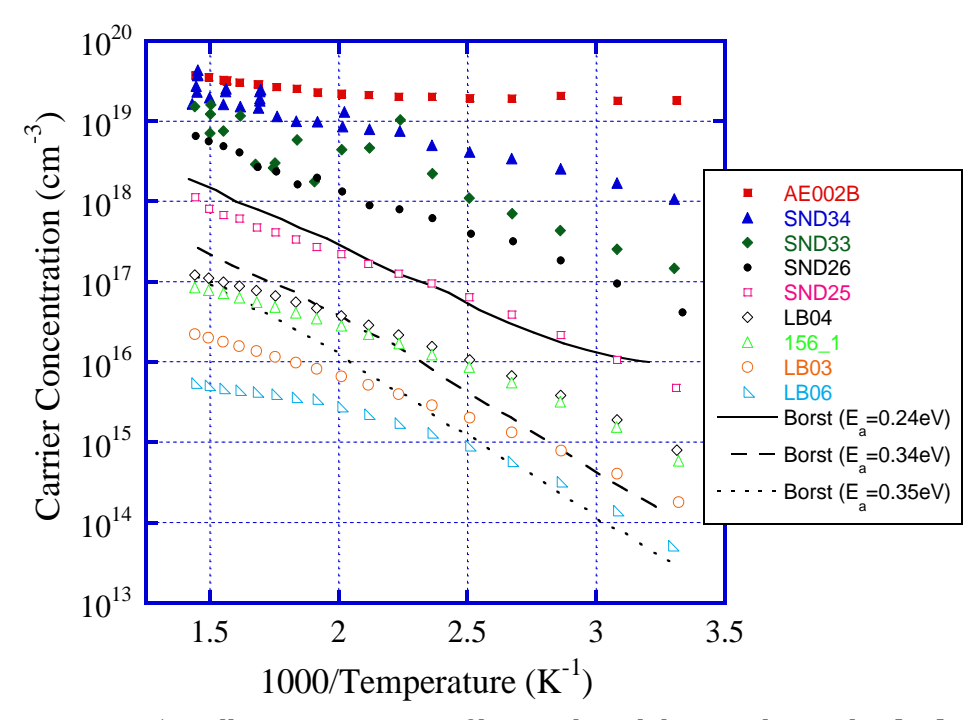


Figure 3.5: Hall measurements of boron doped diamond samples [27]

| Doping               | Hole mobilities (cm <sup>2</sup> /Vs) |       |       | Electron mobilities (cm <sup>2</sup> /Vs) |       |       |  |
|----------------------|---------------------------------------|-------|-------|---|-------|-------|--|
| (cm <sup>-3</sup> )  | 300 K                                 | 450 K | 600 K | 300 K                                     | 450 K | 600 K |  |
| 6.5x10 <sup>15</sup> | 930                                   | 310   | 130   | 540                                       | 560   | 600   |  |
| 3.1x10 <sup>16</sup> | 820                                   | 250   | 100   | 380                                       | 420   | 520   |  |
| 2.5x10 <sup>17</sup> | 800                                   | 230   | 98    | 270                                       | 300   | 490   |  |
| 6x10 <sup>18</sup>   | 150                                   | 90    | 56    | 120                                       | 180   | 475   |  |
| 2x10 <sup>20</sup>   | 39                                    | 32    | 24    | 8   | 140   | 470   |  |

Table 3.2: Hall Mobility Data Obtained from Hall Measurement of the Actual Diamond Samples Grown in MSU Lab [27]

#### 3.2.4 Impact Ionization Model

Impact ionization is a process that occurs in high electric fields. It is an important phenomenon for power device design as it governs the breakdown voltage ( $V_{BR}$ ) of the device. When energetic particles scatter due to a high electric field, this gives excess energy and allows some electrons to be excited into the conduction band. As a result, new electron-hole pairs are created. This process can occur when the particles gain at least the threshold energy for ionization ( $E_i$ ) from the electric field. The impact ionization rates  $\alpha_p$  (for holes) and  $\alpha_n$  (for electrons) are defined as the number of electron-hole pairs generated by the carriers traveling unit distance along the direction of electric field. Empirically, the impact ionization rates can be shown [28, 29] as follows:

$$\alpha_{n,p} = A_{n,p} exp\left(-\frac{B_{n,p}}{E}\right)^{c_{n,p}} \tag{3.7}$$

 $A_{n,p}$ ,  $B_{n,p}$  and  $c_{n,p}$  are fitting parameters and E is the electric field through the semiconductor layer [5]. The fitting parameters are  $A_n$ =4.62x10<sup>5</sup>,  $B_n$ =7.59x10<sup>6</sup>,  $C_n$ =1.0,  $A_p$ =1.93x10<sup>5</sup>,  $B_p$ =4.41x10<sup>6</sup>, and  $C_p$ =1.0. [34]

When impact ionization happens in high electric field region, it can free bound electrons, which also accelerate to velocities that can liberate additional electrons during collisions of particles. This process is called avalanche breakdown at which point the current in a semiconductor will become extremely high [33]. It is crucial to determine  $V_{BR}$  to approximately quantify the blocking capability of diamond power devices in reverse bias. Thus, this model is also included in the Medici simulations.

#### 3.2.5 Metal Contacts to Diamond

Ohmic and Schottky contact are implemented as simple Dirichlet boundary conditions [9]. Medici calculates the surface potential,  $\psi_s$ , at the metal-semiconductor interface by the following equation:

$$\psi_s = \chi_{semi} + \frac{E_g}{2q} + \frac{kT}{2q} \ln\left(\frac{N_c}{N_v}\right) - WORKFUNC + V_{applied}$$
 (3.8)

where  $E_g$  is the bandgap energy,  $\chi_{semi}$  is the electron affinity of the semiconductor,  $N_c$  and  $N_v$  are the electron and hole density of state, respectively, and WORKFUNC is the value of the metal work function used at the contact. All of these values are listed in table 3.3 for diamond. The temperature, T, and the applied voltage,  $V_{applied}$ , in equation 3.8 are the values that can be specified for each simulation. The constant values for the electron charge is  $q = 1.6 \times 10^{-19}$  C and Boltzmann constant  $k = 8.62 \times 10^{-5}$  eV/K.

# 3.3 Summary of Diamond Parameters for the Simulations in this Study

All of the diamond physical parameters that were used in the simulations in this study are listed in table 3.3.

| Diamond Parameters                    | Symbols in | Symbols in        | Values                   | Units            |
|---------------------------------------|------------|-------------------|--------------------------|------------------|
|                                       | Medici     | Dissertation      |                          |                  |
| Bandgap at Room Temperature           | EG300      | Eg                | 5.47                     | eV               |
| Relative Permittivity                 | PERMITTI   | ε                 | 5.7                      |                  |
| Affinity                              | AFFINITY   | χ                 | 1.3                      | eV               |
| Electron Density of State             | NC300      | N <sub>c</sub>    | 1 x 10 <sup>20</sup>     | cm <sup>-3</sup> |
| Impact Ionization Coefficients (for   | AN         | An                | 4.62 x 10 <sup>5</sup>   | cm <sup>-1</sup> |
| electrons)                            |            |                   |                          |                  |
| п                                     | BN         | Bn                | 7.59 x 10 <sup>6</sup>   | V/cm             |
| 11                                    | CN         | Cn                | 1                        |                  |
| Activation Energy (for electrons)     | EB0        | E <sub>A,n</sub>  | 0.59                     | eV               |
| Degeneracy Factor (for electrons)     | GB         | g <sub>a</sub>    | 2                        |                  |
| Ionization Fitting Factor             | ALPHA      | α                 | 3.1 x 10 <sup>-8</sup>   |                  |
| (for electrons)                       |            |                   |                          |                  |
| п                                     | BETA       | α                 | 200                      |                  |
| 11                                    | GAMMA      | Υ                 | 1                        |                  |
| Hole Density of State                 | NV300      | N <sub>v</sub>    | 1 x 10 <sup>20</sup>     | cm <sup>-3</sup> |
| Impact Ionization Coefficients (for   | AP         | Ap                | 1.93 x 10 <sup>5</sup>   | cm <sup>-1</sup> |
| holes)                                |            |                   |                          |                  |
| II                                    | BP         | Bp                | 4.41 x 10 <sup>6</sup>   | V/cm             |
| п                                     | СР         | Cp                | 1                        |                  |
| Activation Energy (for holes)         | EB0        | E <sub>A,p</sub>  | 0.36                     | eV               |
| Degeneracy Factor(for holes)          | GB         | g <sub>a</sub>    | 4                        |                  |
| Ionization Fitting Factor (for holes) | ALPHA      | α                 | 3.037 x 10 <sup>-8</sup> |                  |
| п                                     | BETA       | β                 | 200                      |                  |
| II .                                  | GAMMA      | Υ                 | 0.95                     |                  |
| Workfunction for (AI)                 | WORKFUNC   | Ф <sub>m,Al</sub> | 4.3                      | eV               |
| Workfunction for (Au)                 | WORKFUNC   | Ф <sub>m,Au</sub> | 5.2                      | eV               |

Table 3.3: Diamond Material Parameters Used in All the Simulations of this Work [5,9,11 and 34]

#### **CHAPTER 4**

#### SCHOTTKY DIAMOND DIODE DESIGN AND SIMULATION

Despite the rather simple structure of the Schottky diodes, their simulations can provide meaningful information. Since the mechanisms of charge transport in a basic p\*/p-Schottky diode are identical to multi-layer structures, the knowledge from these simulations serves as the building block for performance optimization in more complicated devices. In this chapter, basic Schottky diode theory that matters to high power applications is introduced. It is followed by the forward bias and reverse bias simulations. Results from the use of field plate structures to control the electric field and increase the breakdown voltage is also reported.

#### 4.1 Schottky diode fundamentals

A Schottky diode has a metal-semiconductor interface which creates a junction known in theory as the Schottky barrier. The structure of a Schottky diamond diode consists of a thin layer of heavily doped diamond on top of a lightly doped layer. Although with different levels of concentration, both layers are doped by boron, which makes this a  $p^+/p^-$  type structure. There are two electrodes, one on the top and the other on the bottom of the structure. The electrode on the  $p^+$  layer forms an Ohmic contact; while the electrode on the  $p^-$  layer forms a Schottky contact. The structure is shown in figure 4.1.

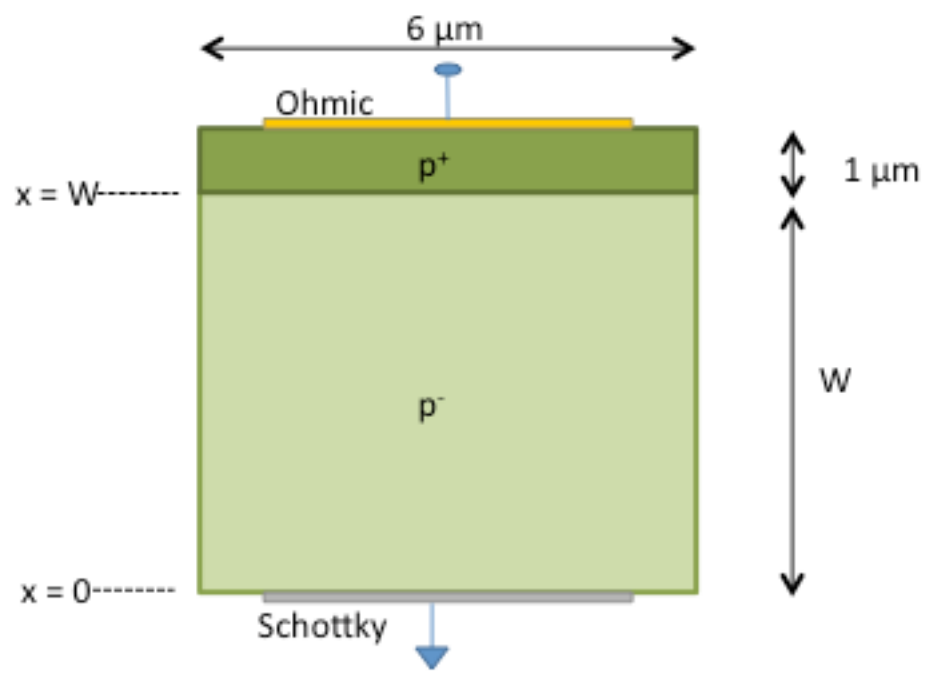
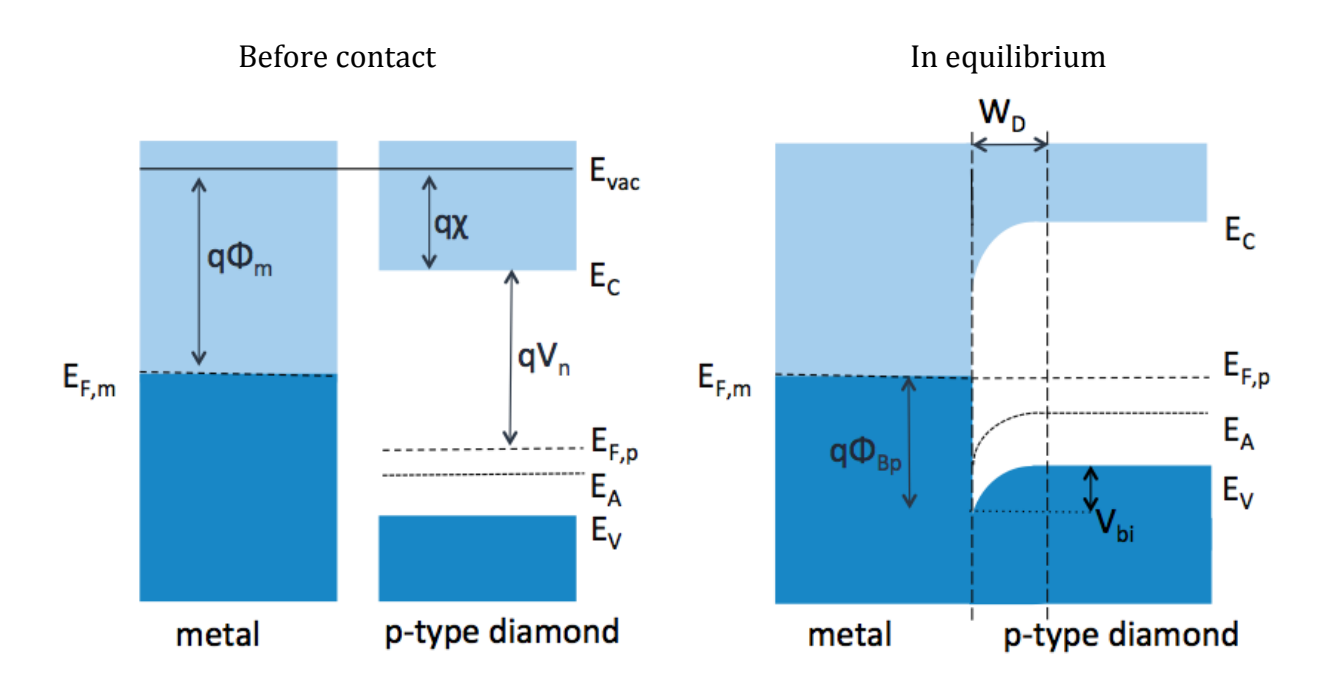


Figure 4.1: Structure of Schottky diamond diode

Unlike PN-junction diodes which are discussed in Chapter 5, Schottky diode is a majority-carrier device. This means for the structure in figure 4.1, the forward current is only due to hole injection from the semiconductor. There can be negligible minority carrier injection which makes the storage of excess minority charge omissible. Thus, Schottky diodes can operate at higher frequency than PN-junction diodes. In figure 4.1, the interface between the p<sup>-</sup> diamond to Schottky contact exhibits a rectifying current-voltage (IV) characteristic. The interface between p<sup>+</sup> diamond and Ohmic contact exhibits a linear IV characteristic. It behaves like a low resistance Ohmic contact.

The band diagrams are depicted in figure 4.2 for the moment before the metal and semiconductor are brought into contact (top left inset), after they are in contact and in equilibrium (top right inset), when the forward bias is applied (bottom left inset) and when the reverse bias is applied (bottom right inset).



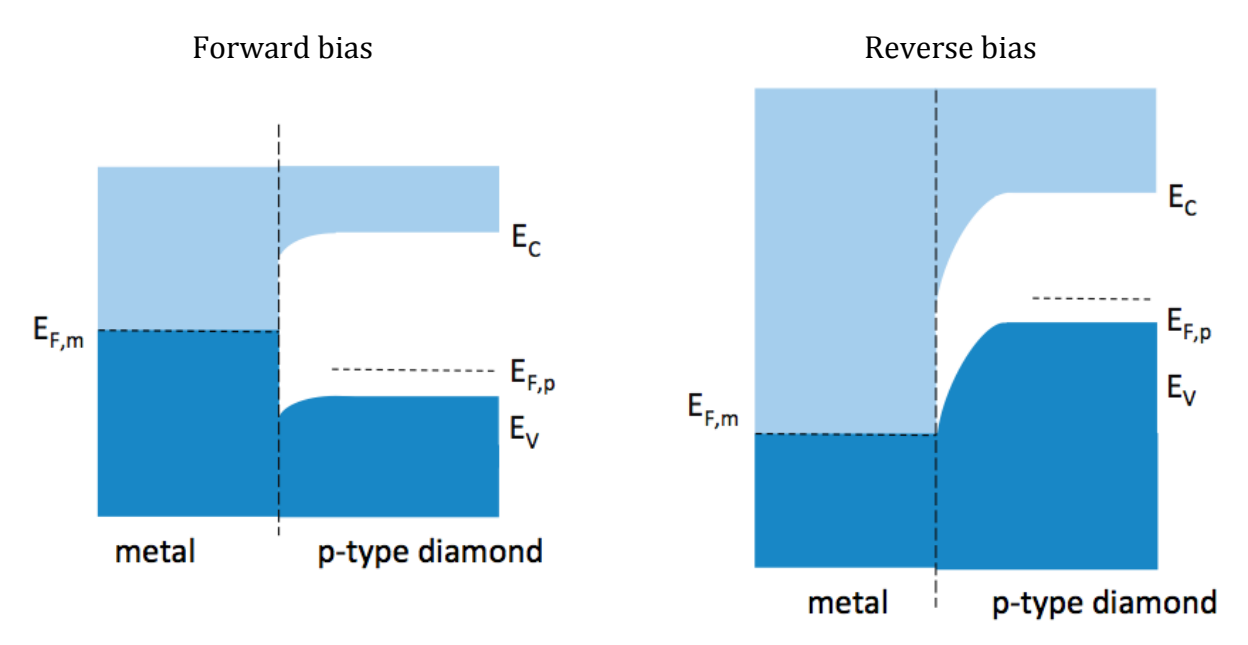


Figure 4.2: Band diagram of Schottky diode

# 4.1.1 Design Parameters in Power Devices

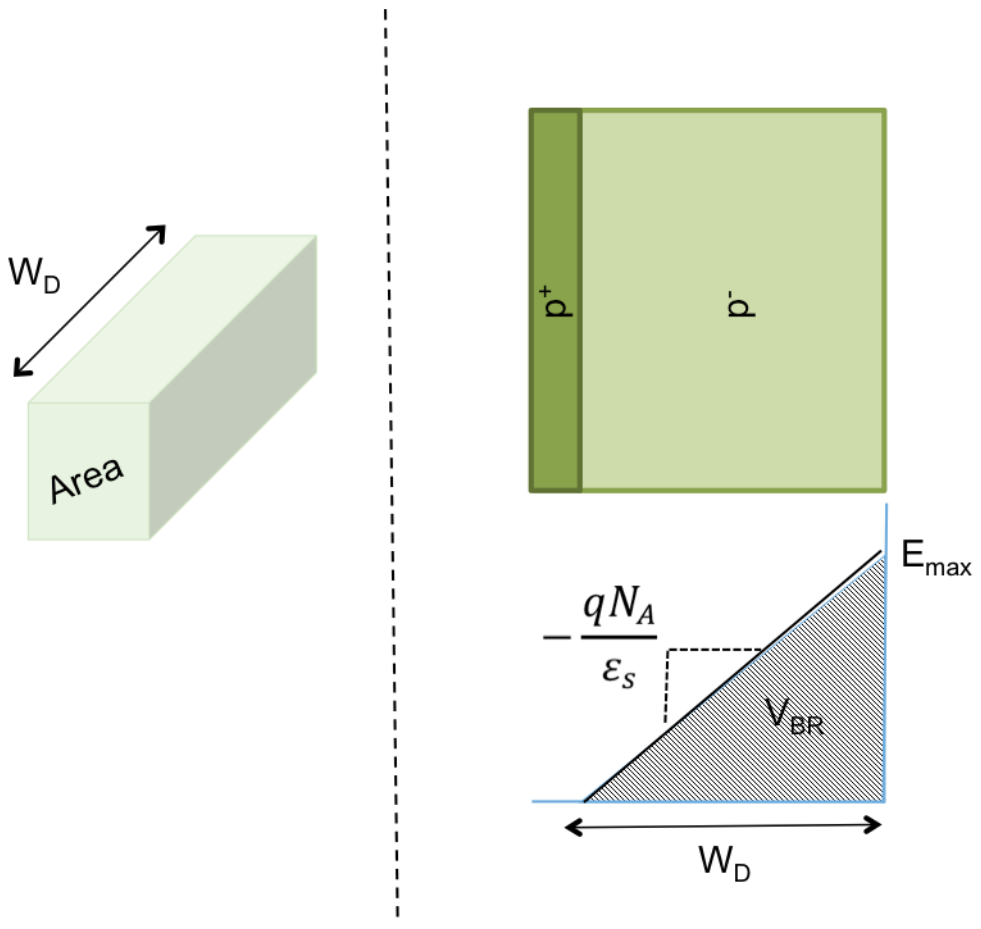


Figure 4.3: Block of semiconductor (left); Electric field distribution in the drift region in reverse bias (right)

The understanding of the relationship between each design parameter starts by the following derivation. Looking at a block of semiconductor in figure 4.3 the left inset, the conductivity ( $\sigma$ ) through the block and resistivity ( $\rho$ ) is given by definition as in equation 4.1 where J is the current density and E is the electric field.

$$\sigma = \frac{1}{\rho} = \frac{J}{E} \tag{4.1}$$

Also, by definition the resistivity is the resistance (R) times the cross-sectional area per unit length ( $W_D$ ) as given in equation 4.2. Note that  $W_D$  is also used to refer to the length of drift layer.

$$\rho = R \times \frac{Area}{W_D} = \frac{E}{I} \tag{4.2}$$

On the right inset of figure 4.3, the electric field distribution in the drift region (p·) for reverse bias is shown when the maximum electric field ( $E_{max}$ ) equals to the critical breakdown electric field ( $E_{c}$ ). The critical breakdown electric field is a physical parameter for each semiconductor material before avalanche breakdown takes place. The carrier concentration can be optimized such that  $E_{max}$  reaches  $E_{c}$  and the drift region is depleted entirely as shown in figure 4.3 (right inset). The breakdown voltage (VBR) is the area under the electric field curve in figure 4.3, which can be written out as in equation 4.3.

$$V_{BR} = \frac{E_c W_D}{2} \tag{4.3}$$

From Poisson's equation, the slope of the electric field plot is determined as shown in figure 4.3, so it can be written in equation 4.4 the relationship between the electric field at the depletion region.

$$E_c = \frac{qN_A}{\varepsilon_S} W_D \tag{4.4}$$

where q is the electron charge,  $N_A$  is the doping concentration in the drift region, and  $\epsilon_s$  is the permittivity of the region. Combining equations 4.3 and 4.4, the doping concentration can be determined as written in equation 4.5.

$$N_A = \frac{\varepsilon_s E_c^2}{2qV_{RR}} \tag{4.5}$$

By definition, the specific on-resistance ( $R_{on,sp}$ ) is an inherent property of a material and is defined by the resistance offered by the unit cross-sectional area of the material when voltage is applied. Back to equation 4.2, with basic knowledge of electric theory it follows that

$$R_{on,sp(ideal)} = R \times Area = W_D \frac{E}{I} = W_D \frac{E}{\sigma E} = \frac{W_D}{q \mu_n N_A}$$
(4.6)

where  $\mu_P$  is the mobility of holes. Equation 4.6 represents the ideal case when the drift region in reverse bias is fully depleted. Combining equations 4.5 and 4.6, the ideal specific on-resistance can also be written as:

$$R_{on,sp(ideal)} = \frac{4V_{BR}^2}{\varepsilon_s \mu_p E_c^3} \tag{4.7}$$

Through equations 4.3 - 4.7, the relationship between the design parameters including  $N_{A}$ ,  $V_{BR}$ ,  $W_{D}$  and  $R_{on,sp}$  are clearly stated. The electric field varies as  $N_{A}$ .  $R_{on,sp}$  is inversely proportional to the electric field.  $V_{BR}$  increases with  $W_{D}$  but is inversely proportional to  $N_{A}$ . These understandings will be important when the simulation results are observed.

There are four basic processes for carrier transport in the forward bias as shown in figure 4.4. Each process is indicated by the arrow showing the location in the band it occurs. These are (1) thermionic emission, (2) tunneling, (3) recombination and (4) diffusion. They can take place at the same time, but usually one process dominates. Since for p<sup>+</sup>/p<sup>-</sup> Schottky diodes, there is only one type of charge carriers and that is hole; the recombination process can be ignored for now. Note that this is also called a unipolar device when there is only one type of charge carriers, either holes or electrons but not both, in the device.

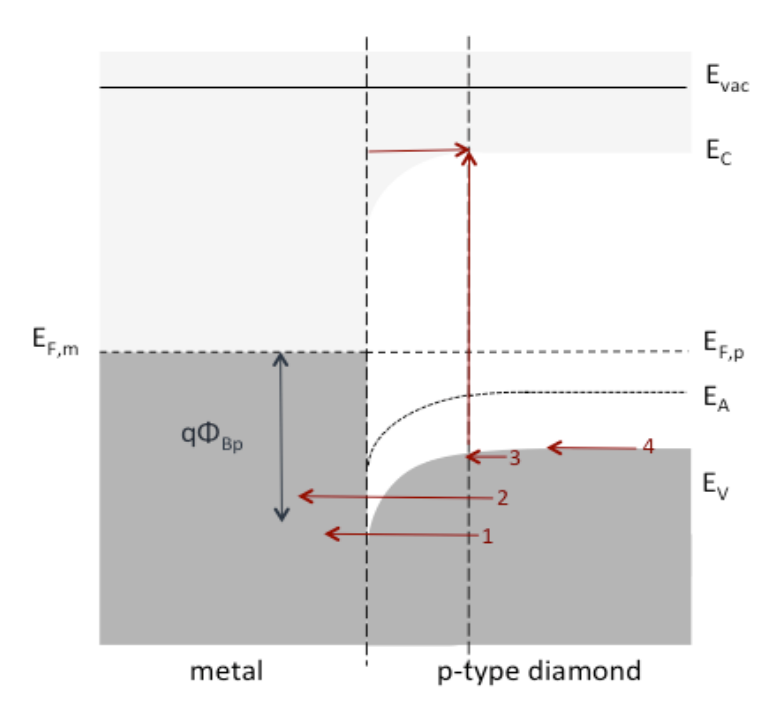


Figure 4.4: Four basic transport processes in forward bias: (1) thermionic emission (2) tunneling (3) recombination and (4) diffusion

The tunneling process where carriers travel through the barrier is often the case for Ohmic contacts and heavily doped ( $>10^{20}$  cm<sup>-3</sup>) semiconductors. For moderately doped semiconductors operating at moderate temperature (like room temperature), the thermionic emission process dominates. Due to the difference in workfunctions, a barrier forms naturally at a metal-semiconductor interface. In the forward bias, the applied voltage allows carriers to travel over the lowered barrier. The injection current based on thermionic emission is represented by the Richardson-Dushman equation as follows. (Note that detailed derivation of this equation can be found in chapter 3 in *Physics of Semiconductor Devices* by Sze.) [35]

$$J = A^* T^2 \exp\left(-\frac{q \Phi_{Bp}}{kT}\right) \exp\left(\frac{qV}{kT} - 1\right)$$
(4.8)

$$A^* = \frac{4\pi m^* k^2}{h^3} \tag{4.9}$$

where  $A^*$  is the Richardson constant, T is the temperature in Kelvin, V is the applied voltage in V,  $\varphi_{Bp}$  is the barrier height of semiconductor in V, V is the Boltzmann constant, V is the electric charge, V is the Planck's constant and V is the effective mass.

Furthermore, there are various numerical models that approximate the amount of charge transport in the semiconductor devices based on certain assumptions. All the models originate from Poisson's and transport equations (described in chapter 2). But the differences come from the type of materials (insulating or semiconductor), dimensions of the device, trapping effects and etc. In any case, the I-V relation of semiconductor devices often follows a universal power law of the form I  $\alpha$  V<sup>m</sup>. The conduction regime varies depending on the value of the exponent m. In the Ohmic conduction regime, m = 1, and the current density J varies linearly with applied voltage V. The Ohmic conduction can be approximated by a simple drift current as shown in the following equation.

$$J = \frac{qn\mu V}{W} \tag{4.10}$$

where q is the electronic charge, n is the density of the carriers,  $\mu$  is the mobility of the carriers, and W is the thickness of the drift layer.

# 4.1.2 Space Charge Limited Conduction (SCLC)

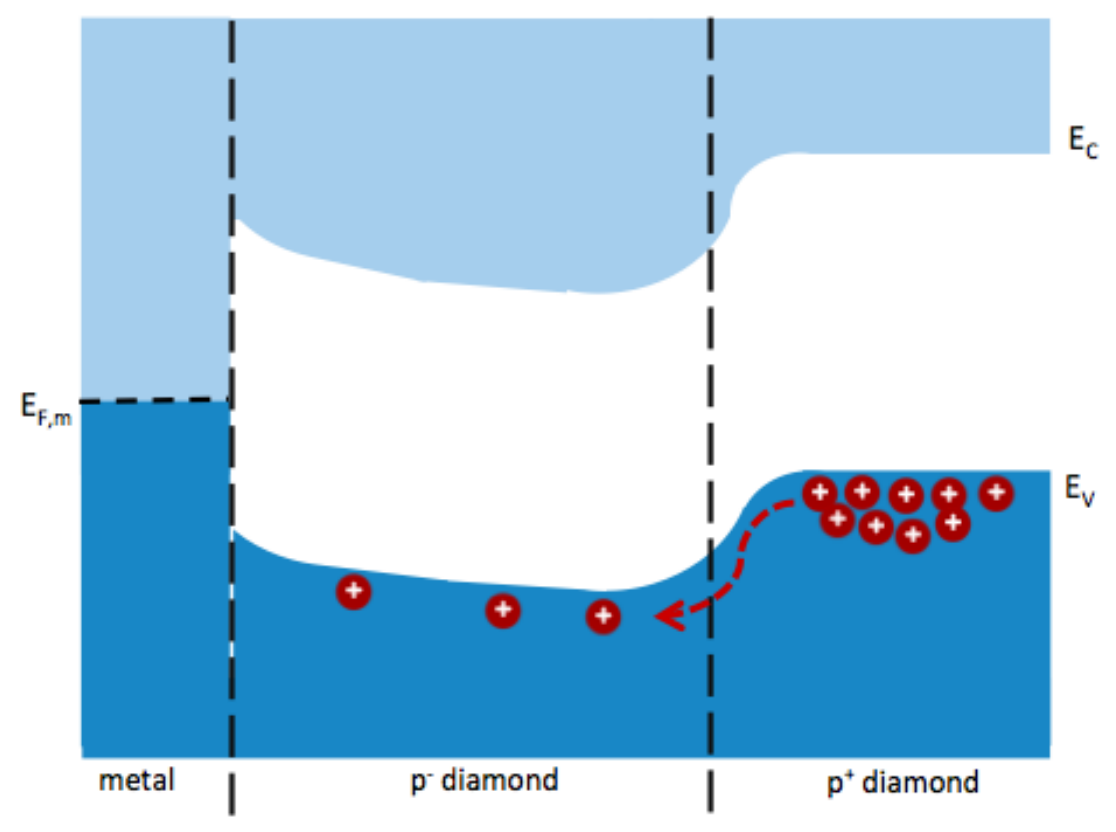


Figure 4.5: Band diagram of Schottky diamond diode in SCLC regime

There is a special situation when the current is controlled by the gradient of charge carriers (space charges) at a certain forward bias. When the density of the injected carriers is large as shown in figure 4.5, the space charge effect occurs, and these injected carriers influence the electric-field profile. In other words, with sufficient forward bias the density of injected carriers is much larger than the equilibrium acceptor levels. This generally happens when the ionization acceptor level is low. The local field, caused by the surplus carriers, yields a large gradient of carrier density and it is responsible for driving the current to the electrode. [36] So the current through a device is limited by the surplus space charges. There is no significant departure from Ohm's low until the average, injected

excess free-electron or free-hole concentration,  $n_{injected}$ , becomes large enough to be noticeable. When  $n_{injected}$  becomes comparable to  $n_0$  (thermal equilibrium free electron concentration), the space-charge-limited (SCL) mechanism becomes noticeable, and the current voltage characteristics change. The situation is depicted in figure 4.5. The bands bend down due to over-compensated acceptor level. [37] This current is referred to as a space-charge limited current (SCLC). Mott-Gurney Law is an analytical theory describing the SCLC. It assumes that the electric field at the charge-injecting interface is zero. If the electric field exists at the interface, it is assumes to be neutralized by the field in the opposite direction generated by the injected p-type free carriers. The Mott-Gurney Law is derived as follows:

With sufficient forward bias,  $p\gg N_a$  it can be approximated that

$$\rho_s = q(p - N_a) \approx qp \tag{4.11}$$

where  $\rho_s$  is the charge density, and p is the hole concentrations.

The Poisson equation becomes independent of doping concentration in this region:

$$\frac{dE}{dx} = \frac{qp}{\varepsilon_s} \tag{4.12}$$

where again E is the electric field. In the lowly doped region with large enough forward bias, the drift current becomes much larger than diffusion current. So the total current can be approximated to the drift current only:

$$J = qp\mu_p E \tag{4.13}$$

Combining equations 4.12 and 4.13:

$$J = \varepsilon_s \mu_p E \frac{dE}{dx} \tag{4.14}$$

Integrate from x = 0 to x = W assuming E(x) = 0 at x = 0 by separating variables yields:

$$\frac{Jx}{\varepsilon_s \mu_p} = \frac{E(x)^2}{2} \to E(x) = \sqrt{\frac{2xJ}{\varepsilon_s \mu_p}}$$
 (4.15)

Integrate from x = 0 to x = W with V(0) = 0 and V(W) = V yields:

$$V = \int_{x=0}^{x=W} E(x) dx = \sqrt{\frac{2J}{\varepsilon_s \mu_p}} \frac{W^{\frac{3}{2}}}{\frac{3}{2}}$$
 (4.16)

Therefore, the Mott Gurney equation is

$$J = \frac{9\varepsilon_s \mu_p V^2}{8W^3} \tag{4.17}$$

SCLC is still part of the ordinary current-voltage characteristics of a majority carrier device in forward bias. Specifically, it describes the case of charge transport by the electric field from the surplus carriers of a highly doped region into another with much lower doping. From the assumptions made in the derivation of SCLC equation, it is evident that the equation holds only for devices in which the entire lowly doped region can be swept over by holes from p<sup>+</sup> region. [37] Hence, such devices have to be thin. The simulations in the following section show that a Schottky diamond diode does produce SCLC under certain design parameters. Furthermore, when those design parameters vary, the forward conduction changes from SCLC to Ohmic regime.

# 4.2 Simulation Setup for Schottky Diamond Diodes

Since Medici allows users the freedom to create arbitrary structures to simulate, for all of the simulations in this entire chapter the p $^+$  layer was 6  $\mu$ m wide and 1  $\mu$ m thick with

the doping concentration of  $10^{20}$  cm<sup>-3</sup>. The p<sup>-</sup> layer was also kept at 6  $\mu$ m wide. Both contacts were 0.1  $\mu$ m thick and 5  $\mu$ m wide – offsetting by 0.5  $\mu$ m from the left and right edge of diamond substrate. The design parameters that affect the performance of Schottky diodes were studied in this section of simulations. These parameters are:

- The p-layer thickness, W (μm)
- The p-layer doping, N<sub>A</sub> (cm<sup>-3</sup>)
- Operating temperature, T (K)

## 4.2.1 Schottky Diamond Diode Simulations in Forward Bias

The I-V characteristics can give some insights about the transport mechanisms of a diamond Schottky diode. The set-up structure for the simulations is displayed in figure 4.1 and the basic parameters are stated in section 4.2. The thickness of  $p^-$  layer, W, was studied first and the results are shown in figures 4.6, 4.7 and 4.8. For these results, the doping concentration in  $p^-$  layer was 1 x  $10^{16}$  cm<sup>-3</sup> with the compensation of 1 x  $10^{14}$  cm<sup>-3</sup> to mimic the actual synthesized doped diamond. The temperature was set to 300 K (room temperature).

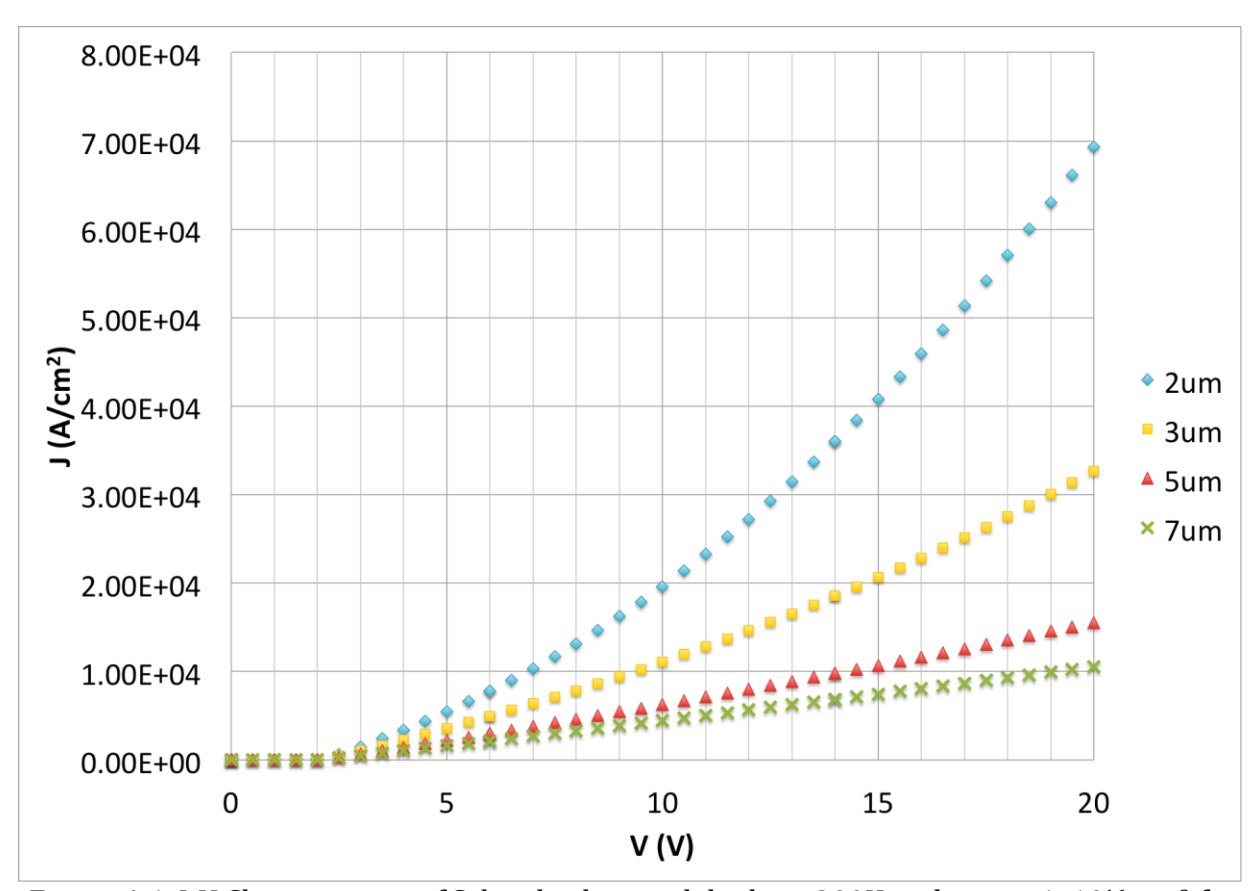


Figure 4.6: I-V Characteristic of Schottky diamond diode at 300K and p<sup>-</sup> was 1x10<sup>16</sup> cm<sup>-3</sup> for different thicknesses of the p<sup>-</sup> layer

The first information from the I-V plot of Schottky diode simulations is that at the bias of 2.0 V the current started to increase above  $100 \text{ A/cm}^2$  and this point is taken as the "on" state ( $V_{on}$ ) of the diode. For all the different thicknesses of the  $p^-$  layer,  $V_{on}$  was the same at 2.0 V.

Next, the Mott Gurney equation (eq. 4.17) when W = 1  $\mu$ m was plotted in figure 4.7 (with the SCLC label) along with the simulations of different thicknesses on the semi-log plot. This is a quick check to see if the diamond model parameters compiled in Chapter 3 agreed with the SCLC theory. Figure 4.7 shows that the simulation result at 1  $\mu$ m agreed quite well with equation 4.17. It is apparent that the model of Schottky diamond diode

produced the forward conduction that matched the SCLC theory as the curves followed each other very closely.

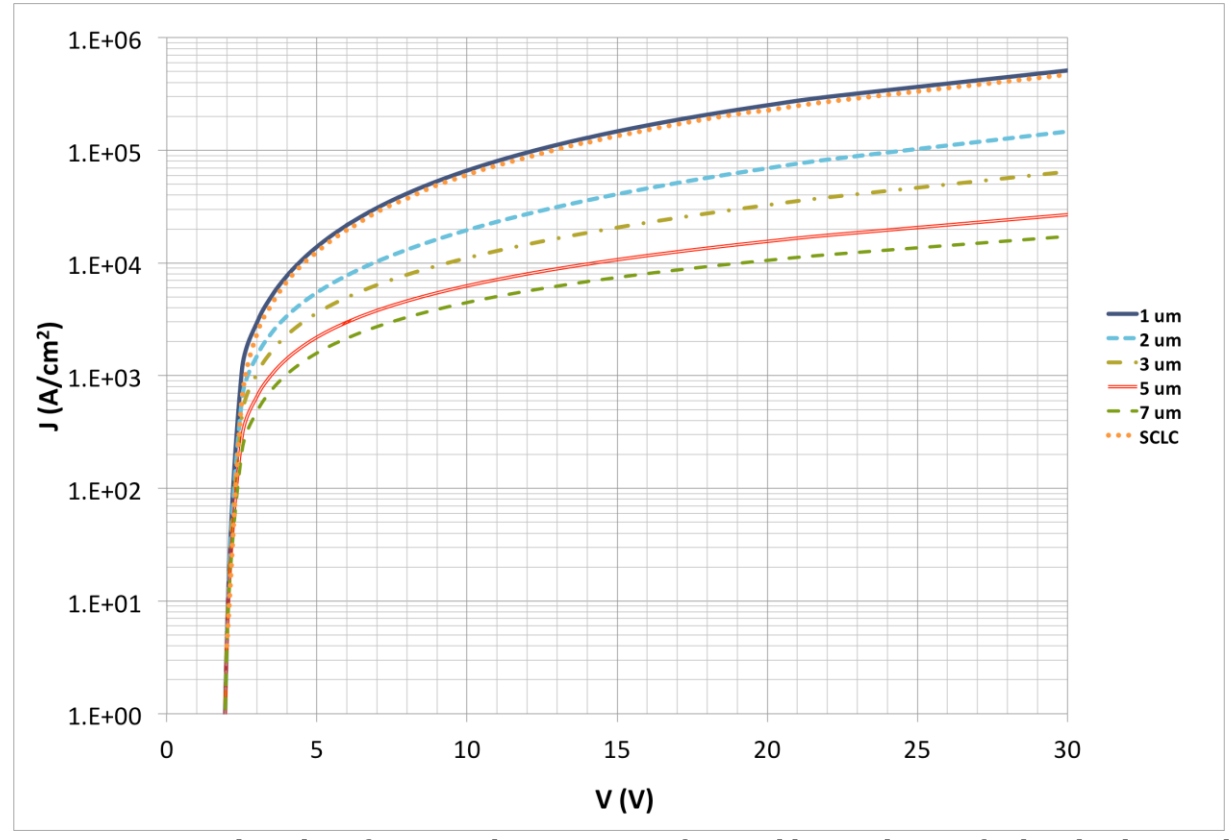


Figure 4.7: Semi-log plot of current density versus forward bias voltage of Schottky diamond diode simulations at 300K and p- was 1x10<sup>16</sup> cm<sup>-3</sup> for different thicknesses of p- layer

Finally, the log(J) versus log(V) plot in figure 4.8 allows us to observe the power law relationship, J  $\alpha$  V<sup>m</sup>., and m can be calculated. When m = 2, J and V relationship followed the Mott-Gurney Law and SCLC was observed. When m = 1, the transport mechanism was in Ohmic regime. In figure 4.8, when the thickness of the lowly doped layer was 1  $\mu$ m, the current density curve follows the same gradient as the theoretical SCLC. As the thickness of the lowly doped layer (W) increased, the gradient of the current density curves decreased towards m = 1, the value of Ohmic conduction. It can be observed that the effect of SCLC was less and less as the thickness increased in figure 4.8. This matches with the

expectation, as it was more difficult for the charges to sweep through the thicker layer according to equation 4.16.

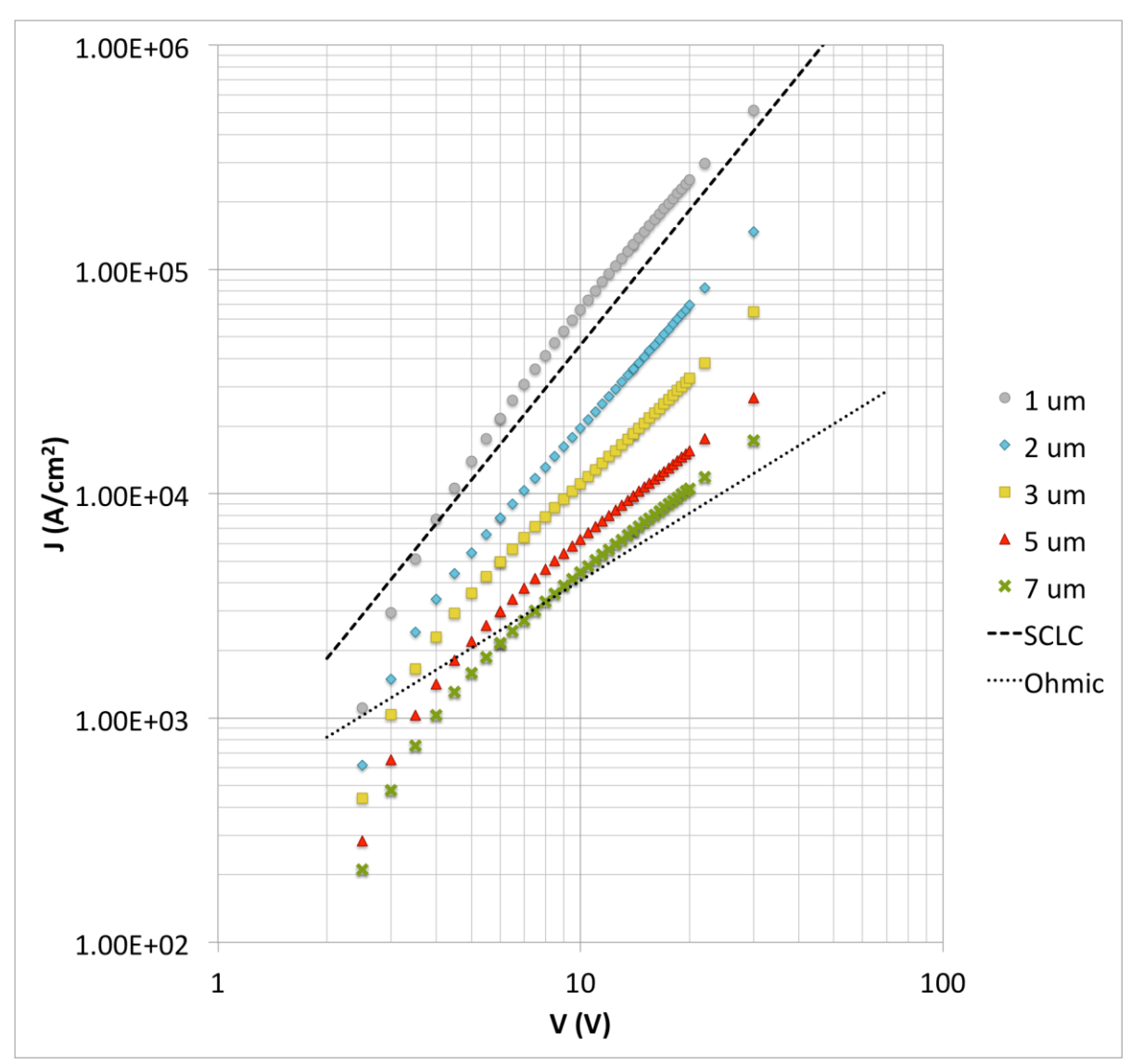


Figure 4.8: Log plot of current densities versus voltage of Schottky diamond diode simulations at 300K and p- was 1x10<sup>16</sup> cm-<sup>3</sup>

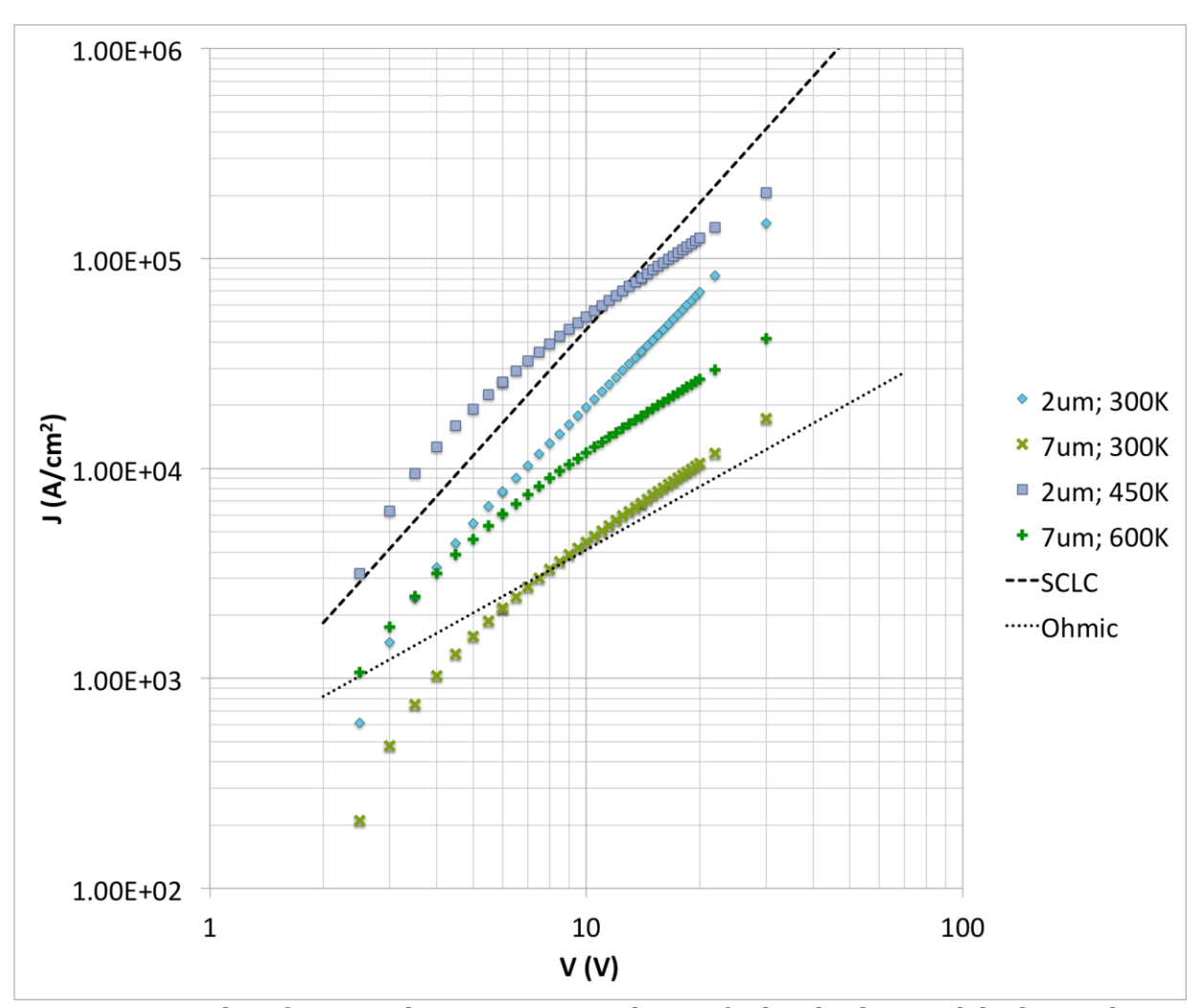


Figure 4.9: Log plot of current densities versus voltage of Schottky diamond diode simulations for varying thickness and temperature based on  $p^-=1x10^{16}~\rm cm^{-3}$ 

When coupled in the effect of SCLC with layer thickness and temperature, the results are shown in figure 4.9. Again as expected, as the thickness and the temperature increased the conduction became more Ohmic. This is also shown in figure 4.10, which is the plot of the slope 'm' versus the thickness for p layer (drift layer) with varying temperature. The 'm' values were calculated between the forward voltages of 5-10 V. Here, it can be concluded that the slope 'm' decreased with increasing layer thickness and temperature.

Thus, the effect of SCLC became less and less (m became closer to 1) with thicker devices and high operating temperature.

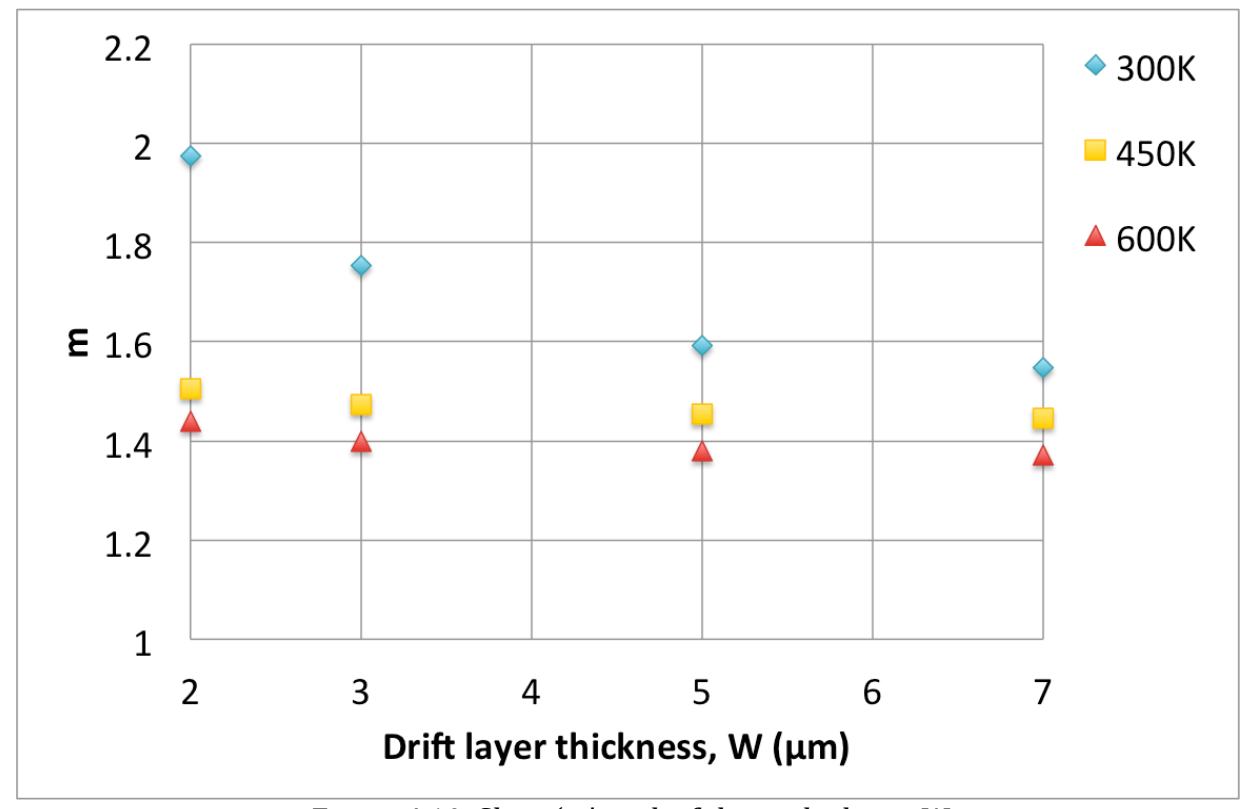


Figure 4.10: Slope 'm' vs. draft layer thickness W

Furthermore, the forward conduction was affected by the doping concentration in the  $p^-$  layer and this is shown in figure 4.11 (which is the simulation when the  $p^-$  layer was 2  $\mu$ m at 300K). Increase in the doping concentration, N<sub>A</sub>, resulted in higher current density. However, the effect of the doping variation on SCLC was less prominent compared to that from the device thickness. The calculated 'm' values ranged between 1.8 – 1.95 for the curves in figure 4.11 when measured between 5 – 10 V.

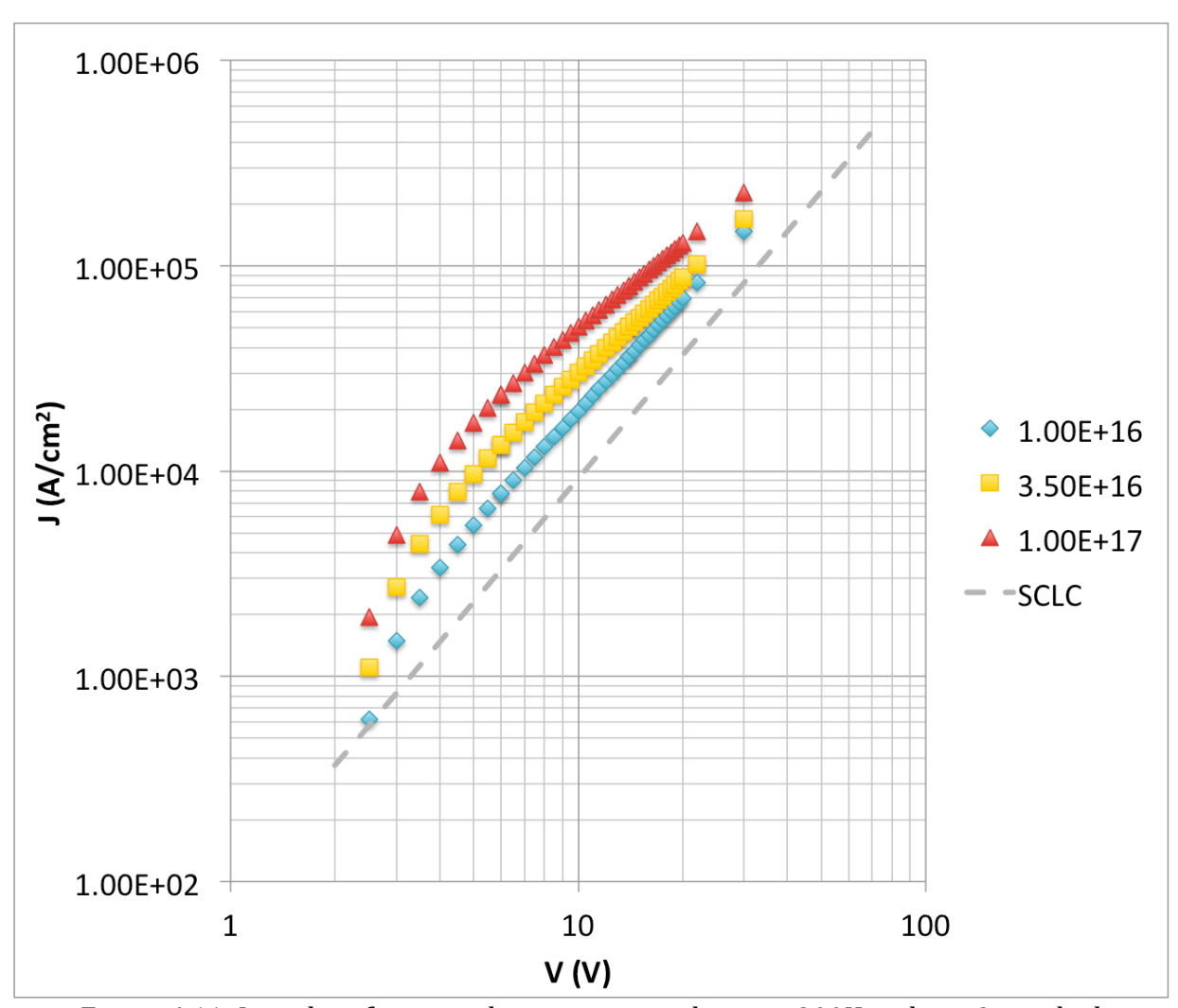


Figure 4.11: Log plot of current density versus voltage at 300K and  $p^- = 2 \mu m$  thick

Therefore, in the forward conduction the design parameter that affected SCLC the most was the thickness of the device. Operating temperature and doping concentration still had some effects but they were less prominent than the thickness of the device.

# 4.2.2 Schottky Diamond Diode Simulations in Reverse Bias

According to equation 4.5, the impurity doping concentration ( $N_A$ ) is the key parameter that affects the breakdown voltage. Hence, it is the design parameter that is discussed first in the reverse bias regime.

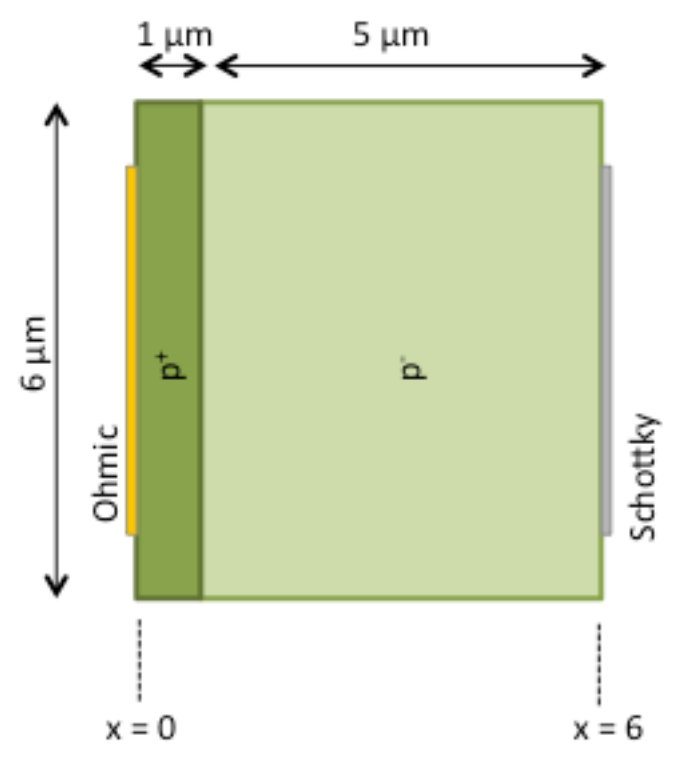


Figure 4.12: Schottky diode structure and dimension for easy electric field comparison

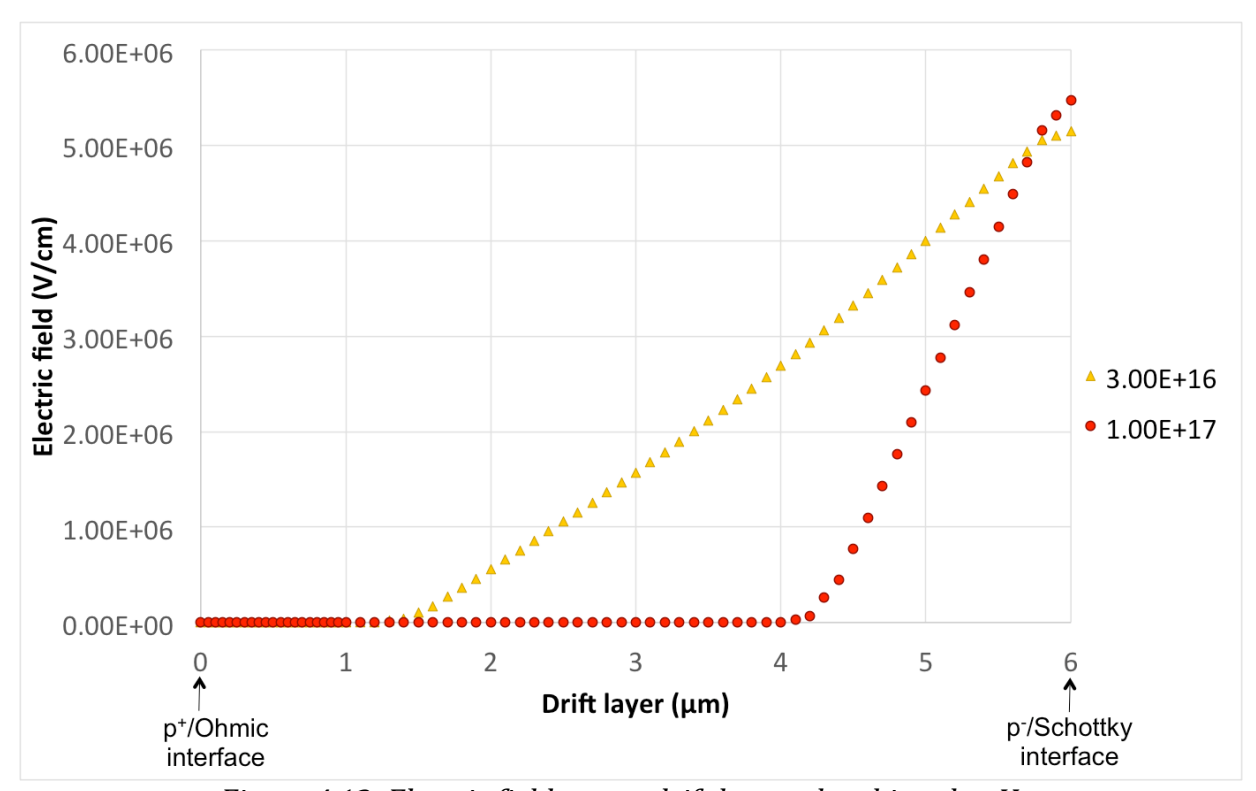


Figure 4.13: Electric field versus drift layer when biased at  $V_{BR}$ 

The structure of Schottky diamond diode for simulations in reverse bias remained the same as shown in figure 4.1. However, figure 4.12 is also given which is just the rotated version of figure 4.1, so that comprehending the electric field plot in figure 4.13 is easier. Note one difference between figure 4.1 and 4.12 in that x=0 is defined at a different location. For figure 4.12, x=0 is at the  $p^+/Ohmic$  contact interface. Figure 4.13 shows the plot of electric field versus device dimension from x=0 to x=6  $\mu m$  for the Schottky diode simulation at 300 K and drift layer is 5  $\mu m$  thick when biased at  $V_{BR}$ . The values of  $V_{BR}$ ,  $R_{On,sp}$  and  $E_{max}$  for each  $N_A$  are also listed in table 4.1.

| 2                                  | 300 K               |                                    |   |  |  |
|------------------------------------|---------------------|------------------------------------|---|--|--|
| N <sub>A</sub> (cm <sup>-3</sup> ) | V <sub>BR</sub> (V) | $R_{on,sp}$ (m $\Omega$ -cm $^2$ ) | E <sub>max</sub> (V/cm)                   |  |  |
| 1x10 <sup>16</sup>                 | 1950                | 4.97                               | 5.04 x 10 <sup>6</sup><br>biased at 1900V |  |  |
| 3x10 <sup>16</sup>                 | 1180                | 3.05                               | 5.15 x 10 <sup>6</sup><br>biased at 1130V |  |  |
| 1x10 <sup>17</sup>                 | 529                 | 1.57                               | 5.48 x 10 <sup>6</sup><br>biased at 500V  |  |  |

Table 4.1: Breakdown Voltages, Specific On-resistance and Maximum Electric Field of Schottky Diamond Diode Simulations at 300 K and Drift Layer, p-, was 5 μm.

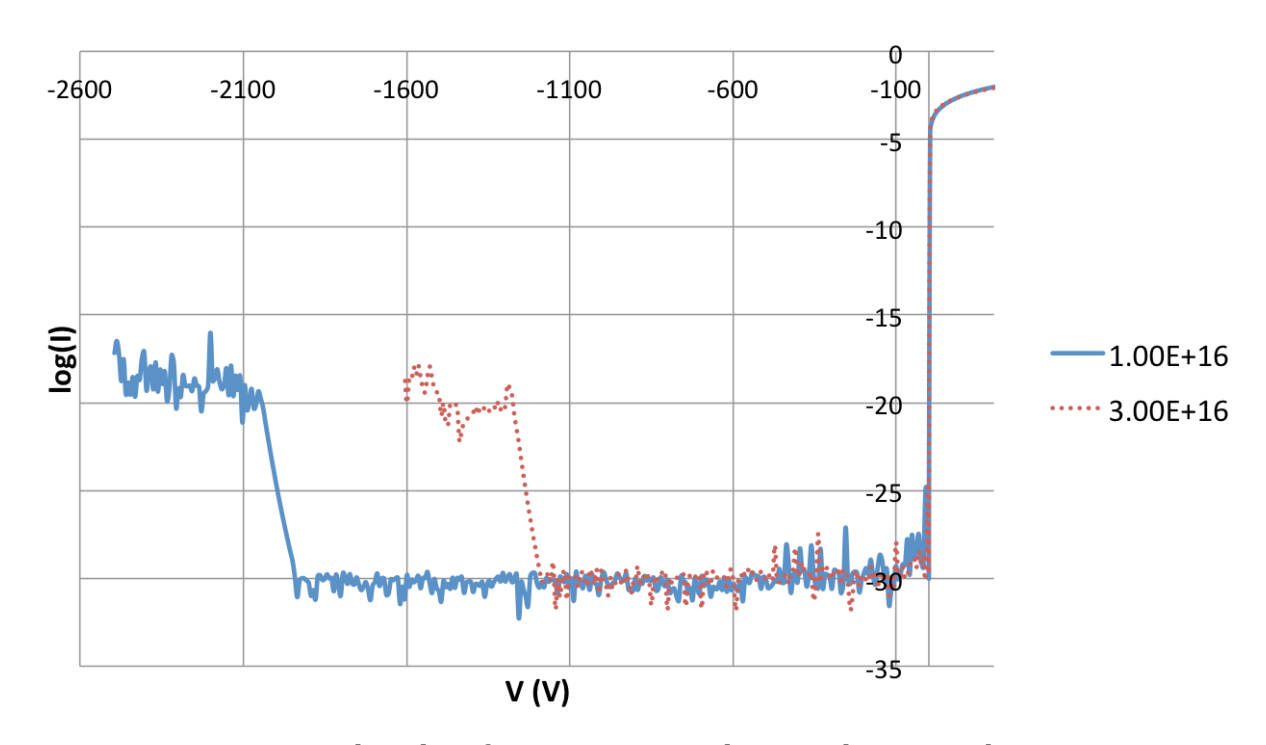


Figure 4.14: Semi-log plot of current versus voltage in the reverse bias at 300 K

As explained earlier in section 4.1, the area under the electric field versus dimension plot equals to  $V_{BR}$ . The area under the yellow curve in figure 4.13 which belongs to  $N_A$  =

 $3x10^{16}$  cm<sup>-3</sup> appears larger compared to the area under the red curve for  $N_A$  =  $1x10^{17}$  cm<sup>-3</sup>. This agrees with the values of  $V_{BR}$  measured from the simulations and shown in table 4.1 such that the breakdown voltage of the lower doped drift layer was higher. This is as expected according to equation 4.5. Also displayed in figure 4.14 is the semi-log plot of current (A/µm) versus voltage in the reverse bias of the structure in figure 4.12 at 300 K. When the drift layer doping was  $1x10^{16}$  cm<sup>-3</sup>, the breakdown voltage was 1950 V. The breakdown voltage reduced to 1180 V as the drift layer doping increased to  $3x10^{16}$  cm<sup>-3</sup>. The results are also listed in table 4.1

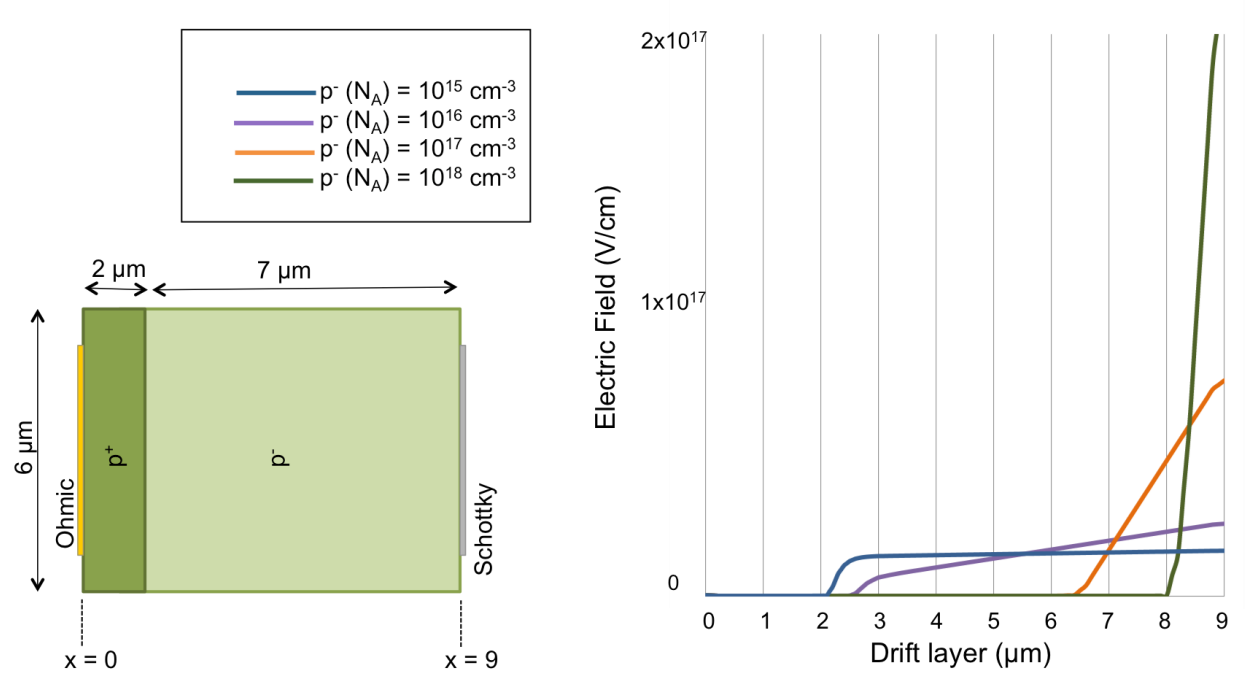


Figure 4.15: Electric field versus drift layer dimension at 300 K at 1000 V reverse bias

Furthermore, figure 4.15 presents another set of results based on slightly different structural dimensions. The p+ layer was 2  $\mu$ m thick while the p- (drift) layer was 7  $\mu$ m. Doping concentration in the p+ layer remained the same as the previous simulations. For the p- layer, the doping concentration was varied from  $1x10^{15}$  to  $1x10^{18}$  cm-3. At 300 K, the

electric filed for each p- doping concentration was plotted for the same 1000 V reverse bias. The results showed the rise in the maximum value of the electric field ( $E_{max}$ ) with increasing doping concentration in the drift layer. Viewing the results from figures 4.13, 4.14 and 4.15 and table 4.1 together, it can be concluded that the electric field varied proportionally as the drift layer doping concentration; while the breakdown voltage was inversely proportional to the electric field and the doping concentration. This conclusion agreed with the theory in equations 4.4 and 4.5.

Results on the variation in operational temperatures are reported in figures 4.16, 4.17 and 4.18. Regardless to the change in the drift layer's dopings or thicknesses, higher temperatures always resulted in slightly greater breakdown voltage.

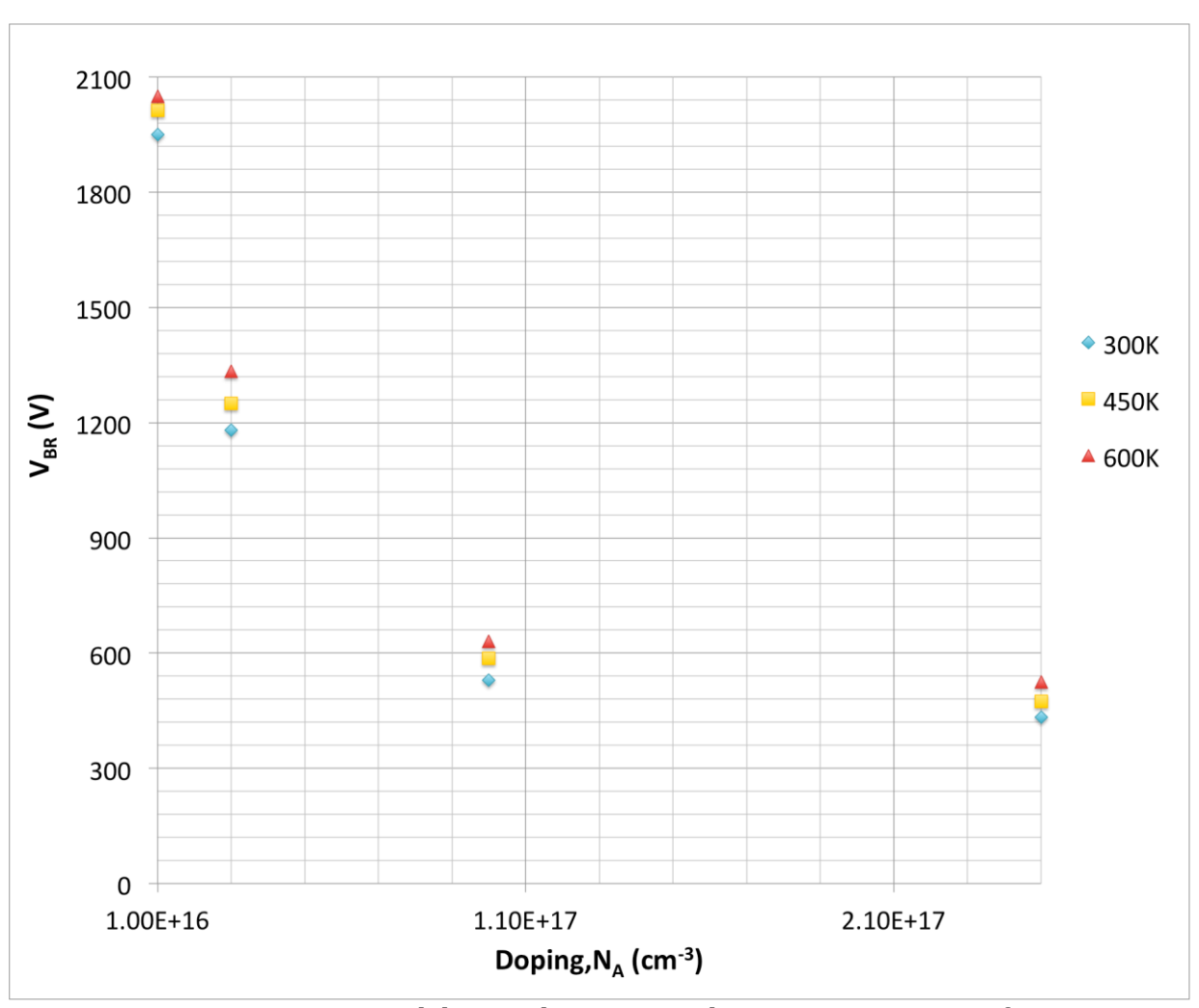


Figure 4.16: Breakdown voltage versus doping concentration of Schottky diamond diode with drift layer (p-) of 5 μm thick

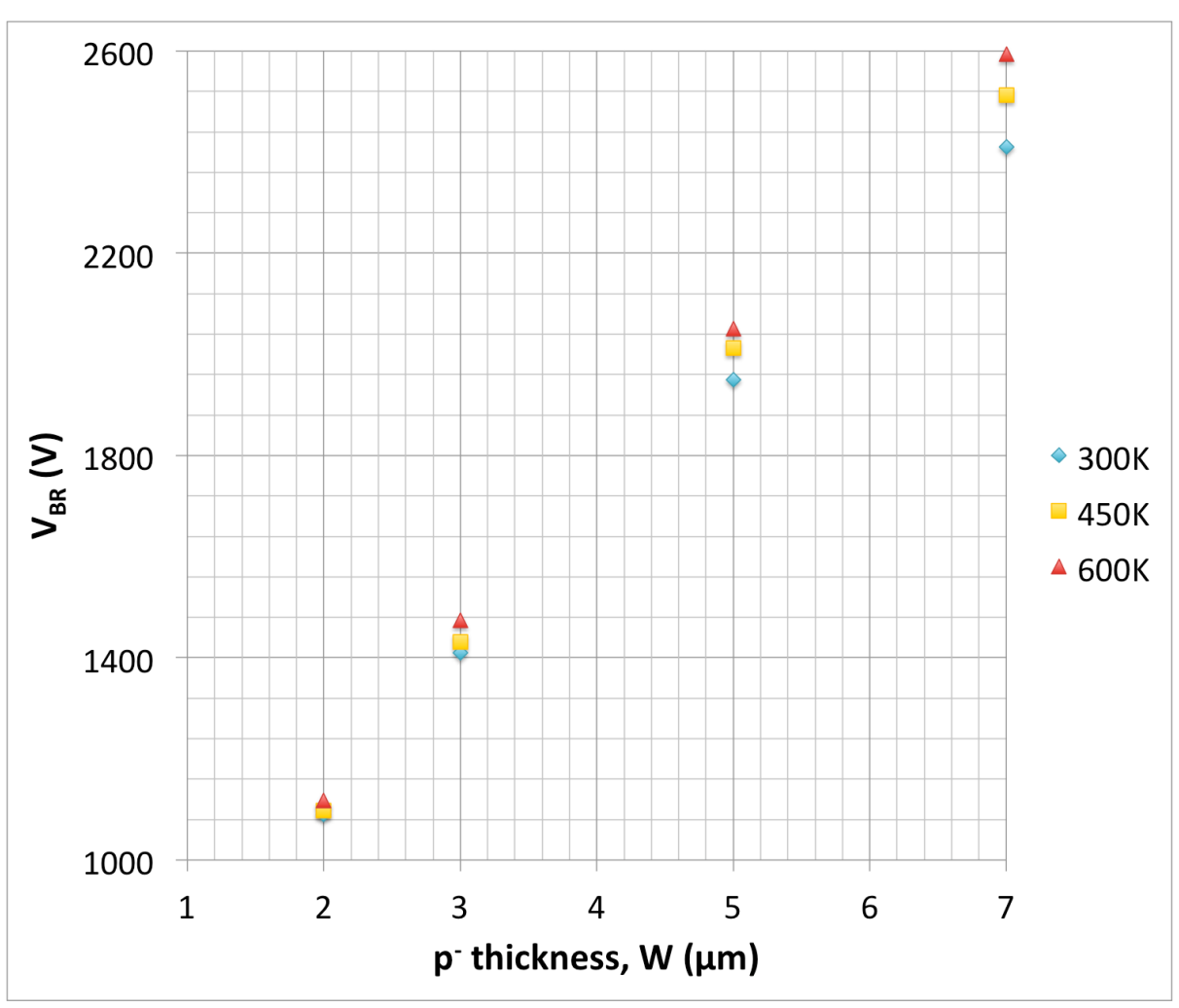


Figure 4.17: Breakdown voltage versus p- layer thickness when p- doping was fixed at 1x10<sup>16</sup> cm<sup>-3</sup>

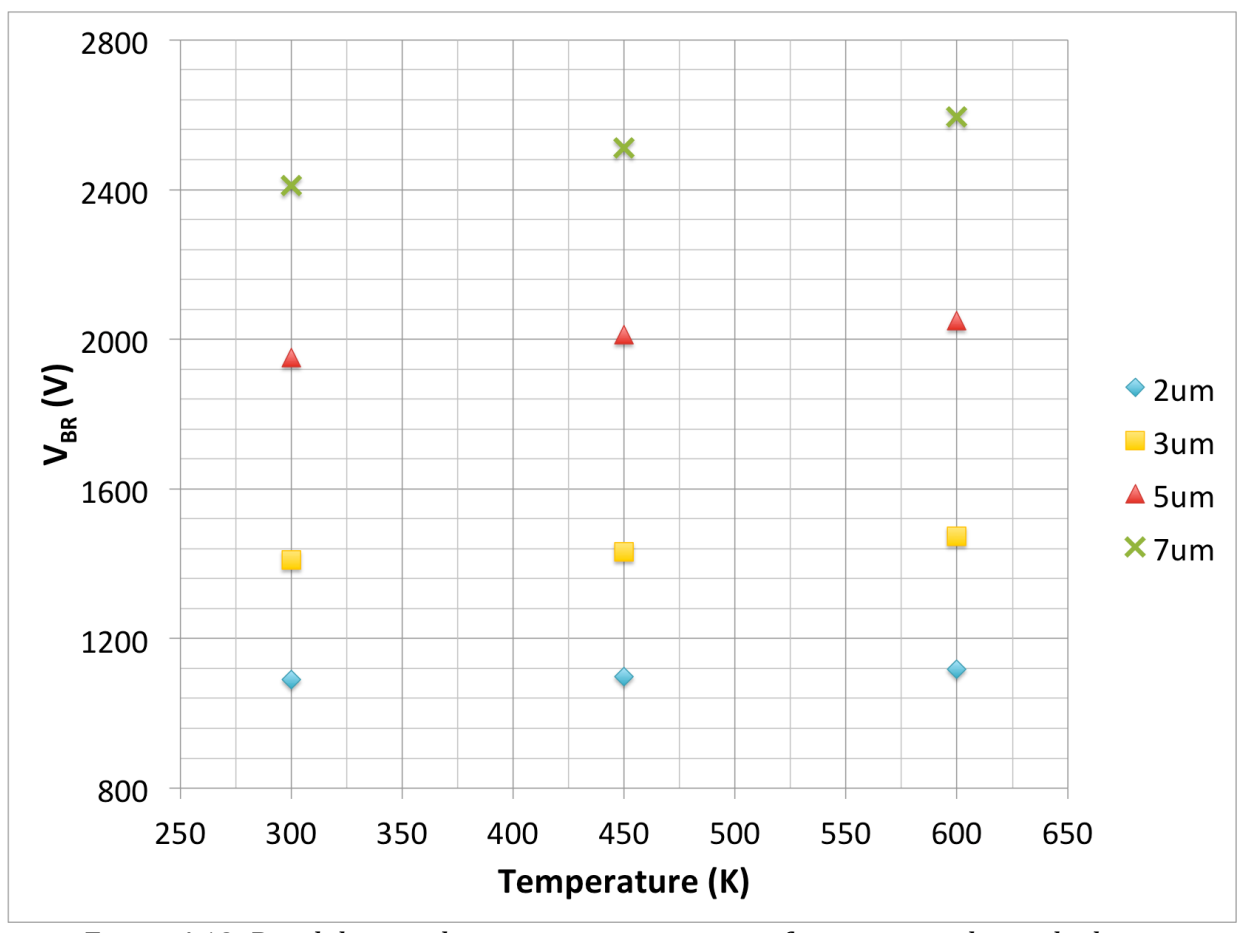


Figure 4.18: Breakdown voltage versus temperature for varying  $p^-$  layer thickness when  $p^-$  doping was fixed at  $1x10^{16}$  cm<sup>-3</sup>

The relationship between breakdown voltage and drift layer thickness is reported in figure 4.17. It was seen that the thicker drift layer yielded a higher breakdown voltage based on the simulations at the doping level of  $1x10^{16}$  cm<sup>-3</sup>, which agreed with equation 4.3. In figure 4.18, the breakdown voltage increased with temperature. The mobility was greatly reduced at higher temperature, with that the peak electric field rose and in turns the higher breakdown voltage resulted.

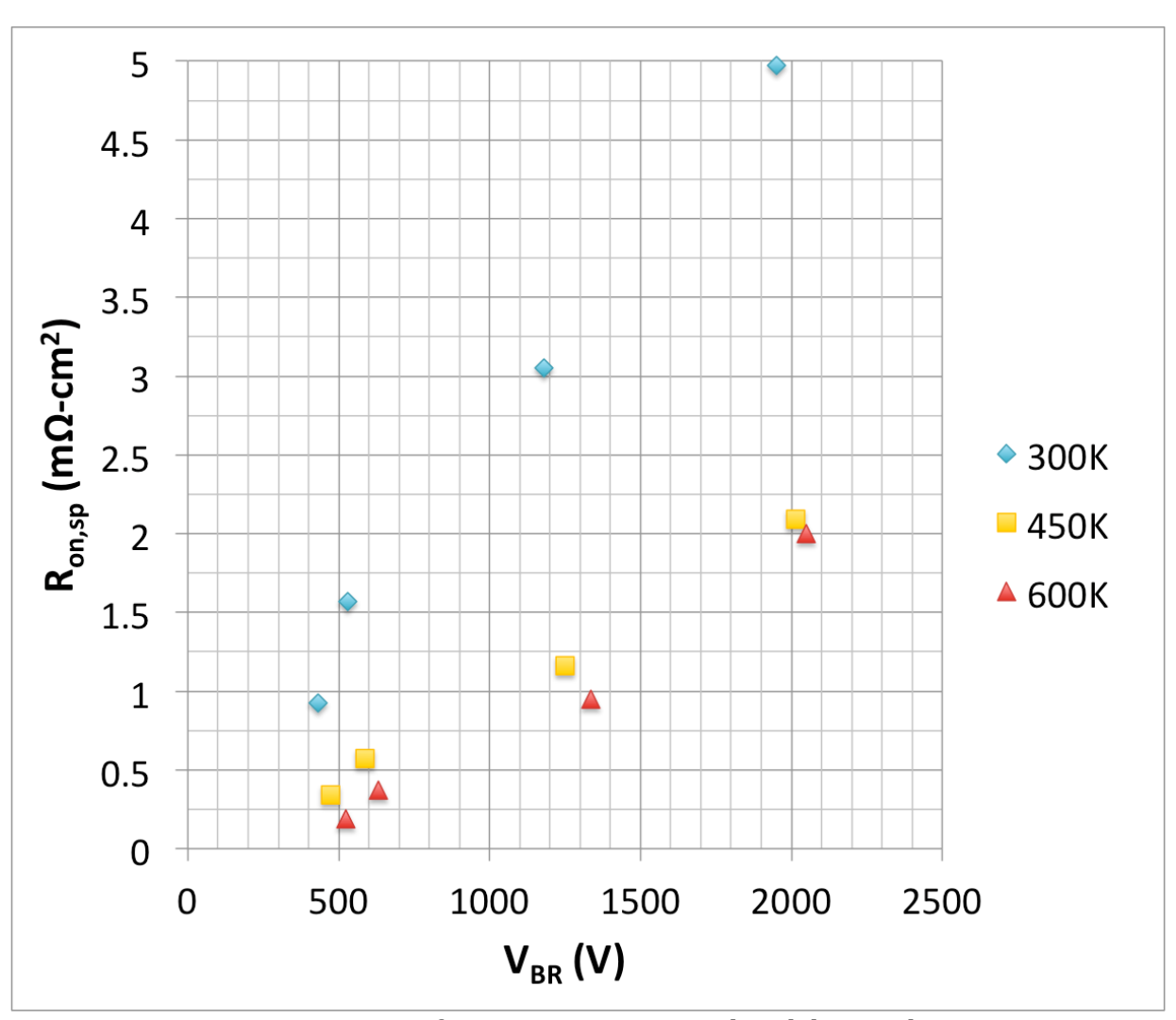


Figure 4.19: Specific on-resistance versus breakdown voltage when  $p^-$  layer thickness was fixed at 5  $\mu$ m and  $p^-$  doping was fixed at 1x10<sup>16</sup> cm<sup>-3</sup>

The reverse bias blocking capability relates to the forward bias performance via the specific on-resistance and breakdown voltage relationship theoretically stated in equation 4.7 and the agreeing results are plotted in figure 4.19. The specific on-resistance rose with increasing breakdown voltage as predicted by equation 4.7. This presents a trade-off in the design of Schottky diodes since normally one would like to increase the voltage blocking capability while minimizing the forward loss.

## 4.3 Schottky Diamond Diode with Field Plate Structures

The effect of high electric field at the edge of Schottky metal contact is exemplified by the simulation results reported in figure 4.20. The simulation of the structure shown in figure 4.20 where the Schottky contact only extended half way across the simulated structure showed the field concentrates higher at the edge of the contact. At 400 V reverse bias, the field at the edge of the Schottky contact was  $1.4 \times 10^7$  V/cm, which was higher than the field in the middle of the contact, which was  $5.2 \times 10^6$  V/cm.

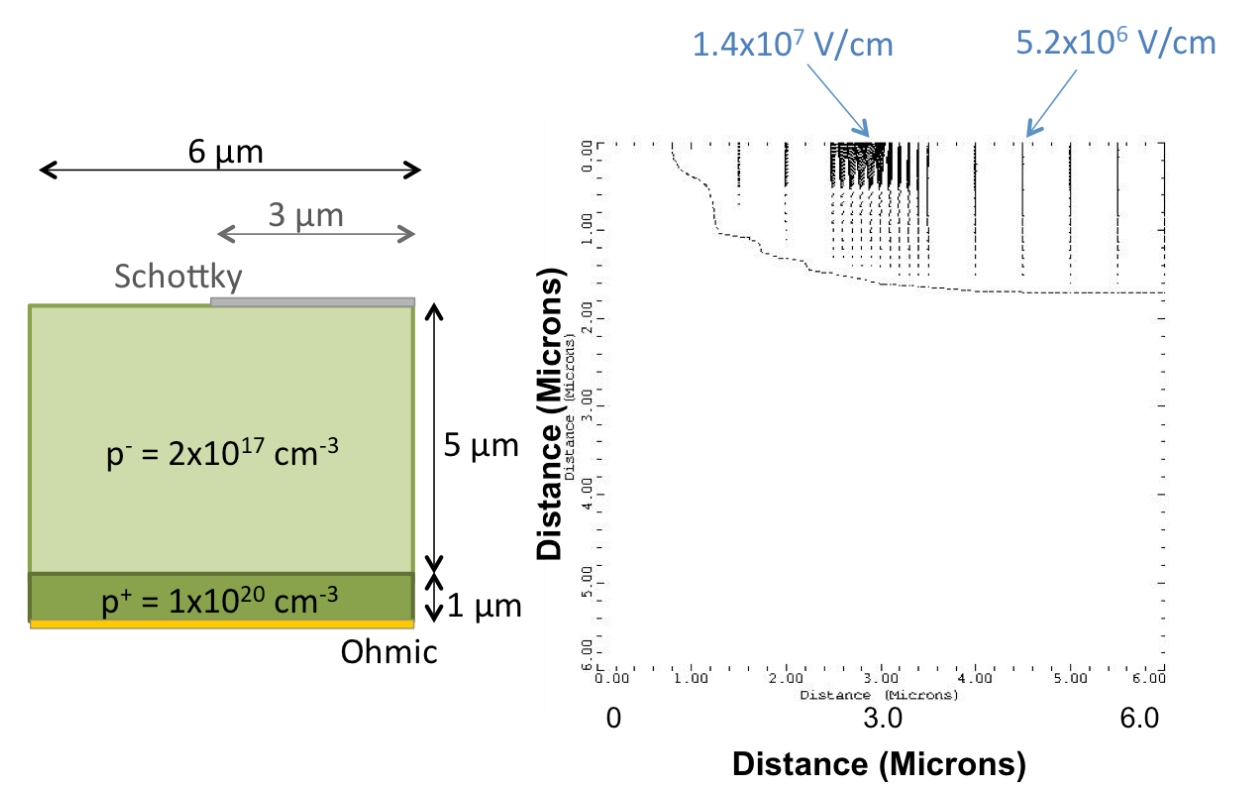


Figure 4.20: Simulation setup and results of electric field vectors in the device at 400 V reverse bias, 300 K

Adding a field plate made of aluminum oxide (dielectric constant,  $\varepsilon_{Al_2O_3}$ = 9.1) to the Schottky barrier as shown in figure 4.21 reduced the high field edge termination problem. Results are reported in table 4.2 and figure 4.21. Both field plate thicknesses yielded improved results in terms of electric field at the edge of the Schottky contact and

breakdown voltage. Between the two thicknesses, the thinner field plate of 0.5  $\mu m$  gave slightly better results.

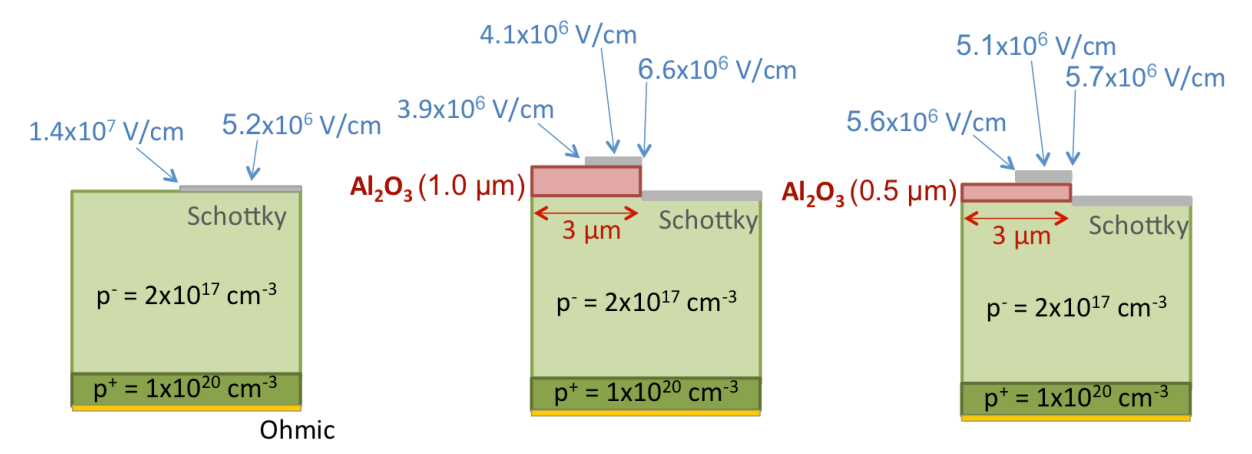


Figure 4.21: Electric field at the edge and middle of Schottky contact without field plate (left); with 1.0  $\mu$ m thick field plate (middle); with 0.5  $\mu$ m thick field plate (right)

| Al <sub>2</sub> O <sub>3</sub> thickness (μm) | Electric field at<br>the edge of contact<br>(V/cm) | V <sub>BR</sub> (V) |
|---|--|---------------------|
| No oxide                                      | 1.4 x 10 <sup>7</sup>                              | 448                 |
| 1   | 6.6x10 <sup>6</sup>                                | 772                 |
| 0.5   | 5.7 x 10 <sup>6</sup>                              | 811                 |

Table 4.2: Electric field at the Edge of Schottky Contact and Breakdown Voltage at 700 V Reverse Bias When Varying Thickness of Field Plate was Used

## 4.4 Summary of Chapter

To summarize this chapter, the following points were deduced from the simulations of Schottky diamond diode with variations in design parameters:

- In the forward conduction the thickness of the device was the most prominent design parameter that would affect the current flow the most. Raising the temperature encouraged more ionization of charges, so the forward conduction improved. Changing the doping concentration did not impact the result as much if space limit current was occurring, however if ohmic conduction was dominating then the doping concentration was important.
- In reverse bias the doping concentration was the most prominent design parameter. Changing the thickness of the device would affect the result until the depletion width equaled the drift layer thickness, after which  $V_{BR}$  would not vary. Raising the temperature did not provide much effect.
- Adding field plate structures made of high dielectric constant material reduced the high electric field at Schottky contact edges. Hence, greater breakdown voltage could be achieved.

#### **CHAPTER 5**

#### COMPARISON OF DIAMOND DIODE DESIGNS

This chapter presents the simulation results of the PN-junction and merged diamond diodes. The basic operational mechanism of the different structures and their attributes are first introduced. The results from different diode designs are then compared. The chapter is organized into the following sections including (1) PN-junction diamond diode with consideration of the basic operation of PN-junction diodes, simulation of PN-junction diamond diodes, and performance comparison of Schottky and PN-junction diamond diodes and (2) merged diamond diodes with consideration of basic operation of merged diode structures, simulation of merged diamonds and comparison of Schottky, PN-junction and merged diamond diodes.

## 5.1 PN-junction Diamond Diode

Unlike the Schottky barrier formed by a semiconductor-to-metal interface, a PN-junction is formed by bringing two semiconductor materials with dissimilar Fermi energies together. The PN-junction structure performs like a rectifier, but due to its semiconductor-to-semiconductor interface, its operational mechanisms are different from the ones seen in Schottky diamond diode in the previous chapter. In fact the physics in the forward conduction is more complicated in PN-junction diode as it is a minority carrier device in which movements of both electrons and holes take place.

## 5.1.1 Basic Operation of PN-junction Diode

The basic operational mechanism of a PN-junction is depicted in figure 5.1. When p-type and n-type semiconductors are brought in contact, initially some diffusion occurs when some free electrons in the n-region move across the interface (leaving behind some positive donor ions) to combine with the holes in the p region yielding some negative acceptor ions. This results in the area near the junction of the p and n type material having a space charge built up, which is called the depletion region. The space charge region with its electric field prevents any further electron transfer in the equilibrium. In forward bias, the applied voltage will cause the electrons to diffuse across the depletion region to the p-type region and holes to diffuse across the depletion region to the n-type region. Electrons and holes also can partially recombine in the depletion region. In reverse bias, electrons and holes are pulled away from the junction. The depletion region width increases. Breakdown occurs when the applied voltage creates an electric field large enough that impact ionization occurs.

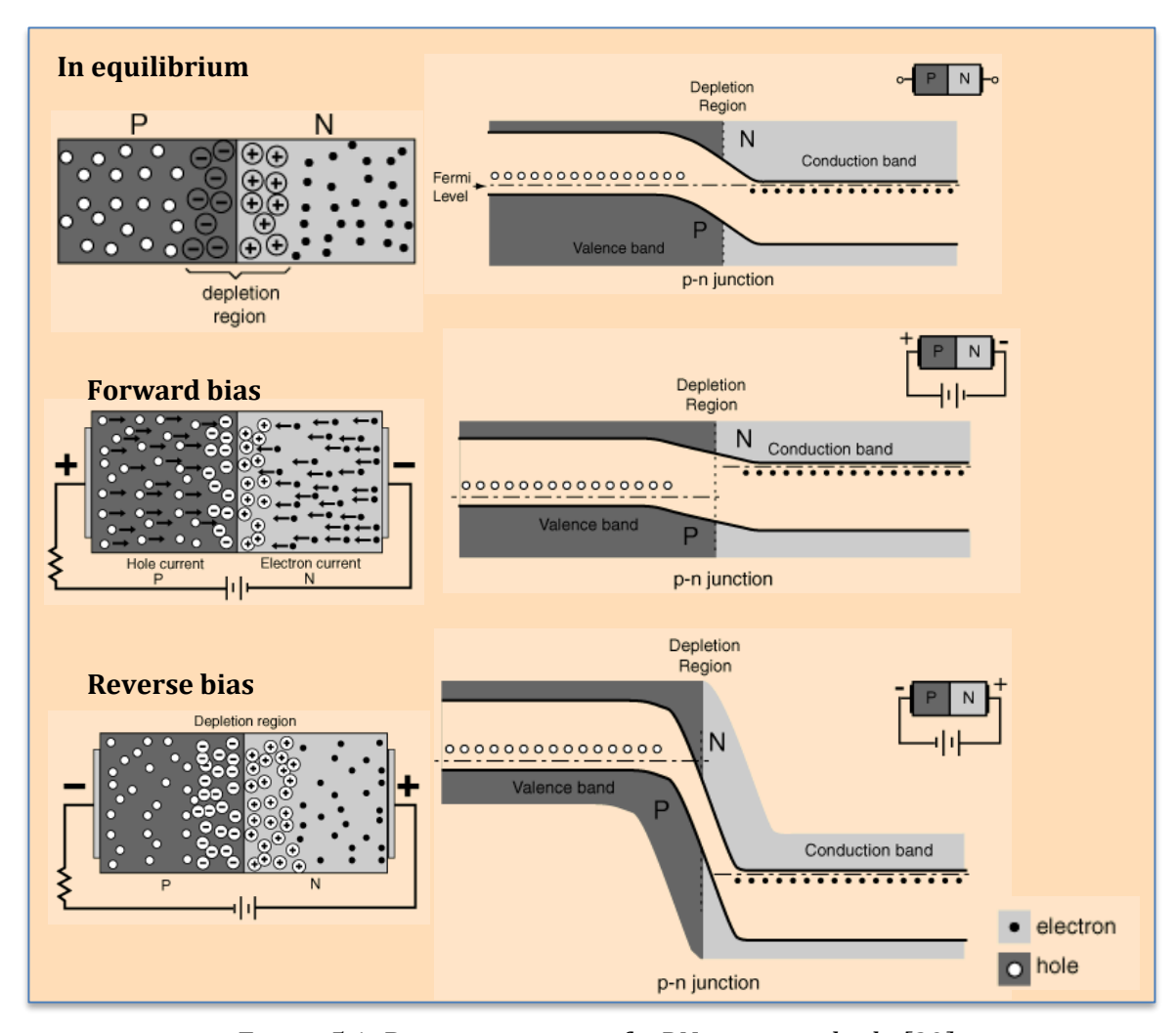


Figure 5.1: Basic operations of a PN-junction diode [39]

Because there are movements of holes and electrons in the drift region for PN-junction diodes, the resistance in the area is lowered and changing depending on the amount of forward bias applied. Hence, at higher forward bias the current density is normally large when compared to Schottky diode at higher voltage. This is called conduction modulation, which is the process that Schottky diode is lacking.

When either side of the semiconductor is much more heavily doped,  $p^+/n$  or  $n^+/p$ , the situation is referred to as a one-sided abrupt junction. The depletion region primarily extends into the lightly doped region; any extension into the highly doped area can be

neglected. Detailed theoretical derivations and explanations about PN-junction diodes can be found in chapter 2 of *Physics of Semiconductor Devices* by Sze. [35]

For the  $n^+/p^-$  junction in the simulations in the next section,  $N_D >> N_A$  and the depletion width is given in equation 5.1. The built-in potential and breakdown voltage are given in equations 5.2 and 5.3 respectively. [35]

$$W_D = \sqrt{\frac{2\varepsilon_s \psi_{bi}}{q N_A}} = \frac{2V_{BR}}{E_{max}} \tag{5.1}$$

$$\psi_{bi} \approx \frac{kT}{q} ln \left( \frac{N_D N_A}{n_i^2} \right) \tag{5.2}$$

$$V_{BR} = \frac{\varepsilon_s E_{max}^2}{2qN_A} \tag{5.3}$$

where  $\varepsilon_s$  is permittivity of the semiconductor (diamond in this case), k is the Boltzmann constant, T is the temperature, q is the electric charge,  $E_{max}$  is the peak electric field,  $N_D$  is the donor impurity concentration,  $N_A$  is the acceptor impurity concentration, and  $n_i$  is the intrinsic carrier concentration. Equations 4.3-4.7 are also applicable for the PN-junction structure. [35] The built-in potential in equation 5.2 is larger than the barrier potential in Schottky diodes. As a result, higher turn-on voltage is to be expected.

### 5.1.2 Structure Setup and Simulation of PN-junction Diamond Diode

The structure of the PN-junction diode used in all of the simulations in this chapter is shown in figure 5.2. It looks similar to the structure in figure 4.1 for Schottky diode simulations. The difference was the thin and heavily doped layer is n-type with the concentration of 1 x  $10^{20}$  cm<sup>-3</sup> and thickness of 1  $\mu$ m. Phosphorus was assumed as the n-type dopant and its parameters which were necessary for the simulations are listed back in

chapter 3. The lowly doped layer is p-type and was 5  $\mu$ m thick. Two ohmic contacts were formed; one was placed on top of the n<sup>+</sup> layer while the other was on the bottom side of p-layer. Both were 100 nm thick, and 5  $\mu$ m long. (Note that Medici assumes the 2-dimensional structure has 1  $\mu$ m depth into the page for figure 5.2).

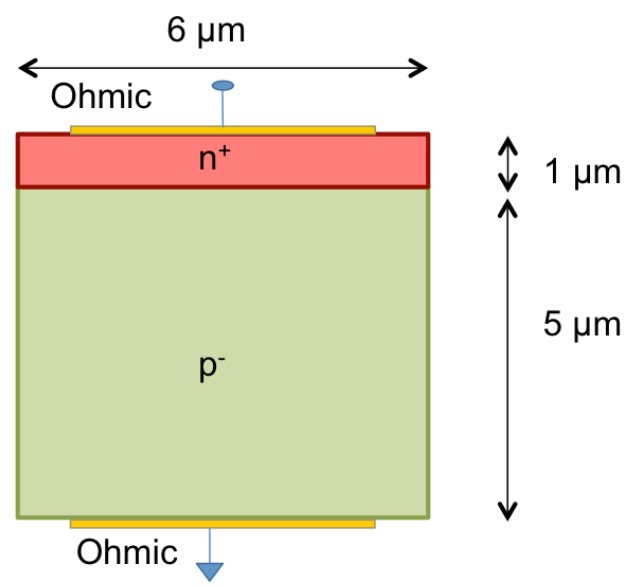


Figure 5.2: Setup structure of PN-junction diode

The structure in figure 5.2 was simulated by varying the operating temperature from 300 to 600 K and the doping concentration in the p<sup>-</sup> layer (N<sub>A</sub>) from  $1x10^{16}$  –  $2.5x10^{17}$  cm<sup>-3</sup>. The values of breakdown voltages (V<sub>BR</sub>) and the calculated specific on-resistance (R<sub>on,sp</sub>) from the I-V plots of the simulation results are listed in table 5.1. Similar to the Schottky diamond diode, as the operating temperature rose the incomplete ionization effect became less, resulting in higher current density in the forward bias as seen in the J-V plot in figure 5.3. Also when keeping the operating temperature fixed at 450 K and only varying N<sub>A</sub>, the current densities increased with the level of doping concentration as shown in figure 5.4. In figure 5.5, the specific on-resistance decreased with increasing doping level, which agreed with equation 4.6.

| 300                                |                     | ) K 450 K                      |                     | 600 K                       |                     |                                |
|------------------------------------|---------------------|--------------------------------|---------------------|-----------------------------|---------------------|--------------------------------|
| N <sub>A</sub> (cm <sup>-3</sup> ) | V <sub>BR</sub> (V) | R <sub>on,sp</sub><br>(mΩ-cm²) | V <sub>BR</sub> (V) | R <sub>on,sp</sub> (mΩ-cm²) | V <sub>BR</sub> (V) | R <sub>on,sp</sub><br>(mΩ-cm²) |
| 1x10 <sup>16</sup>                 | 2114                | 0.526                          | 2160                | 0.069                       | 2223                | 0.0395                         |
| 3x10 <sup>16</sup>                 | 1313                | 0.342                          | 1355                | 0.0404                      | 1404                | 0.0179                         |
| 1x10 <sup>17</sup>                 | 728                 | 0.182                          | 830                 | 0.0221                      | 919                 | 0.00787                        |
| 2.5x10 <sup>17</sup>               | 467                 | 0.104                          | 543                 | 0.0146                      | 613                 | 0.00458                        |

Table 5.1: Results of PN-junction Diamond Diode Simulations (structure displayed in figure 5.1) with Varying Temperature and Doping Concentration

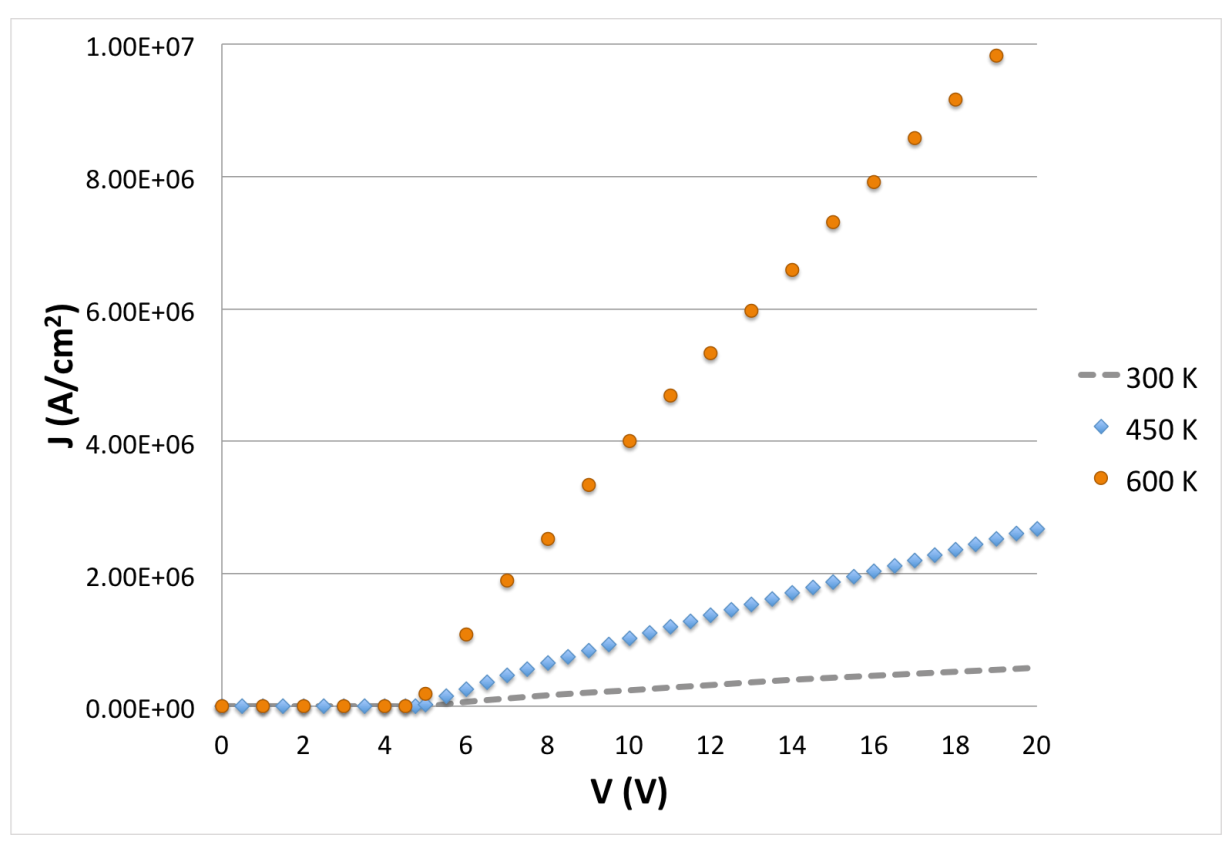


Figure 5.3: J-V plot of a PN-junction diamond diode when  $N_A$  in p- layer was  $1x10^{17}$  cm<sup>-3</sup> and 5  $\mu$ m thick

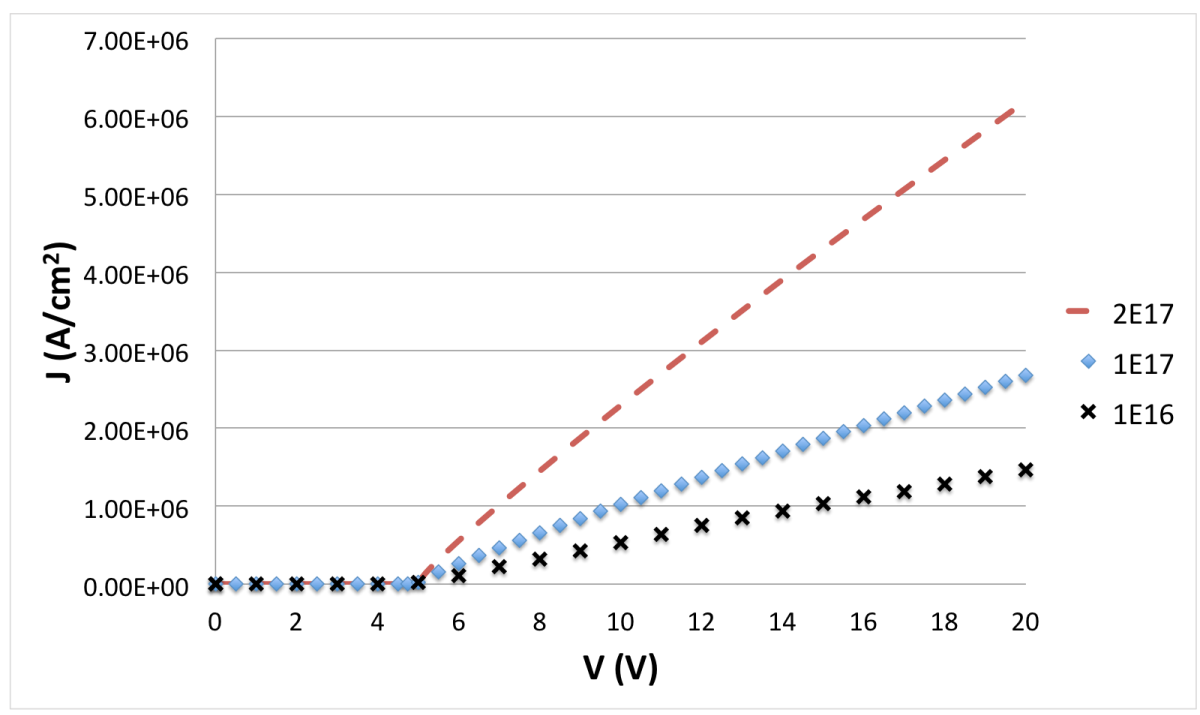


Figure 5.4: J-V plot of a PN-junction diamond diode when  $p^{-}$  layer was 5  $\mu$ m thick and operating temperature was 450K

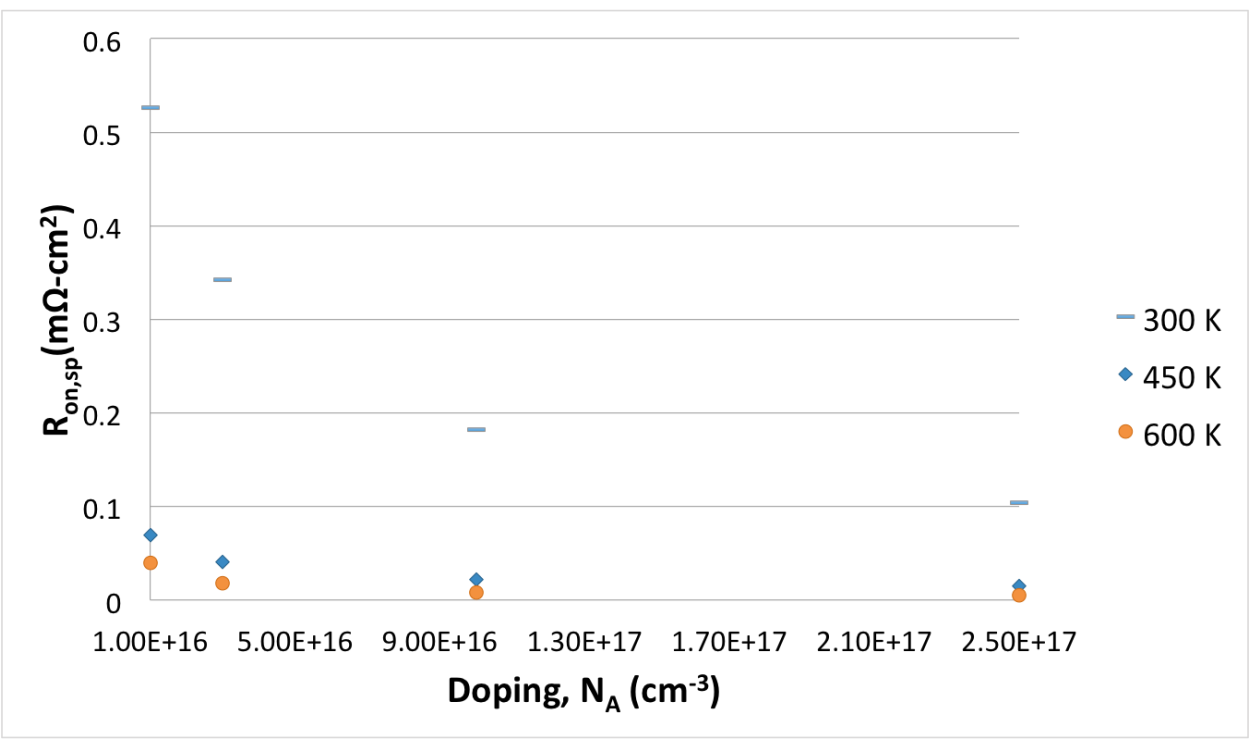


Figure 5.5: Specific on-resistance versus doping concentration in the drift layer of PN-junction diode

In the reverse bias, the values of peak electric field ( $E_{max}$ ) measured at 450 K were recorded at the breakdown voltage. When the drift layer doping was  $1x10^{16}$  cm<sup>-3</sup>,  $E_{max}$  was  $5.57x10^6$  V/cm. When doping was increased to  $1x10^{17}$  cm<sup>-3</sup>,  $E_{max}$  went up to  $6.24x10^6$  V/cm. This also agreed with the theoretical equation 4.4 since increasing drift layer doping resulted in higher peak electric field at breakdown in the reverse bias. This led to the results in figure 5.6. Since the breakdown voltage was inversely proportional to the peak electric field, the breakdown voltage decreased with increasing p<sup>-</sup> layer (drift layer) doping concentration as shown in figure 5.6.

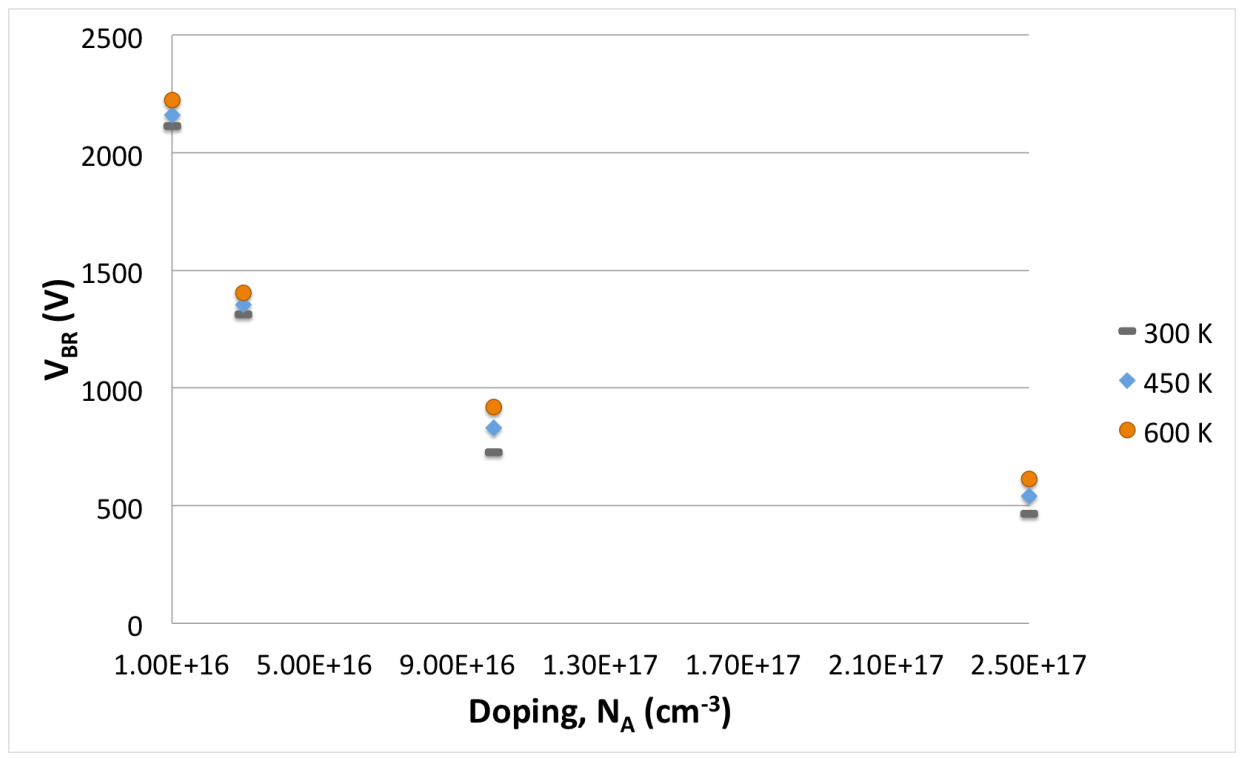


Figure 5.6: Breakdown voltage versus drift layer doping concentration of a PN-junction diamond diode based on 5-µm thick drift layer

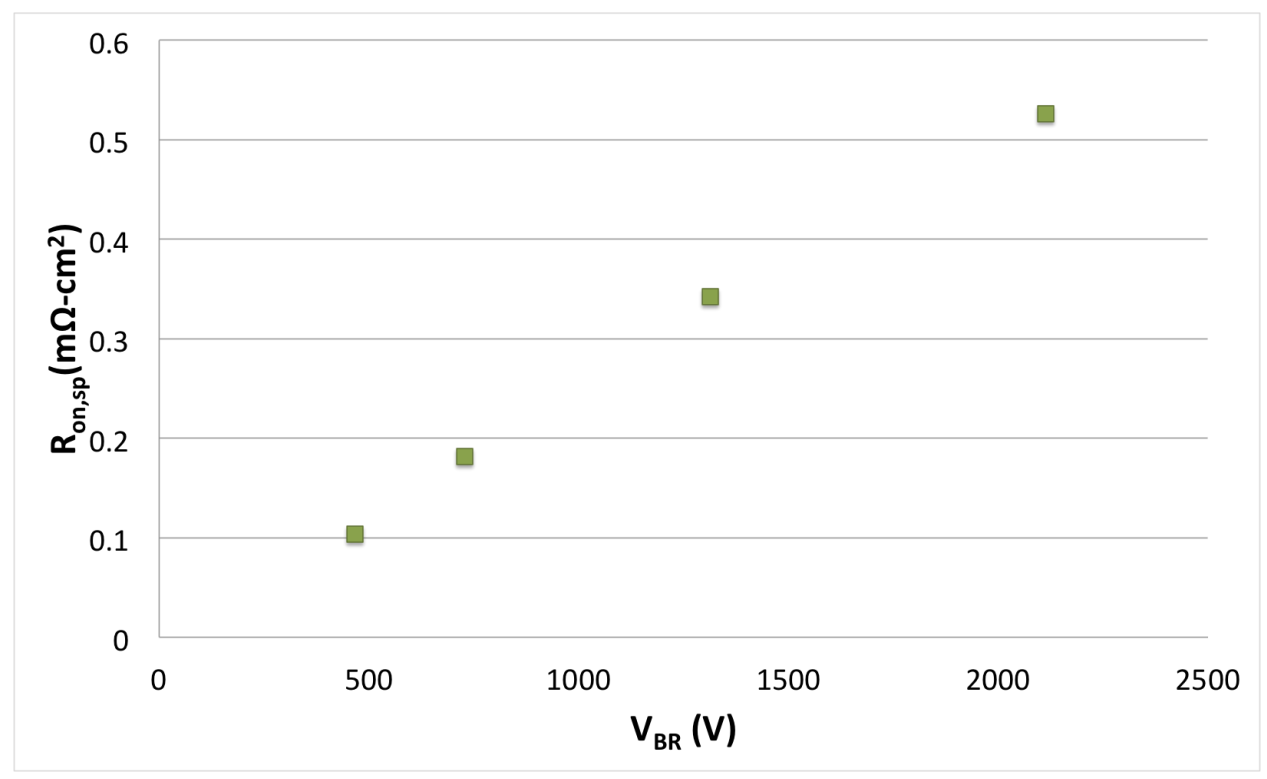


Figure 5.7: Specific on-resistance versus breakdown voltage of PN-junction diamond diode at 300 K

The specific on-resistance of PN-junction diode versus the blocking capability is plotted in figure 5.7. The result matched the expectation based on the theoretical derivation in equation 4.7. This suggests that higher voltage blocking capability comes with greater power loss.

## 5.1.3 Performance Comparison of Schottky and PN-junction Diamond Diode

In this section, the simulation results between the two types of diodes are compared. Depicted in figure 5.8 is a plot of current density versus voltage in the forward bias of the Schottky and PN-junction diodes - both of which had the  $p^-$  layer doping concentration of 1 x  $10^{17}$  cm<sup>-3</sup> and thickness of 5  $\mu$ m at 450 K. It can be observed that the turn-on voltage ( $V_{on}$ ) was approximately 2 V for Schottky diode and 4.8 V for PN-junction

diode. This was as expected since the Schottky barrier height between metal and semiconductor was lower. Thus, lower built-in potential was required to transport carriers. However, the PN-junction diode conducted more current as a result of high carrier injection.

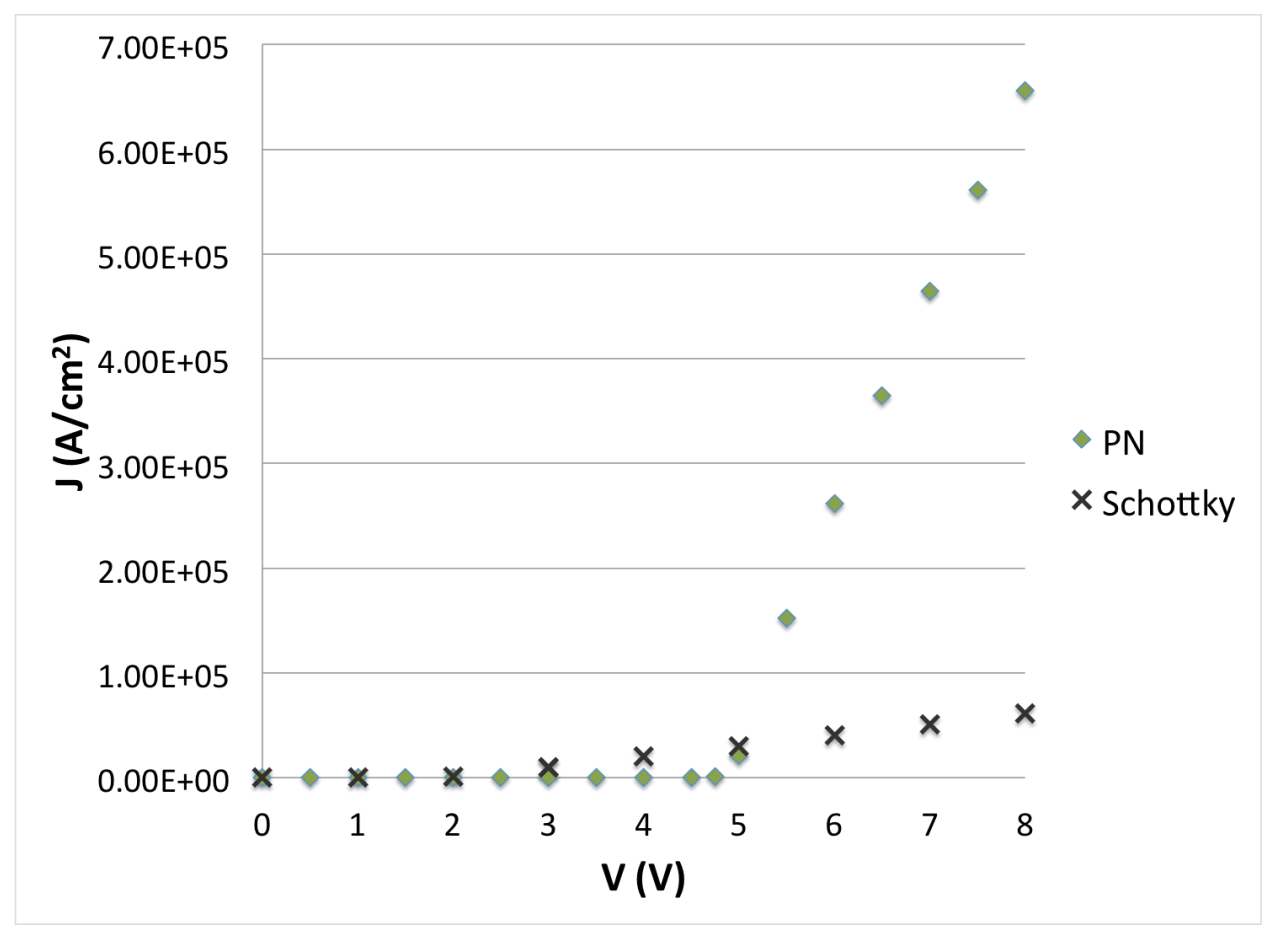


Figure 5.8: Comparison of the turn-on voltages ( $V_{on}$ ) of Schottky and PN-junction diodes at 450 K based on N<sub>A</sub> of 1 x 10<sup>17</sup> cm<sup>-3</sup> and p<sup>-</sup> was 5  $\mu$ m thick

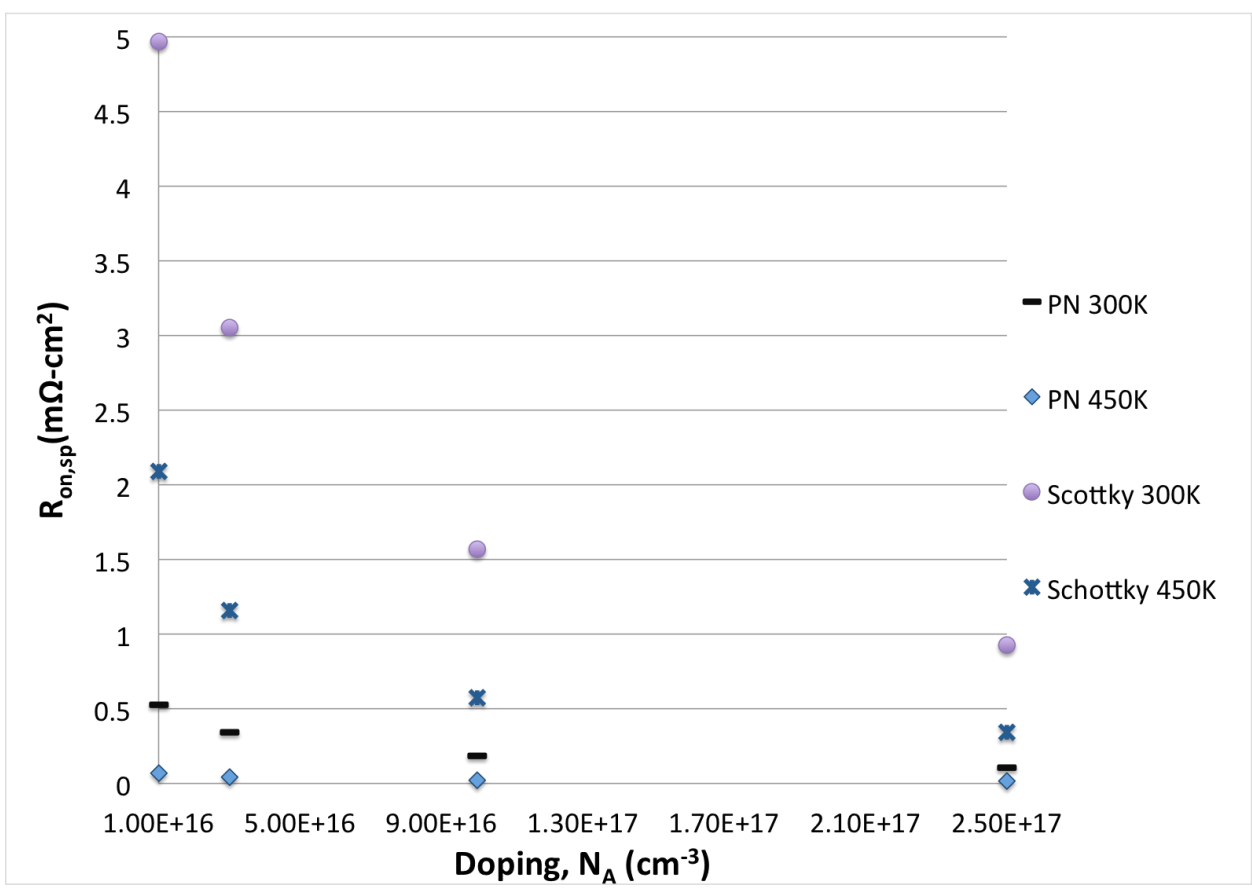


Figure 5.9: Comparison of  $R_{on,sp}$  of PN junction and Schottky diamond diodes

Additionally, a comparison between the specific on-resistance ( $R_{on,sp}$ ) of Schottky and PN-junction diodes are plotted in figure 5.9. Again,  $R_{on,sp}$  was calculated by determining the differential resistance from the current density versus voltage data obtained from the simulation output multiplied by the area of the contact area through which the current flowed (which was 5  $\mu m$  x 1  $\mu m$ ) . The differential resistance was calculated around the forward voltage of 10 V. Since PN-junction diodes produced higher current as seen in figure 5.8, intuitively they had lower loss in the forward conduction.

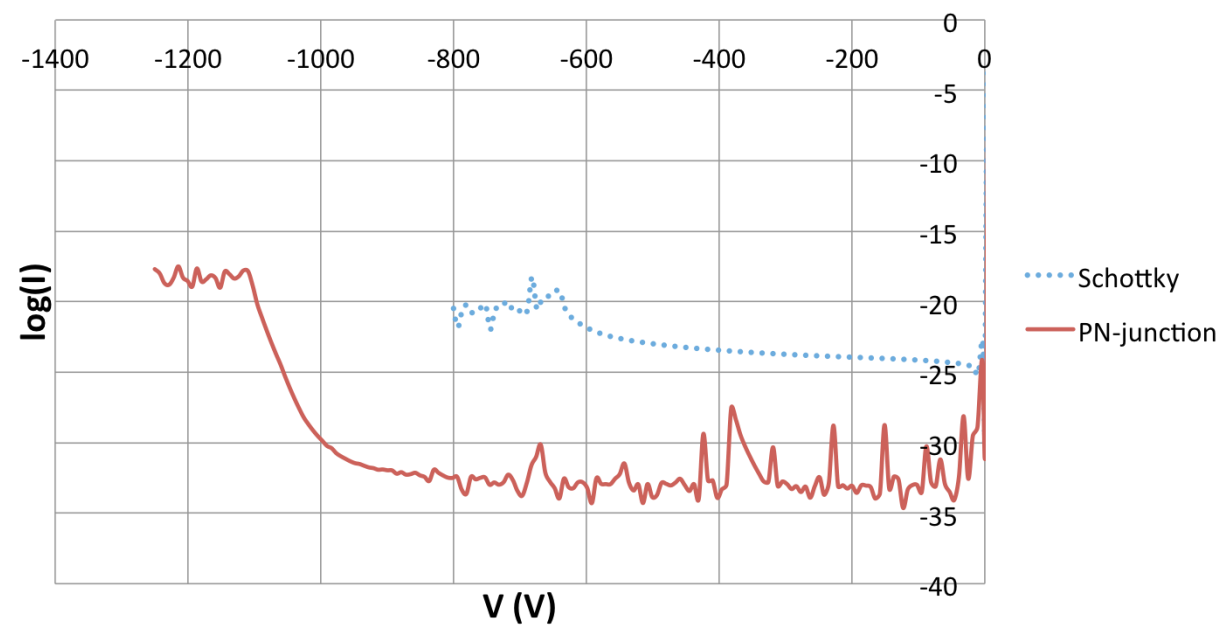


Figure 5:10 Semi-log plot of current versus voltage in reverse bias of Schottky and PN-junction diamond diodes at 450 K and drift layer doping of 4x10<sup>17</sup> cm<sup>-3</sup>

As for the reverse bias, the PN-junction diamond diodes were expected to perform better and they did when comparing the simulation results shown in figure 5.10. Additionally, figure 5.11 also displays the breakdown voltage versus doping concentration in the drift layer of Schottky and PN-junction diamond diodes at 300 K and 450 K. The peak electric field at breakdown of PN-junction and Schottky diodes are reported in table 5.2. For the same doping concentration, the field peaked higher in PN-junction diodes and this accounted for its better voltage-blocking attribute.

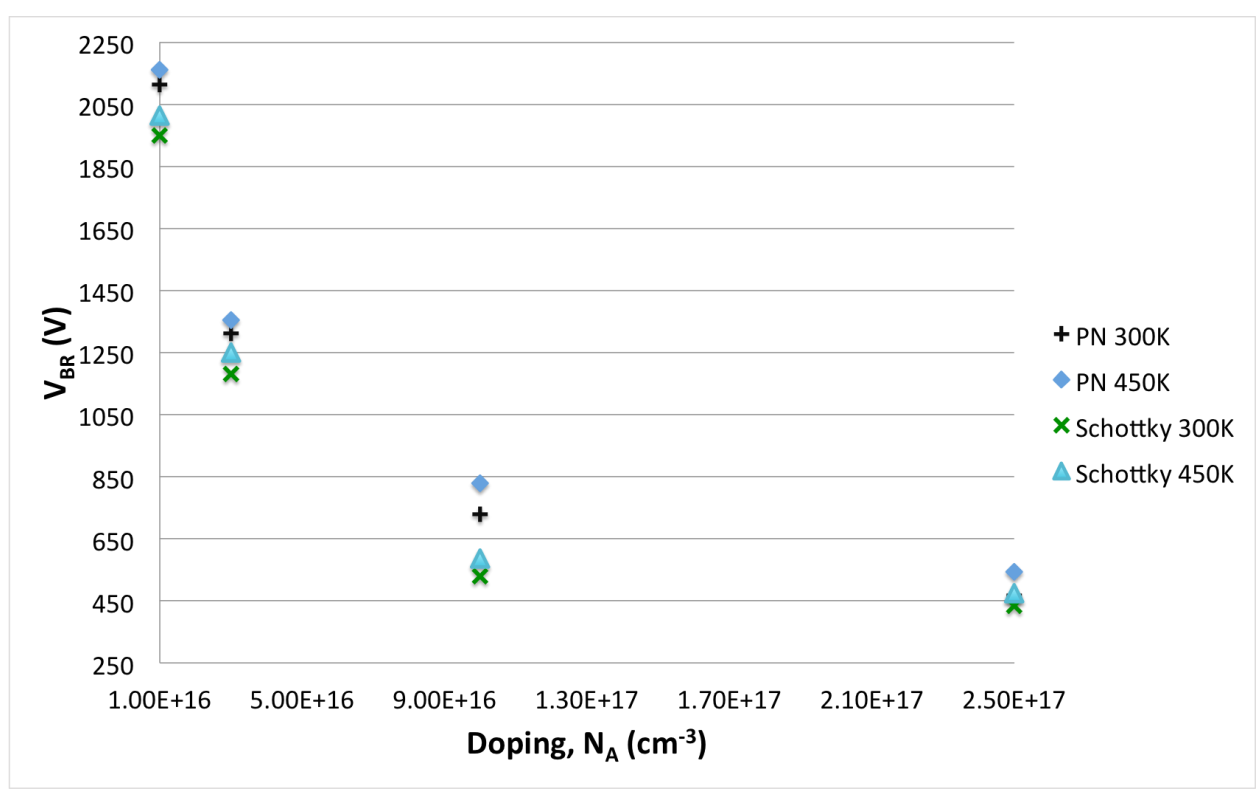


Figure 5.11: Breakdown voltage versus p layer doping concentration of Schottky and PN-junction diamond diodes based on p layer of 5 µm thick and operating temperatures at 300 K and 450 K

| PN                                 |                     | unction                 | Schottky            |                         |
|------------------------------------|---------------------|-------------------------|---------------------|-------------------------|
| N <sub>A</sub> (cm <sup>-3</sup> ) | V <sub>BR</sub> (V) | E <sub>max</sub> (V/cm) | V <sub>BR</sub> (V) | E <sub>max</sub> (V/cm) |
| 1x10 <sup>16</sup>                 | 2160                | 5.57x10 <sup>6</sup>    | 2013                | 5.19x10 <sup>6</sup>    |
| 1x10 <sup>17</sup>                 | 830                 | 6.24x10 <sup>6</sup>    | 586                 | 5.9x10 <sup>6</sup>     |

Table 5.2: Peak Electric Field at Breakdown of PN-junction and Schottky Diode at 450 K

## 5.2 Merged Diamond Diode

## 5.2.1 Basic Operation of Merged Diode Structures

Incorporating the best operating attributes of Schottky and PN-junction diodes into one discrete device have many benefits and it has been previously done with other wide bandgap materials. [40] The structure of the proposed merged diode design is depicted in figure 5.12. It can be thought of as putting a Schottky diode in parallel with the PN-junction diodes.

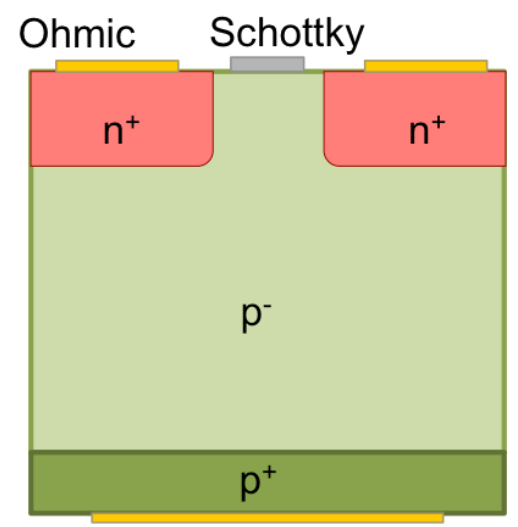


Figure 5.12: Structure of merged diode design

At low forward bias, the merged diode will start to conduct and current will flow through the Schottky contact. So it incorporates the low turn-on voltage attribute from the Schottky diode that offers lower potential barrier to current flow. Under reverse bias conditions, depletion regions formed at the  $n^+/p^-$  interface spread out and intersect under the area where the Schottky contact is placed as depicted in figure 5.13. This depletion region establishes a potential barrier under the Schottky contact that can reduce the high field in the area.

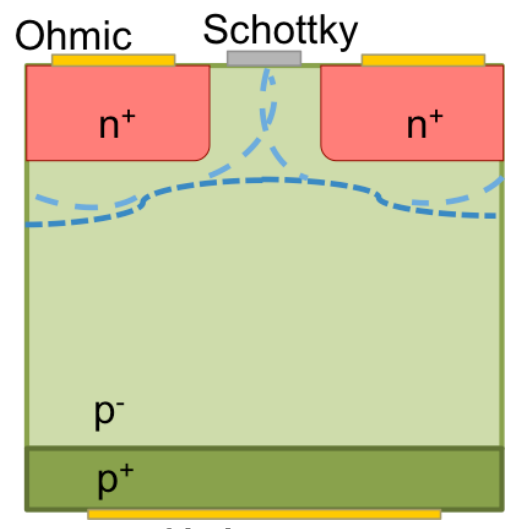


Figure 5.13: The intersection of depletion regions in merged diamond diode under reverse bias

## 5.2.2 Structure Setup and Simulation of Merged Diamond Diode

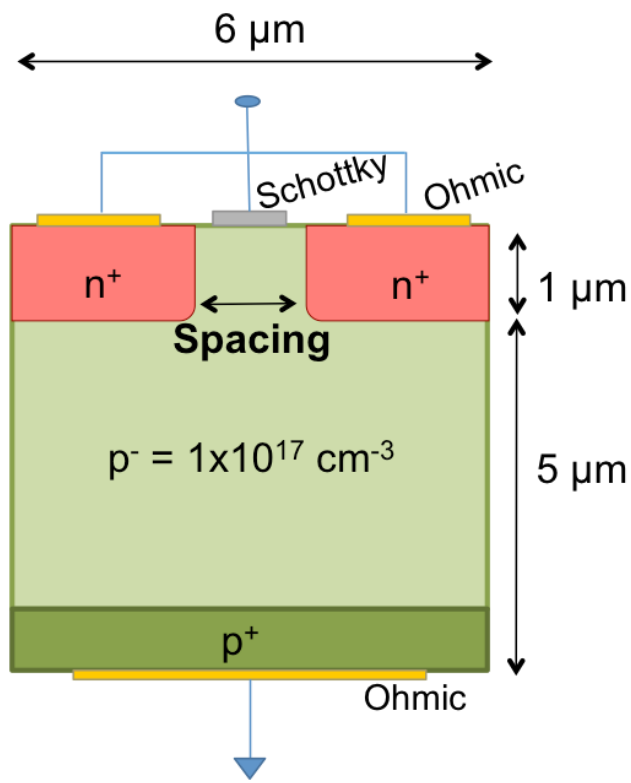


Figure 5.14: Merged diode setup for simulations

The structural setup of merged diode for simulations is exemplified in figure 5.14. The doping concentration in  $p^+$  layer ( $N_A$ ) was 1 x  $10^{20}$  cm<sup>-3</sup>. Boron was used for p-type doping. Phosphorus was used for the  $n^+$  regions and the concentration was 1 x  $10^{20}$  cm<sup>-3</sup>. The dimension of each  $n^+$  region was 1  $\mu$ m thick while the width varied depending on the *spacing* width between them. Since the spacing is the area where the depletion regions from each  $n^+/p^-$  interface would merge, it became one of the design parameters in the simulations. A Schottky contact was placed on top of this spacing area, it was 100nm thick. An Ohmic contact on the  $p^+$  layer was 100 nm thick and 5  $\mu$ m wide, while the ones on the  $n^+$  regions had the same thickness but the width varied according to the spacing. Three values of the spacing width were simulated, the dimension of  $n^+$  width, the Schottky contact above the spacing, and the Ohmic contacts above the  $n^+$  regions were configured as shown in figure 5.15.

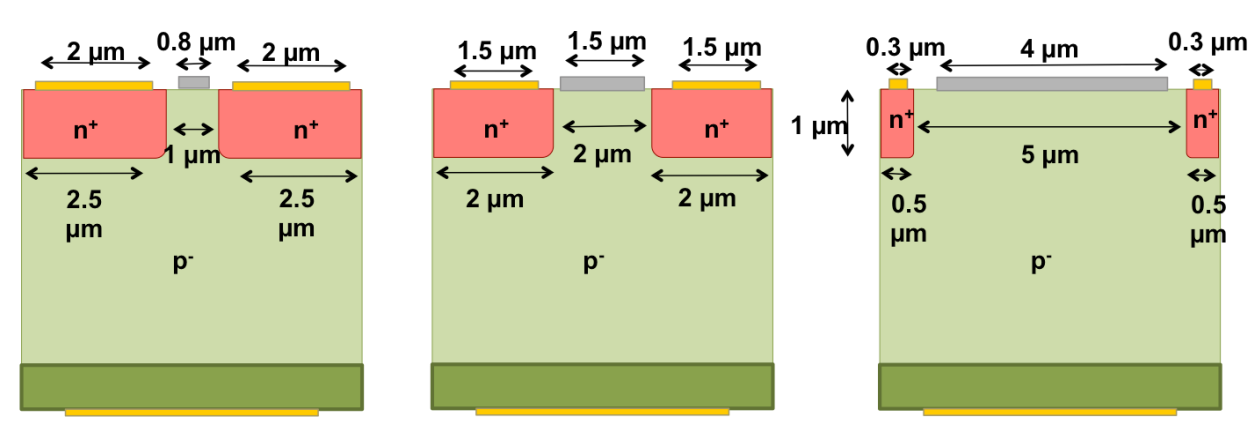


Figure 5.15: Dimension configurations of merged diode dimensions

It should be noted that the surface area that current flowed through for merged diodes was different from that of the Schottky and PN-junction diodes. In fact, for the three dimension configurations shown in figure 5.15, the surface area of current flow was different. This is important when the specific on-resistance was calculated. For the results

reported in the next sections, the specific on-resistance was determined by obtaining the differential resistance from the current density versus voltage plot where the voltage was about 10 V then multiplied by each surface area of the Schottky contact.

### 5.2.3 Comparison of Schottky, PN-junction and Merged Diamond Diodes

Values of breakdown voltage, turn-on voltage and specific on-resistance from different diode designs are reported in table 5.3 based on the simulation at 450 K and the drift layer doping of  $1x10^{17}$  cm<sup>-3</sup>. At a quick glance at table 5.3, the merged diodes had low turn-on voltage like the Schottky diode and higher voltage blocking capability like the PN-junction diode.

| Design type              | V <sub>BR</sub> (V) | V <sub>on</sub> (V) | R <sub>on,sp</sub><br>(mΩ-cm²) |
|--------------------------|---------------------|---------------------|--------------------------------|
| PN-junction              | 830                 | 5                   | 0.0221                         |
| Schottky                 | 586                 | 2                   | 0.575                          |
| Merged<br>(1-μm spacing) | 880                 | 2                   | 0.0184                         |
| Merged<br>(2-μm spacing) | 730                 | 2                   | 0.0422                         |
| Merged<br>(5-μm spacing) | 664                 | 2                   | 0.285                          |

Table 5.3: Breakdown Voltage, Turn-on Voltage and Specific On-resistance for PN-junction, Schottky and Merged Diamond Diodes Simulated at 450 K and Drift Layer Doping of 1x10<sup>17</sup> cm<sup>-3</sup>

Among the merged diodes, the structure that had 1-µm spacing offered the highest breakdown voltage. The breakdown voltage dropped as the spacing width increased. The

1- $\mu$ m spacing structure also had the lowest specific on-resistance. Smaller area of the PN-junctions yielded higher resistance. This can be interpreted that the smaller spacing allowed the depletion regions formed by each p-/n+ interface to merge more easily. The situation is depicted in figure 5.16 through the electric field vector at each biasing. At equilibrium (0 V), as indicated by the empty field vector in the drift region, no current was flowing yet. At the forward bias of 10 V, field vectors existed through out the drift region indicating current flow. In the reverse bias of -180 V, the longer field vectors indicated higher field values, which were located in the depletion regions at the p-/n+ interface. The depletion regions intersected in the spacing area (below the Schottky contact) forming a potential barrier as indicated by the line enclosing the field vectors. No field vectors existed below the potential barrier. The high electric field that conventional Schottky diodes experience at breakdown was reduced by this mechanism allowing the merged diode to have larger voltage blocking capability.

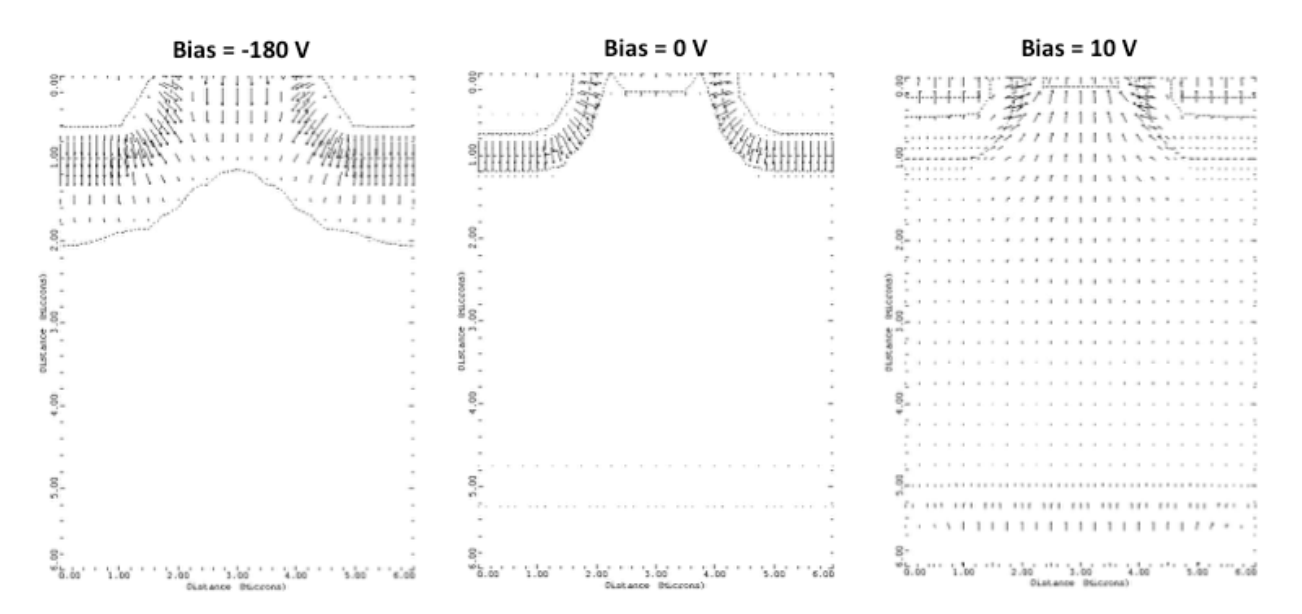


Figure 5.16: Electric field vector of the merged diode with 2- $\mu$ m spacing, drift layer doping of  $1x10^{17}$  cm<sup>-3</sup> and simulated at 450 K

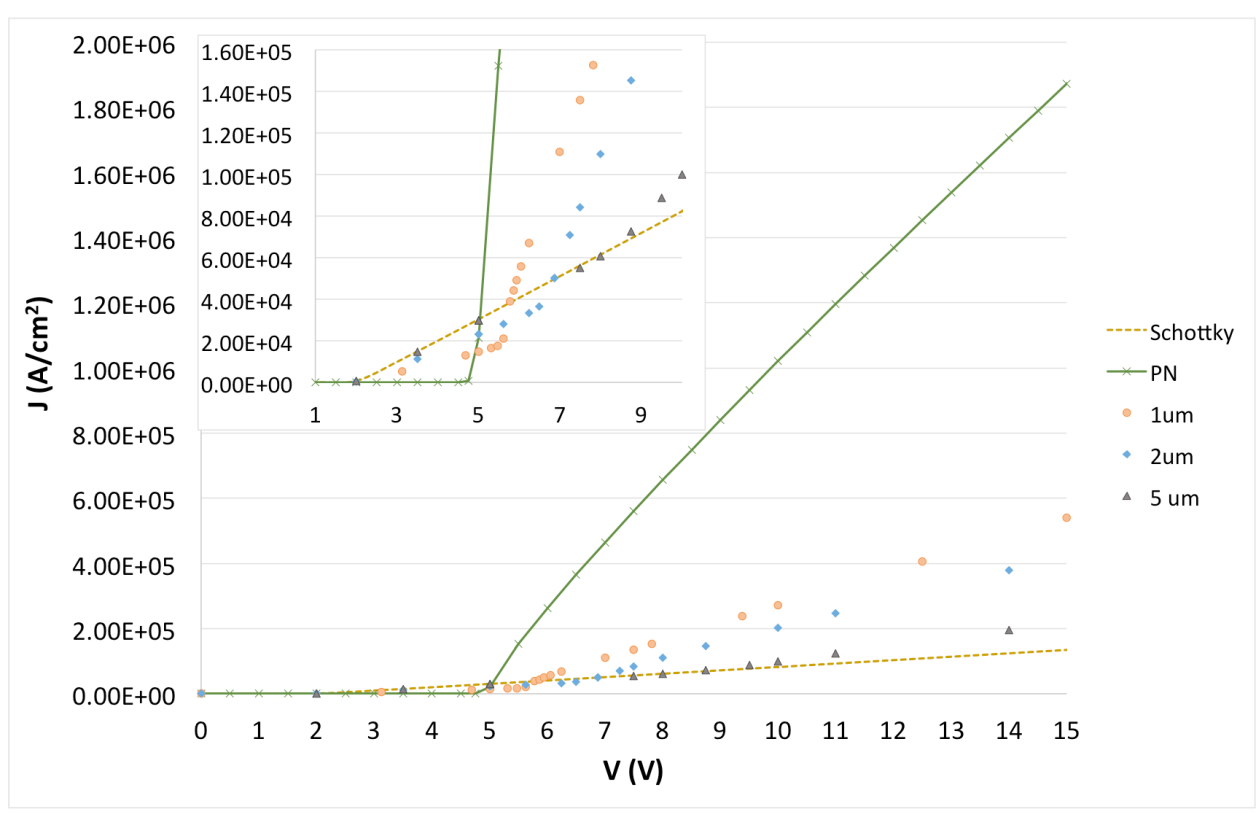


Figure 5.17: Forward conduction of Schottky, PN junction and merged diamond diode simulated at 450 K and drift layer doping of  $1 \times 10^{17}$  cm<sup>-3</sup> (the inset is zoomed in on the x and y axes)

Looking at the inset of figure 5.17, the merged diodes and Schottky diode started to conduct before the PN-junction diode. It was seen that the currents by the merged diodes followed the trend of the Schottky diode from 2 V up until 5 V. As previously reported, the Schottky diode turned on at 2 V while the PN-junction diode turned on at 5 V. Above 5.5 V, the merged diode currents increased significantly especially for the 1- $\mu$ m spacing, and they no longer looked similar to that of the Schottky diode. This can be explained that as forward voltage increased, the p-/n+ junction began to inject some minority carriers into the drift region in p- layer. The resistance in the drift region was lessened due to the presence of the minority carriers. As a result, more current was flowing. This process is

called conductivity modulation when increasing number of carriers lowers the drift layer resistance allowing more current to flow. [40]

## 5.3 Summary of Chapter

Simulations of PN-junction diodes yielded agreeable results to the theory. They provided higher voltage blocking capability and higher forward current than the Schottky diodes. Although being a minority carrier device, the reverse recovery time between the on and off state would not be as fast as the Schottky diodes.

The merged diode structure combined the low turn-on voltage of the Schottky diode and high breakdown voltage of the PN-junction diode. However, the performance depended greatly on the structure design particularly the spacing width between the interfaces  $(p^-/n^+)$  that form depletion regions.

#### **CHAPTER 6**

#### CONCLUSION AND FUTURE RESEARCH

### 6.1 Conclusion of Findings

This study developed a set of diamond physical parameters with the most up-to-date models in the literature and from the measurements of the experimental work at Michigan State University. Models for incomplete ionization, temperature-and-impurity dependent mobility, and impact ionization, along with diamond bulk parameters were included for this compilation, which was used for device simulations of diamond diode designs.

In this study, the design parameters for diamond diodes included the doping concentration in the drift layer, thickness of the drift layer, operational temperature, and spacing width between depletion regions when applicable. Diode performance metrics for high power, high voltage and high temperature applications included the breakdown voltage, turn-on voltage, and specific on-resistance. Three different structures of diamond diodes were simulated versus changes in the design parameters. These structures were the Schottky, PN-junction and merged Schottky/PN-junction diodes. The design parameters affect the performance metrics of each diode structure as follows.

In Schottky diamond diodes, the thickness and doping level of the drift layer are the most prominent design parameters in the forward conduction. The space-charge-limited conduction (SCLC) current was observed in the forward bias when the drift layer thickness was thin. The forward current entered the Ohmic conduction regime as the drift layer thickness increased. The increase in operational temperature also caused the forward

conduction to become more Ohmic. The specific on-resistance reduced as the doping concentration and temperature increased. Higher temperature enabled more carriers to be ionized, while higher doping concentration also gave more carriers in the drift region. Both of these effects reduced the series resistance in the drift layer.

As for the reverse bias performance of the Schottky diamond diodes, the drift layer doping concentration has the highest impact. The doping concentration inversely affected the breakdown voltage - causing the reduced breakdown voltage as the doping increased. The larger thickness of the drift layer caused the peak electric field at breakdown to increase yielding higher breakdown voltage. The thin aluminum oxide field plate reduced the high field associated to the edge termination problem of the Schottky contact. The field plate thickness of 0.5  $\mu$ m yielded the most improved result by lowering the field and giving the significant increase in breakdown voltage.

In the PN-junction diamond diodes, the same trend of the design parameter effects on the performance metrics was observed. The breakdown voltage had the inverse relationship with the drift layer doping concentration; while its relationship to temperature was positive. The specific on-resistance varied as the doping concentration and opposite to the temperature.

The performance comparison from the simulations between the Schottky and PN-junction diamond diodes matched their conventional and well-known attributes in both directions of conduction. In the forward bias, the turn-on voltage by the Schottky diamond diodes was lower than that of the PN-junction diamond diodes. This agrees with the known fact that the barrier potential of Schottky diodes is lower than the built-in potential of PN-junction diodes. However, the Schottky diamond diodes produced more forward loss, as

their specific on-resistances were larger resulting in the much lower current density at the higher conducting voltage. This stems from the fact that Schottky diodes are unipolar device that lack the high carrier injection condition from the process of carrier recombination and generation seen in bipolar devices like PN-junction diodes. Conventionally, PN-junction diodes have higher voltage blocking capability when compared to Schottky diodes. This results from the higher field at breakdown of the PN-junction structure. In the simulations of this study, the PN-junction diamond diodes yielded the higher breakdown voltages than the values produced by the Schottky diamond diodes – agreeing with the convention. Additionally, the higher breakdown voltage for PN-junction diodes are due to the elimination of the edge effect found in the Schottky diodes.

The merged diamond diodes combined the benefits of the Schottky and PN-junction diamond diodes. As seen in the reverse bias of the PN-junction diodes, the merged diamond diodes also produced high voltage breakdown capability. This was achieved from the intersection of the depletion regions, which created the potential barrier that reduced the electric field at its Schottky contact resulting in the high breakdown voltage. The turn-on voltage of the merged diamond diodes was low like that of the Schottky diamond diodes because its forward conduction path involved the Schottky barrier. As the forward voltage reached pass the higher turn-on voltage of the PN-junction diamond diodes, the merged diamond diodes started to deviate from the trend of Schottky diamond diodes and produced higher current density due to conductivity modulation. The performance of the merged diamond diodes depended greatly on the spacing width between the interfaces that form depletion regions. The performance deteriorated as the spacing width widened.

#### 6.2 Future research

For the high voltage, high power and high temperature applications of diamond devices, further study on the aspects not covered in this study are required. These aspects are the following:

- Extend the performance metrics to include the leakage current since it can give high
  power loss especially as the temperature increases. This can be done by plotting the
  J versus V characteristic of the simulation results similar to figure 4.14 and 5.10. The
  leakage current densities can then be observed and compared for different cases of
  design structures.
- 2. Model the forward current of the PN-junction diamond diodes. In particular, determine the design parameters that affect the ideality factor and the high injection regime. Similar methods that were used for the study of the forward current in Schottky diamond diodes in chapter 4 can be used.
- 3. Fabricate diamond diodes based on the simulated designs and compare the performance outcomes. Ultimately, a physical diamond device that is working as predicted is the goal.
- 4. Improve the carrier mobility database as more experimental results become available especially at high temperatures. The theoretical models indicate the lower rate of carrier mobility at higher temperature due to carrier scattering. As more doped diamond samples in p-type and n-type become available, the Hall measurement method can be used to measure the mobilities at various temperatures. The data can be from in-house measurements or gathered from the literature when available.

5. Apply the findings to the design and simulation of diamond field effect transistors (FETs). The findings from diamond diode simulations serve as the fundamentals from which more complicated diamond devices can be achieved. **APPENDICES** 

# APPENDIX A: Input File of Schottky Diamond Diode $(p^- = 1 \times 10^{17} \text{ cm}^{-3}; 450 \text{ K})$

TITLE Schottky Diamond Diode p-/p+

#### MESH SMOOTH=1

| X.MESH | WIDTH=6.0 N=10   |
|--------|------------------|
| Y.MESH | DEPTH=1.0 H1=0.1 |
| Y.MESH | DEPTH=5.0 H1=0.2 |

REGION NAME=SUB DIAMOND

ELECTR NAME=Anode X.MIN=0.8 X.MAX=5.2 TOP

ELECTR NAME=Cathode X.MIN=0.8 X.MAX=5.2 BOTTOM

PROFILE P-TYPE N.PEAK=1E17 UNIFORM OUT.FILE=DDT1

PROFILE N-TYPE N.PEAK=1E14 UNIFORM

PROFILE P-TYPE N.PEAK=1E20 X.MIN=0.0 WIDTH=6.0 Y.MIN=0 Y.JUNC=1.00

MATERIAL DIAMOND PERMITTI=5.7 EG300=5.47 AFFINITY=1.3 AN=4.62E5 +BN=7.59E6 CN=1.0 AP=1.93E5 BP=4.41E6 CP=1.0 NC300=1E20 NV300=1E20 +TAUP0=1E-9

IMPURITY NAME=N-TYPE REGION=SUB GB=2 EB0=0.59 ALPHA=3.1E-8 BETA=200 +GAMMA=1 HDT.MIN=3E19 HDT.MAX=3E20

IMPURITY NAME=P-TYPE REGION=SUB GB=4 EB0=0.36 ALPHA=3.037E-8 BETA=200 +GAMMA=0.95 HDT.MIN=3E19 HDT.MAX=3E20

CONTACT NAME=Cathode WORKFUNC=4.3 CONTACT NAME=Anode WORKFUNC=7.2

COMMENT mobilities by Dr. Hogan's Hall Measurements

COMMENT MOBILITY DIAMOND CONCENTR=(6.5E15, 3.1E16, 2.5E17, 6E18, 2E20)

COMMENT at 300K HOLE=(930, 820, 800, 150, 39) ELECTRON=(540, 380, 270, 120, 8)

COMMENT at 450K HOLE=(310, 250, 230, 90, 32) ELECTRON=(560, 420, 300, 180, 140)

COMMENT at 600K HOLE=(130, 100, 98, 56, 24) ELECTRON=(590, 520, 490, 475, 470)

MOBILITY DIAMOND CONCENTR=(6.5E15, 3.1E16, 2.5E17, 6E18, 2E20)

- + HOLE= (310, 250, 230, 90, 32)
- + ELECTRON= (560, 420, 300, 180, 140)
- + PR.TABLE

PLOT.2D GRID TITLE="Grid" FILL SCALE DEVICE=POSTSCRIPT PLOT.OUT=DiT1.ps

REGRID DOPING LOG RATIO=2 SMOOTH=1 IN.FILE=DDT1

PLOT.2D GRID TITLE="Doping Regrid" FILL SCALE DEVICE=POSTSCRIPT +PLOT.OUT=DiT2.ps

MODELS SRH AUGER CONMOB INCOMPLE HIGH.DOP ENERGY.L IMPACT.I +TEMPERAT=450

SYMB NEWTON CARRIERS=2

SOLVE INITIAL

SOLVE V(Anode)=0

SOLVE V(Anode)=5

SOLVE V(Anode)=10

SOLVE V(Anode)=200 ELEC=Anode VSTEP=-7 NSTEP=400

PLOT.1D E.FIELD X.START=3.0 X.END=3.0 Y.START=0.0 Y.END=6.0 TITLE="EFvsDist" +PRINT DEVICE=POSTSCRIPT PLOT.OUT=TGEF.ps

PLOT.1D Y.LOGARI Y.AXIS=I(Anode) X.AXIS=V(Anode) POINTS COLOR=2 TITLE="IV +Schottky REV 450K" DEVICE=POSTSCRIPT PLOT.OUT=DiT6HogCom.ps

PLOT.1D POTENTIA X.START=3.0 X.END=3.0 Y.START=0.0 Y.END=6.0 TITLE="PoTentail" +PRINT DEVICE=POSTSCRIPT PLOT.OUT=TGPP.ps

PLOT.1D Y.LOGARI HOLES X.START=3.0 X.END=3.0 Y.START=0.0 Y.END=3.0 +TITLE="Holes" PRINT DEVICE=POSTSCRIPT PLOT.OUT=TGHoles.ps

SOLVE V(Anode)=-5 ELEC=Anode VSTEP=0.5 NSTEP=50
PLOT.1D Y.AXIS=I(Anode) X.AXIS=V(Anode) POINTS COLOR=2 TITLE="IV Schottky FWD +450K" PRINT DEVICE=POSTSCRIPT PLOT.OUT=DiT3HogCo.ps

# APPENDIX B: Input File of Schottky Diamond Diode with Field Plate $(p^- = 1 \times 10^{17} \text{ cm}^{-3}; 450 \text{ K})$

## TITLE Diamond Test1 Field Plate p/p+

#### MESH

X.MESH WIDTH=1.0 H1=0.5

X.MESH WIDTH=1.0 H1=0.1

X.MESH WIDTH=0.5 H1=0.25

X.MESH WIDTH=1.0 H1=0.1

X.MESH WIDTH=2.5 H1=0.5

COMMENT Y.MESH NODE=1 L=-1.0

COMMENT Y.MESH NODE=11 L=0

Y.MESH NODE=1 L=-0.5

Y.MESH NODE=6 L=0

Y.MESH WIDTH=0.5 H1=0.025

Y.MESH WIDTH=4.5 H1=0.10

Y.MESH WIDTH=1.0 H1=0.20

REGION NAME=SUB DIAMOND

REGION OXIDE X.MIN=0 X.MAX=3 Y.MIN=-0.5 Y.MAX=0

ELECTR NAME=Anode X.MIN=1.5 X.MAX=3.0 TOP

ELECTR NAME=Anode2 X.MIN=3.001 X.MAX=6.0 Y.MAX=0.0

ELECTR NAME=Cathode BOTTOM

PROFILE P-TYPE N.PEAK=1E17 UNIFORM OUT.FILE=DDT2

PROFILE P-TYPE N.PEAK=1E20 Y.JUNC=1.0 Y.MIN=5.0 Y.MAX=6.0 X.MIN=0.0

+WIDTH=6.0 XY.RATIO=0.75

MATERIAL DIAMOND PERMITTI=5.7 EG300=5.47 AFFINITY=1.3 AN=4.62E5 +BN=7.59E6 CN=1.0 AP=1.93E5 BP=4.41E6 CP=1.0 NC300=1E20 NV300=1E20 +TAUP0=1E-9

MATERIAL OXIDE PERMITTI=9.1

IMPURITY NAME=P-TYPE REGION=SUB GB=4 EB0=0.36 ALPHA=3.037E-8 BETA=200 +GAMMA=0.95 HDT.MIN=3E19 HDT.MAX=3E20

CONTACT NAME=Cathode WORKFUNC=7.2

CONTACT NAME=Anode WORKFUNC=4.3

CONTACT NAME=Anode2 WORKFUNC=4.3

COMMENT mobilities by Dr. Hogan's Hall Measurements

COMMENT MOBILITY DIAMOND CONCENTR=(6.5E15, 3.1E16, 2.5E17, 6E18, 2E20)

COMMENT at 300K HOLE=(930, 820, 800, 150, 39) ELECTRON=(540, 380, 270, 120, 8)

COMMENT at 450K HOLE=(310, 250, 230, 90, 32) ELECTRON=(560, 420, 300, 180, 140)

COMMENT at 600K HOLE=(130, 100, 98, 56, 24) ELECTRON=(590, 520, 490, 475, 470)

MOBILITY DIAMOND CONCENTR=(6.5E15, 3.1E16, 2.5E17, 6E18, 2E20)

- + HOLE= (310, 250, 230, 90, 32)
- + ELECTRON= (560, 420, 300, 180, 140)
- + PR.TABLE

PLOT.2D GRID TITLE="Grid" FILL SCALE DEVICE=POSTSCRIPT PLOT.OUT=DiT2.ps

REGRID DOPING LOG RATIO=2 SMOOTH=1 IN.FILE=DDT2

PLOT.2D GRID TITLE="Doping Regrid" FILL SCALE DEVICE=POSTSCRIPT PLOT.OUT=DiT2.ps

MODELS SRH AUGER CONMOB INCOMPLE IMPACT.I HIGH.DOP TEMPERAT=450

SYMB NEWTON CARRIERS=2

SOLVE INITIAL SOLVE V(Cathode) = 0

COMMENT SOLVE V(Cathode) =-5 ELEC=Cathode VSTEP=1 NSTEP=25

SOLVE V(Cathode)=50 ELEC=Cathode VSTEP=-7 NSTEP=150

COMMENT SOLVE V(Cathode)=0 ELEC=Cathode VSTEP=-7 NSTEP=100

PLOT.1D E.FIELD X.START=3.0 X.END=3.0 Y.START=-1.0 Y.END=6.0 TITLE="EF -700V+Bias" PRINT DEVICE=POSTSCRIPT PLOT.OUT=DiT2EF.ps

PLOT.1D E.FIELD X.START=1.5 X.END=1.5 Y.START=-1.0 Y.END=6.0 TITLE="EF -700V+Bias" PRINT DEVICE=POSTSCRIPT PLOT.OUT=DiT2EF1.ps

PLOT.1D E.FIELD X.START=0.75 X.END=0.75 Y.START=-1.0 Y.END=6.0 TITLE="EF -700V+Bias" PRINT DEVICE=POSTSCRIPT PLOT.OUT=DiT2EF2.ps

PLOT.1D E.FIELD X.START=1.75 X.END=1.75 Y.START=-1.0 Y.END=6.0 TITLE="EF -700V+Bias" PRINT DEVICE=POSTSCRIPT PLOT.OUT=DiT2EF3.ps

PLOT.2D JUNCTION DEPLETION SCALE TITLE="E-field Vector Struc3" +DEVICE=POSTSCRIPT PLOT.OUT=DiT2EFC.ps

VECTOR E.FIELD

PLOT.2D BOUND JUNC DEPL FILL SCALE TITLE="Potential Contours at -700V Struc3" +DEVICE=POSTSCRIPT PLOT.OUT=DiT2CC.ps

## CONTOUR POTENTIA

PLOT.1D Y.AXIS=I(Cathode) X.AXIS=V(Cathode) POINTS COLOR=2 TITLE="Log IV Struct3" +PRINT DEVICE=POSTSCRIPT PLOT.OUT=DiT2b.ps

**EXTRACT IONIZATI** 

# APPENDIX C: Input File of PN-junction Diamond Diode $(p^- = 1x10^{17} \text{ cm}^{-3}; 450 \text{ K})$

TITLE PN-junction Diamond Diode p-/n+

MESH

X.MESH WIDTH=6.0 N=10 Y.MESH WIDTH=1.0 H1=0.10 Y.MESH WIDTH=5.0 H1=0.20

REGION NAME=SUB DIAMOND

ELECTR NAME=Anode X.MIN=0.8 X.MAX=5.2 TOP

ELECTR NAME=Cathode X.MIN=0.8 X.MAX=5.2 BOTTOM

PROFILE P-TYPE N.PEAK=1E17 UNIFORM OUT.FILE=DDT1

PROFILE N-TYPE N.PEAK=1E14 UNIFORM

PROFILE N-TYPE N.PEAK=1E20 X.MIN=0.0 WIDTH=6.0 X.CHAR=6 Y.MIN=0.0 Y.JUNC=1.0

PROFILE P-TYPE N.PEAK=1E20 Y.MIN=5.0 Y.JUNC=5.5 X.MIN=0 X.MAX=6

MATERIAL DIAMOND PERMITTI=5.7 EG300=5.47 AFFINITY=1.3 AN=4.62E5 +BN=7.59E6 CN=1.0 AP=1.93E5 BP=4.41E6 CP=1.0 NC300=1E20 NV300=1E20 +TAUP0=1E-9

IMPURITY NAME=N-TYPE REGION=SUB GB=2 EB0=0.59 ALPHA=3.1E-8 BETA=200 +GAMMA=1 HDT.MIN=3E19 HDT.MAX=3E20

IMPURITY NAME=P-TYPE REGION=SUB GB=4 EB0=0.36 ALPHA=3.037E-8 BETA=200 +GAMMA=0.95 HDT.MIN=3E19 HDT.MAX=3E20

CONTACT NAME=Cathode CONTACT NAME=Anode

COMMENT mobilities by Dr. Hogan's Hall Measurements

COMMENT MOBILITY DIAMOND CONCENTR=(6.5E15, 3.1E16, 2.5E17, 6E18, 2E20)

COMMENT at 300K HOLE=(930, 820, 800, 150, 39) ELECTRON=(540, 380, 270, 120, 8)

COMMENT at 450K HOLE=(310, 250, 230, 90, 32) ELECTRON=(560, 420, 300, 180, 140)

COMMENT at 600K HOLE=(130, 100, 98, 56, 24) ELECTRON=(590, 520, 490, 475, 470)

MOBILITY DIAMOND CONCENTR=(6.5E15, 3.1E16, 2.5E17, 6E18, 2E20) + HOLE= (310, 250, 230, 90, 32)

- + ELECTRON= (560, 420, 300, 180, 140)
- + PR.TABLE

PLOT.2D GRID TITLE="Grid" FILL SCALE DEVICE=POSTSCRIPT PLOT.OUT=DiT1.ps

REGRID DOPING LOG RATIO=2 SMOOTH=1 IN.FILE=DDT1

PLOT.2D GRID TITLE="Doping Regrid" FILL SCALE DEVICE=POSTSCRIPT +PLOT.OUT=DiT2.ps

MODELS SRH AUGER CONMOB INCOMPLE HIGH.DOP ENERGY.L IMPACT.I +TEMPERAT=450

SYMB NEWTON CARRIERS=2

**SOLVE INITIAL** 

SOLVE V(Cathode)=0
COMMENT SOLVE V(Cathode)=-5 ELEC=Cathode VSTEP=5 NSTEP=30
COMMENT PLOT.1D Y.AXIS=I(Cathode) X.AXIS=V(Cathode) POINTS COLOR=2 TITLE="IV +PN 1E16 5um Compensated 450K" PRINT DEVICE=POSTSCRIPT +PLOT.OUT=DiT3HogCo.ps

COMMENT PLOT.1D E.FIELD X.START=3.0 X.END=3.0 Y.START=0.0 Y.END=6.0 TITLE="EFvsDist" PRINT DEVICE=POSTSCRIPT PLOT.OUT=TGEF.ps COMMENT PLOT.1D POTENTIA X.START=3.0 X.END=3.0 Y.START=0.0 Y.END=6.0 TITLE="PoTentail" PRINT DEVICE=POSTSCRIPT PLOT.OUT=TGPP.ps COMMENT PLOT.1D Y.LOGARI HOLES X.START=3.0 X.END=3.0 Y.START=0.0 Y.END=6.0 TITLE="Holes" PRINT DEVICE=POSTSCRIPT PLOT.OUT=TGHoles.ps

SOLVE V(Cathode)=10 ELEC=Cathode VSTEP=-9 NSTEP=400 PLOT.1D Y.LOGARI Y.AXIS=I(Cathode) X.AXIS=V(Cathode) POINTS COLOR=2 TITLE="IV+PN 350K" DEVICE=POSTSCRIPT PLOT.OUT=DiT3HogPN.ps

PLOT.1D E.FIELD X.START=3.0 X.END=3.0 Y.START=0.0 Y.END=6.0 TITLE="EFvsDist" +PRINT DEVICE=POSTSCRIPT PLOT.OUT=TGEF.ps

APPENDIX D: Input File of Merged Diamond Diode  $(p^- = 1x10^{17} \text{ cm}^{-3}; 450 \text{ K}; \text{ spacing} = 1 \mu\text{m})$ 

TITLE Diamond Merged N+/P-/P+ Diode

COMMENT Specify a rectangular mesh MESH SMOOTH=1

COMMENT Specify the width of the mesh and the spacing is 0.125 micron X.MESH WIDTH=6.0 H1=0.25

Y.MESH N=1 L=0

COMMENT Specify the spacing between y=0 and y=2.5um is 0.125um for P-Y.MESH DEPTH=5.0 H1=0.25

COMMENT Specify the spacing between y=2.5 and y=3um is 0.25um for P+Y.MESH DEPTH=1.0 H1=0.5

COMMENT Eliminate all nodes between y=1.1um and y=2um ELIMIN COLUMNS Y.MIN=5.1

REGION NAME=SUB DIAMOND

COMMENT Electrode definition

ELECTR NAME=Ohmic X.MIN=1.0 X.MAX=5.0 BOTTOM
ELECTR NAME=Left X.MIN=0.4 X.MAX=1.8 TOP
ELECTR NAME=Right X.MIN=4.2 X.MAX=5.6 TOP
ELECTR NAME=Mid X.MIN=2.7 X.MAX=3.3 TOP

COMMENT Specify impurity profiles and fixed charge

PROFILE P-TYPE N.PEAK=1E17 UNIFORM OUT.FILE=MDEX1DS

PROFILE N-TYPE N.PEAK=1E14 UNIFORM

PROFILE P-TYPE N.PEAK=1E20 Y.MIN=5.0 Y.JUNC=5.5 X.MIN=0 X.MAX=6

PROFILE N-TYPE N.PEAK=1E20 Y.JUNC=1.0 X.MIN=0.0 WIDTH=1.5 XY.RAT=1.0 PROFILE N-TYPE N.PEAK=1E20 Y.JUNC=1.0 X.MIN=4.5 WIDTH=1.5 XY.RAT=1.0

MATERIAL DIAMOND PERMITTI=5.7 EG300=5.47 AFFINITY=1.3 AN=4.62E5 +BN=7.59E6 CN=1.0 AP=1.93E5 BP=4.41E6 CP=1.0 NC300=1E20 NV300=1E20 +TAUP0=1E-9

IMPURITY NAME=N-TYPE REGION=SUB GB=2 EB0=0.59 ALPHA=3.1E-8 BETA=200 +GAMMA=1 HDT.MIN=1E15 HDT.MAX=1E21

IMPURITY NAME=P-TYPE REGION=SUB GB=4 EB0=0.36 ALPHA=3.037E-8 BETA=200 +GAMMA=0.95 HDT.MIN=1E15 HDT.MAX=1E21

CONTACT NAME=Left
CONTACT NAME=Right
CONTACT NAME=Ohmic
CONTACT NAME=Mid WORKFUNC=4.3

COMMENT mobilities by Dr. Hogan's Hall Measurements

COMMENT MOBILITY DIAMOND CONCENTR=(6.5E15, 3.1E16, 2.5E17, 6E18, 2E20)

COMMENT at 300K HOLE=(930, 820, 800, 150, 39) ELECTRON=(540, 380, 270, 120, 8)

COMMENT at 450K HOLE=(310, 250, 230, 90, 32) ELECTRON=(560, 420, 300, 180, 140)

COMMENT at 600K HOLE=(130, 100, 98, 56, 24) ELECTRON=(590, 520, 490, 475, 470)

MOBILITY DIAMOND CONCENTR=(6.5E15, 3.1E16, 2.5E17, 6E18, 2E20)

- + HOLE= (310, 250, 230, 90, 32)
- + ELECTRON= (560, 420, 300, 180, 140)
- + PR.TABLE

PLOT.2D GRID TITLE="Initial Grid" FILL SCALE + DEVICE=POSTSCRIPT PLOT.OUT=GRID.ps

COMMENT Regrid on doping
REGRID DOPING LOG RATIO=2 SMOOTH=1
+ IN.FILE=MDEX1DS

PLOT.2D GRID TITLE="Doping Regrid" FILL SCALE
+ DEVICE=POSTSCRIPT PLOT.OUT=REGRIDDOPING.ps

MODELS SRH AUGER CONMOB INCOMPLE IMPACT.I TEMPERAT=450 SYMB NEWTON CARRIERS=2

SOLVE V(Ohmic)=-5 ELEC=Ohmic VSTEP=1 NSTEP=30

PLOT.1D Y.AXIS=I(Ohmic) X.AXIS=V(Ohmic) POINTS COLOR=2 TITLE="Merged Di Diode +1um sep" PRINT DEVICE=POSTSCRIPT PLOT.OUT=MED1.ps

SOLVE V(Mid)=0 V(Left)=0 V(Right)=0 V(Ohmic)=1 ELEC=Ohmic VSTEP=-7 NSTEP=300

PLOT.1D Y.LOGARI Y.AXIS=I(Ohmic) X.AXIS=V(Ohmic) POINTS COLOR=2 TITLE="Log +Merged Di Diode 1um sep" PRINT DEVICE=POSTSCRIPT PLOT.OUT=MED2.ps

BIBLIOGRAPHY

#### **BIBLIOGRAPHY**

- [1] International Energy Agency (IEA), World Energy Outlook 2013: Renewable energy outlook, www.iea.org. 2013.
- [2] International Energy Agency (IEA), World Energy Outlook 2015: Renewable energy outlook, www.iea.org. 2015.
- [3] S. Kone, G. Civrac, H. Schneider, K. Isoird, R. Issaoui, J. Achard, A. Gicquel, "CVD diamond Schottky barrier diode, carrying out and characterization," *Diamond and Related Materials*, vol. 19, pp. 792-795. 2010.
- [4] J. Isberg, J. Hammersberg, E. Johansson, T. Wikstrom, D. J. Twitchen, A. J. Whitehead, S. E. Coe, and G. A. Scarsbrook, "High carrier mobility in single-crystal plasma-deposited diamond," *Science*, vol. 297, pp. 1670-1672. 2002.
- [5] M. E. Levinshtein, S. L. Rumyantsev, and M. S. Shur, "Handbook series on semiconductor parameters," *World Scientific*, vol. 1, Singapore. 1996.
- [6] M E. Levinshtein, S. L. Rumyantsev, and M. R. Shur, *Properties of advanced semiconductor materials GaN, AIN, SiC, BN, SiGe,* John Wiley & Sons, Inc., New York. 2001.
- [7] J. Isberg, J. Hammersberg, D J. Twitchen, A J. Whitehead, "Single crystal diamond for electronic applications," *Diamond and Related Materials*, vol. 13, pp. 320-324. 2004.
- [8] C. Wort, R. Balmer, "Diamond as an electronic material," *Materials Today*, vol. 11, pp. 22-28. 2008.
- [9] Synopsys, *Medici User's Manual*, Mountain View, CA. 2007.
- [10] S. Kone, G. Civrac, J. Schneider, K. Isorid, R. Issaoui, J. Achard, A. Gicquel, "CVD diamond Schottky barrier diode, carrying out and characterization," *Diamond and Related Materials*, vol. 19, pp. 792-795. 2010.
- [11] S. J. Rashid, A. Tajani, D. J. Twitchen, L. Coulbeck, F. Udrea, T. Butler, N. L. Rupesinghe, M. Brezeanu, J. Isberg, A. Garraway, M. Dixon, R. S. Balmer, D. Chamund, P. Taylor and G. A. J. Amaratunga, "Numerical parameterization of chemical-vapor-deposited (CVD) single-crystal diamond for device simulation and analysis," *IEEE Transactions of Electron Devices*, vol. 55, no. 10, pp. 2744-2756. 2008.
- [12] T. Makino, H. Kato, N. Tokuda, M. Ogura, D. Takeuchi, K. Oyama, S. Tanimoto, H. Okushi, and S. Yamasaki, "Diamond Schottky-PN diode without trade-off relationship between on-resistance and blocking voltage," *Phys. Status Solidi A*, vol. 207, no. 9, pp. 2105-2109. 2010.

- [13] T. Matsumoto, H. Kato, N. Tokuda, T. Makino, M. Ogura, D. Takeuchi, H. Okushi and S. Yamasaki, "Reduction of n-type diamond contact resistance by graphite electrode," *Phys. Status Solidi RRL*, vol. 8, no. 2, pp.137-140. 2014.
- [14] D. J. Twitchen, A. J. Whitehead, S.E. Coe, J. Isberg, J. Hammersberg, T. Wikstrom, and E. Johansson, "High-voltage single-crystal diamond diodes," *IEEE Transactions on Electron Devices*, vol. 51, no. 5, pp. 826-828. 2004.
- [15] M. Kubovic, H. El-Hajj, J.E. Butler, E. Kohn, "Diamond merged diode," *Diamond and Related Materials*, vol. 16, pp. 1033-1037. 2007.
- [16] H. Umezawa, S. I. Shikata, and T. Funaki, "Diamond Schottky barrier diode for high-temperature, high-power, and fast switching applications," *Japanese Journal of Applied Physics*, vol. 53, pp. 05FP061-05FP064. 2014.
- [17] H. Elhajj, A. Denisenko, A. Bergmaier, G. Dollinger, M. Kubovic and E. Kohn, "Characteristics of boron delta-doped diamond for electronic applications," *Diamond and Related Materials*, vol. 17, no. 4, pp. 409-414. 2008.
- [18] G. Chicot, T. N. Tran Thi, A. Fiori, F. Jomard, E. Gheeraert, E. Bustarret and J. Pernot, "Hole transport in boron delta-doped diamond structures," *Applied Physics Letter*, vol. 101, no. 16, pp. 162101-162104. 2012.
- [19] D. Kuech, H. El-Hajj, A. Kaiser, and E. Kohn, "Surface-channel MESFET with boron-doped contact layer," *Diamond & Related Materials*, vol. 17, pp. 732 735. 2008.
- [20] H. Kawarada, H. Tsuboi, T. Naruo, T. Yamada, D. Xu, A. Daicho, T. Saito and A. Hiraiwa, "C-H surface diamond field effect transistors for high temperature (400 C) and high voltage (500 V) operation," *Applied Physics Letters*, vol. 105, pp. 013510. 2014.
- [21] J. Liu, M. Liao, M. Imura, E. Watanabe, H. Oosato, and Y. Koide, "Diamond field effect transistors with a high dielectric constant  $Ta_2O_5$  as gate material," *J. Phys. D: Appl. Phys.*, vol. 47. 2014.
- [22] C. Kao, H. Chen, J. Chiu, K. Chen, and Y. Pan, "Physical and electrical characteristics of the high-k Ta<sub>2</sub>O<sub>5</sub> dielectric deposited on the polycrystalline silicon," *Applied Physics Letters*, vol. 96, pp. 112901. 2010.
- [23] H. Cheng, L. Sang, M. Liao, J. Liu, M. Imura, H. Li and Y. Koide, "Integration of high dielectric constant Ta<sub>2</sub>O<sub>5</sub> oxides on diamond for power devices," *Applied Physics Letters*, vol. 101, pp. 232907. 2012.
- [24] C. E. Nebel and M. Stutzmann, "Handbook," *Diamond Related Materials*, pp. 40-45. 2000.

- [25] B. A. Fox, M. L. Hartsell, D. M. Malta, H. A. Wynands, C.-T. Kao, L. S. Plana, G. J. Tessmer, R. B. Henard, J. S. Holmes, A. J. Tessmer, and D. L. Dreifus, "Diamond devices and electrical properties," *Diamond Related Materials*, vol. 4, no. 5, pp. 622-627. 1995.
- [26] D. M. Caughey and R. E. Thomas, "Carrier mobilities in silicon empirically related to doping and field," *Proc. IEEE*, vol. 55, no. 12, pp. 2192-2193. 1967.
- [27] I. Berkun, S. Demlow, N. Suwanmonkha, T. Hogan, and T. Grotjohn, "Hall Effect Measurement System for Characterization of Doped Crystal Diamond," *MRS Fall Meeting*, vol. 1511. 2013.
- [28] R. Van Overstraeten and H. Demann, "Measurement of the ionization rates in diffused silicon p-n junctions," *Solid State Electron*, vol. 13, no. 5, pp. 583-608. 1970.
- [29] A. G. Cysnoweth, "Ionization rates for electrons and holes in silicon," *Phys. Rev.*, vol. 109, no. 5, pp. 1537-1540. 1958.
- [30] S. Selberherr, *Analysis and simulation of semiconductor devices*, New York: Springer-Verlag. 1984.
- [31] R. Raghunathan and B. J. Baliga, "Measurement of electron and hole impact ionization coefficients for SiC," *Proc. IEEE Int. Symp. Power Semicond. Devices*, pp. 173-176. 1997.
- [32] J. Isberg, M. Gabrysch, A. Tajani, and D. J. Twitchen, "High-field electrical transport in single crystal CVD diamond diodes," *Advances Sci. Technol.*, vol. 48, pp. 73-76. 2006.
- [33] B. J. Baliga, *Modern Power Devices*, New York: Wiley. 1987.
- [34] A. Hiraiwa and H. Kawarada, "Figure of merit of diamond power devices based accurately estimated impact ionization processes," *Journal of Applied Physics*, vol. 114, pp. 034506. 2013.
- [35] S. Sze and K. Kwok, *Physics of Semiconductor Devices*, New York: Wiley-Interscience. 2007.
- [36] K. Böer, *Introduction to Space Charge Effects in Semiconductors*, Berlin: Springer-Verlag. 2010.
- [37] P. Stallinga, *Electrical characterization of organic electronic materials and devices*, New York: Wiley. 2009.
- [38] T. Makino, S. Tanimoto, Y. Hayashi, H. Kato, N. Tokuda, M. Ogura, D. Takeuchi, K. Oyama, H. Ohashi, H. Okushi and S. Yamasaki, "Diamond Schottky- p n diode with high

forward current density and fast switching operation," *J. Appl. Phys.*, vol. 94, pp. 262101. 2009.

[39] C. Hu, *Modern Semiconductor Devices for Integrated Circuits*. New Jersey: Pearson Prentice Hall. 2010.

[40] B. J. Baliga, "Analysis of a high-voltage merged P-i-N (MPS) rectifier: a high voltage, high speed power diode," *IEEE Electron Device Lett.*, vol. EDL-8, pp. 407-409. 1987.